uOttawa

L'Université canadienne
Canada's university

FACULTÉ DES ÉTUDES SUPÉRIEURES ET POSTOCTORALES

uOttawa

L'Université canadienne
Canada's university

FACULTY OF GRADUATE AND POSDOCTORAL STUDIES

Matias Alvarez-Saavedra

AUTEUR DE LA THÈSE / AUTHOR OF THESIS

M.Sc. (Biochemistry)

GRADE / DEGREE

Department of Biochemistry, Microbiology and Immunology

FACULTÉ, ÉCOLE, DÉPARTEMENT / FACULTY, SCHOOL, DEPARTMENT

MicroRNA-132-Dependent Post-Transcriptional Regulation of Clock Entrainment Physiology Via Modulation of Chromatin Remodeling and Translational Control Gene Targets

TITRE DE LA THÈSE / TITLE OF THESIS

Mary Cheng

DIRECTEUR (DIRECTRICE) DE LA THÈSE / THESIS SUPERVISOR

CO-DIRECTEUR (CO-DIRECTRICE) DE LA THÈSE / THESIS CO-SUPERVISOR

David Lohnes

Adam Rudner

Gary W. Slater

Le Doyen de la Faculte des etudes superieures et postdoctorales / Dean of the Faculty of Graduate and Postdoctoral Studies

MicroRNA-132-Dependent Post-Transcriptional Regulation of Clock Entrainment Physiology Via Modulation of Chromatin Remodeling and Translational Control Gene Targets

M.Sc. Thesis

in partial fulfillment of the requirements

for the degree Master of Science (M.Sc.)

in the Biochemistry Program at the

University of Ottawa, Faculty of Medicine

Ottawa, Ontario, Canada

Submitted by

Your file Votre référence
ISBN: 978-0-494-73802-3
Our file Notre référence
ISBN: 978-0-494-73802-3

Thesis Supervisor:

Dr. Hai-Ying Mary Cheng, Department of BMI, University of Ottawa

Thesis Examiners:

Dr. David Lohnes, Department of CMM, University of Ottawa

Dr. Adam Rudner, Department of BMI, University of Ottawa

Date of Thesis Submission: August 20th, 2010.

ABSTRACT

Mammalian circadian rhythms of behaviour are synchronized to external time by daily resetting of the master pacemaker, the suprachiasmatic nucleus (SCN), in response to light, in a process known as light-induced clock entrainment. microRNA-132 (miR-132) is induced by light within the SCN via a MAPK-CREB-dependent mechanism and has the capacity to attenuate the entraining effects of light. However, the identity of the genes that miR-132 regulates and their roles in the light-entrainment process have not yet been characterized. This thesis describes that 2 gene clusters involved in chromatin remodeling (i.e. *Mecp2, Ep300, Jarid1a*) and translational control (i.e. *Btg2, Paip2a*) are under the regulation of miR-132 in the SCN and coordinated regulation of these genes underlies miR132-dependent modulation of *mPeriod1* (*mPer1*) and *mPeriod2* (*mPer2*) and the light-entrainment process. I find that the *Period* genes are bound and transcriptionally modulated by MeCP2. In addition, *Paip2a* acts as a repressor of *Period* translation. This work further proposes that miR-132 is enriched for chromatin and translation-associated target genes-and, thus, miR-132 is an important orchestrator of chromatin remodeling and protein translation within the SCN clock, thereby fine-tuning clock entrainment.

ACKNOWLEDGEMENTS

Dr. Hai-Ying Mary Cheng, my supervisor, for guiding me through the chronobiology field and, very importantly, for financial support.

Dr. Odette Laneuville, the mediator of this thesis, for constant support through the final stages of this thesis.

Dr. David Lohnes, for advice and for being a constant member of my thesis advisory committee from the early stages of this work.

Members of the Cheng lab for discussion, in particular Dr. Reynaldo Oliva-Hernández for help with the mouse colony, tissue harvesting as well as for his friendship and Daniel Cornejo-Palma for help with quantitations and friendship.

Dr. Juan I. Young, my previous mentor, for introducing me into the epigenetics field, and for *Mecp2*$^{Floxed/y}$ mice. Many thanks for his friendship and for comments on the revised manuscript (circa March 2010) that arose from this thesis.

Dr. Karl Obrietan and Heather Dziema for mouse cannulations and antagomir infusions.

Dr. Carolina Perez-Iratxeta for bioinformatics analysis of microRNA-132 targets.

Drs. Nahum Sonenberg and Akiko Yanagiya for *Paip2a*$^{-/-}$ mice.

Dr. Zhaolan (Joe) Zhou for the anti-pS421 MeCP2 antibody.

Dr. David Weaver for anti-mPER2, anti-mCLOCK and anti-mBMAL1 antibodies.

Dr. Steven Reppert for anti-mPER1 antibody.

Dr. Luc Berthiaume for anti-GFP antibodies.

Dr. Berge Minassian for h-MeCP2-e1-myc vector

Dr. Hitoshi Okamura for pcDNA3-mPER1 and pBS-mPER2 vectors.

Dr. Emilio Lopéz-Vidriero, my close friend, for advice.

Dr. Rabih Kashouty, my dear friend, for always being there and for believing in me.

My family (Victoria, Felipe, Rodrigo & Matías Ignacio) for spiritual and financial support.

Sulman Caballero for her unconditional love and spiritual support.

My eternal gratitude to Dr. Linda Hsu, Professor Emeritus and my first scientific mentor, for having given me the opportunity to become a researcher during my undergraduate years at Seton Hall University.

TABLE OF CONTENTS

ABBREVIATIONS

AHR: Aryl Hydrocarbon Receptor
ARNT: Aryl Hydrocarbon Receptor Nuclear Translocator
AVP: Arginine Vasopressin
BMAL1: ARNT-Like Protein 1, Brain and Muscle
BTG2: B-Cell Translocation Gene 2
B-TRCP1: Beta-Transducin Repeat-Containing Protein
CAR: Calretinin
c-FOS: cellular Fos (Finkel-Biskis-Jinkins murine osteogenic sarcoma virus)
ChIP: Chromatin Immunoprecipitation
CK1δ: Casein Kinase 1 Delta
CK1□: Casein Kinase 1 Epsilon
CLOCK: Circadian Locomotor Output Cycles Kaput
CRE: Cyclic-AMP Response Element
CREB: c-AMP Response Element Binding Protein
CT: Circadian Time
DD: Dark:Dark
DICER: Helicase with RNA Motif, Drosophila Homolg
DOX: Doxycycline
dpc: days post-coitum
DROSHA: Nuclear Ribonuclease III, Drosophila Homolog
DSPS: Delayed Sleep-Phase Syndrome
ECFP: Enhanced Cyan Fluorescent Protein
ENK: Enkephalin
ENU: *N*-ethyl-*N*-nitrosourea
EP300: E1A-Binding Protein, 300kD
FASPS: Familial Advanced Sleep-Phase Syndrome
FBXL3: F-Box and Leucine-Rich Repeat Portein 3
GHT: Geniculohypothalamic Tract
GABA: γ-amino-butyric acid
GFP: Green Fluorescent Protein
GRP: Gastrin-Releasing Polypeptide
GTP: Guanosine Triphosphate
HAT: Histone Acetyltransferase
HDAC: Histone Deacetylase
H3: Histone 3
H3K4Me3: Trimethylated Histone 3 at Lysine 4
IGL: Intergeniculate Leaflet
ir: immunoreactivity
JARID1A: Jumonji AT-Rich Interactive Domain 1A
LacZ: β-galactosidase
LD: Light:Dark
LL: Light:Light
MAPK: Mitogen-Activating Protein Kinase

MECP2: Methyl-CpG-Binding Protein 2
MOP3: Member of PAS superfamily 3
miR-132: microRNA-132
miRNP: microRNA ribonucleoprotein
MRE: microRNA
mRNA: messenger RNA
N2A: Neuroblastoma 2A
NCOR1: Nuclear Receptor Corepressor 1
NMDA: N-Methyl-D-Aspartate
NR1D1: Nuclear Receptor Subfamily 1, group D, member 1
nt: nucleotide
NT: Neurotensin
PABP: PolyA-Binding Protein
PAC1: Pituitary Adenyl Cyclase Receptor 1
PACAP: Pituitary Adenyl Cyclase Activating Peptide
PAIP2A: polyadenylate-Binding Protein-Interacting Protein 2
p-ERK: phosphorylated ERK
PER1: PERIOD1
PER2: PERIOD2
PER3: PERIOD3
PEST: Proline-Glutamic Acid-Serine-Threonine
PKC: Protein Kinase C
PPAR: Perixosome Proliferator-Activated Receptor-Alpha
pre-miRNA: precursor-microRNA
pri-miRNA: primary-microRNA
qPCR: Quantitative Polymerase Chain Reaction
qRT-PCR: Quantitative Real-Time Polymerase Chain Reaction
RAR: Retinoic Acid Receptor
RAS: Rat Sarcoma (RAS superfamily of proteins)
RGC: Retinal Ganglion Cell
RHT: Retinohypothalamic Tract
RISC: RNA-Induced Silencing Complex
RNase: Ribonuclease
ROR: RAR-Related Orphan Receptor
RORC: RAR-related Orphan Receptor C
RT-qPCR: Reverse-Transcriptase Quantitative Polymerase Chain Reaction SCN: Suprachiasmatic Nucleus
SIM: Single-Minded, Drosophila Homolog
SACO: Serial Analysis of Chromatin Occupancy
SIRT1: Sirtuin 1
SP: Substance P
SS: Somatostatin
TIM: Timeless
TSS: Transcription Start Site UTR: Untranslated Region
VIP: Vasoactive Intestinal Peptide
WT: Wild-Type

ZT: *Zeitgeber* Time

INTRODUCTION

i. Principles of circadian rhythms

Most organisms on Earth have evolved to regulate their daily physiological activities to the rotation of the Earth, its revolution around the sun and the moon's revolution around the earth. As a consequence, terrestrial and marine organisms across phyla exhibit rhythmic behaviour in association with the daily alterations of light and darkness. These rhythms of behaviour have been defined by biologists as "circadian" rhythms, from the Latin *circa* meaning "about" and *dian* meaning "day" (circadian = about a day) due to their near 24-hour length (or 24-hour periodicity). In mammals, circadian rhythmicity is present in sleeping and feeding patterns as well as body temperature regulation, blood pressure, hormone secretion, cell regeneration and many other daily biological activities that are necessary for survival. From a sociological perspective, circadian rhythmicity regulates human social behaviour, having implications in human cognition and social health. Biologically, the circadian system plays a key role in the measurement and interpretation of day length, a phenomenon termed photoperiodism, that is, the physiological reaction of organisms to the length of day and/or night (1).

Mechanistically, circadian rhythms allow organisms to anticipate environmental changes and adapt their physiological needs accordingly. Interestingly, the physiological responses to day and night continue even when organisms are maintained in constant light (LL) or constant dark (DD) environments. In some organisms, these rhythmic behaviors persist for some time, while in others they persist indefinitely. Thus, by definition biological rhythms that continue to persist with a period of about a day (~24 hrs) are called circadian rhythms.

The first historical evidence for the existence of circadian rhythms has been attributed to the Greek philosopher Androsthenes of Thasus. He traveled through North Africa and India and observed the daily opening and nightly closing of the leaves of the tamarind tree (*Tamarindus indica*). He hypothesized that the daily rhythms of plant movements must be reactions to environmental signals, such as sunlight (2). Nevertheless, it was not until the 18th century A.D. that the French astronomer Jean-Jacques de Mairan provided the first evidence that circadian clocks are endogenous to organisms. De Marian reported in the plant *Mimosa pudica* that its leaves fold up along the midline during the night and open up during the day. Plants were then placed in constant darkness and the leaves still opened during the day and closed during the night (3,4). This observation indicated that leaf folding rhythms do not require daily rhythms of sunlight. Nevertheless, the existence of endogenous rhythmicity is not demonstrated by this observation, since they were speculated to be attributed to geophysical factors.

A few years later, the Swiss botanist Augustin Pyramus de Candolle, who also used the *Mimosa pudica* plant as a model organism, observed that the rhythms still persisted in constant illumination, similarly to de Mairan. However, he showed that the duration of the cycle (i.e. the period of the rhythm) was shorter than 24 hours (4,5). This observation suggested that the machinery (i.e. the clock) responsible for the length of the period must reside within the plant and cannot be attributed to an outside geophysical factor. Hence, Candolle elegantly provided the first evidence suggesting the existence of an endogenous circadian clock. It was many years later that the location, genetics and molecular machinery of this clock were discovered.

Circadian rhythms are defined via three key properties: I) they are endogenous, that is, they are able to persist even in the absence of environmental cues and have a periodicity of ~24-hours (under these conditions, they are said to be "free-running"); II) they can be synchronized and reset by environmental cues; and III) they are temperature compensated. On Earth, the most potent and predominant cue that resets the clock is light (i.e. sunlight).

The field of *chronobiology* (i.e. the study of biological timing) rapidly expanded in the 1950s through the novel experimental paradigms and discoveries of the three fathers of chronobiology, Jürgen Aschoff, Colin Pittendrigh and Franz Halberg. Dr. Aschoff designated the term *zeitgeber* (German for "timegiver") to denote a periodic environmental signal that resets or synchronizes the time of a circadian rhythm (4). The process of entrainment is defined as a synchronization of two or more rhythmic cycles. Since circadian rhythms are synchronized to environmental cues (light being the most potent), chronobiologists refer to time as defined by these environmental cues, hence calling it *zeitgeber time,* or ZT (also referred to in experimental paradigms as circadian time, or CT). A change in the timing of the *zeitgeber*, results in a shift of the phase of the rhythm. For example, in nocturnal rodents, a light stimulus in the early night (e.g. CT15) induces a phase delay, that is the clock "delays" its time for the subsequent cycles in order to adjust itself to the new *zeitgeber.* Conversely, a light stimulus in the late night (e.g. CT22) induced a phase advance which makes the clock "advance" its time for the subsequent cycles. In the laboratory, light-induced phase shifts are paradigms used to measure the responsiveness and sensitivity of circadian clocks.

ii. Genetic basis for circadian rhythmicity

In the 1930s, Kalmus and Bunning demonstrated that *Drosophila* possess a circadian rhythm of eclosion (i.e. the emergence of an adult fly from its pupal case; 6,7). Subsequently, *Drosophila pseudoobscura* and *Drosophila melanogaster* were used as the primary model organisms to study circadian rhythms. In 1971, Ronald Konopka and Seymour Benzer isolated the first single-gene "clock" mutants in *Drosophila melanogaster* (8). These fly models trigerred the genetic analysis of clock mechanisms. In this report, they describe three different mutations induced by ethyl methane sulfonate treatment, in which the 24-hr rhythms of eclosion and locomotor activity were drastically changed. One mutant was arrhythmic; another had a period of 19 hrs; and the third had a period of 28 hrs. Hence, the authors concluded that because the period of the rhythm under constant conditions is altered, then the mutations must be affecting the basic oscillator. This report is the first to describe a genetic basis for circadian rhythmicity and coined the name *"Period"* gene (8).

With the rapid expansion of the molecular genetics field at the time, it became possible to isolate some of the genes involved in the regulation of circadian rhythms of *Drosphila,* such as *dPeriod (dPer), dDoubletime (dDbt)* and *Timeless (dTim).* Therefore, the combination of molecular genetics and biochemical tools in flies led to more profound understanding of clock mechanisms. Fortunately for biologists, the mammalian clock shares many of the genes involved in circadian rhythmicity (with broad sequence conservation) to the genes used by the *Drosophila* clock. Therefore, many of the mechanistic models derived from *Drosophila* have been adapted to the mammalian clock, and later experimentally validated.

In 1988, the first description of a single-gene mutation that specifically alters the circadian rhythms in a mammalian species was reported (9). The *tau* hamster, named so because the mutation affects the period (the period is also referred to as *tau* by chronobiologists) of locomotor running-wheel rhythms, has a drastically reduced *tau.* Hamsters heterozygote for the *tau* allele have a period of ~22 hrs, whereas hamsters homozygous for the mutated allele have a period of ~20 hrs, opposed to the wild-type (WT) hamsters with a period of ~24 hrs. Many years later, it was shown that the *tau* locus corresponds to the *Casein Kinase 1ε* (*CK1ε*) gene, involved in the phosphorylation-dependent degradation of the PERIOD proteins (10).

In 1997, two reports provided evidence for the existence of the mammalian homolog of the *dPer* gene, via sequence homology to the bHLH-PAS (basic helix-loop-helix; PER-ARNT-SIM) domain of the fly protein (11,12). These reports show that the mammalian *Period* transcript (later designated as *Period1*) shows robust 24-hr rhythms in the suprachiasmatic nucleus of the hypothalamus and the retina and is also highly expressed in other brain regions. A few months later, a second mammalian homolog of the *dPer* gene was characterized and designated *Period2 (Per2*; 13,14). In conjunction, these reports show that both *Per1* and *Per2* transcripts have a ~24-hr periodicity in the SCN and that *Per1* is induced throughout the night, whereas *Per2* is phase-restricted and is only induced in the early night. Also in 1997, another bHLH-PAS domain-containing protein was discovered and designated CLOCK (Circadian Locomotor Output Cycles Kaput; 15). Via random *n*-ethyl-*n*-nitrosurea (ENU) mutagenesis in the mouse, the authors show that the *in-vivo* mutation affects at least two fundamental properties of the circadian system: 1) the length of the free-running period; and 2) the persistence of

circadian rhythmicity in constant darkness (15). This is the first report demonstrating that a single-gene mutation alters the circadian locomotor activity rhythms of the mouse. With the major discoveries and advances in the field of homologous recombination in mouse embryonic stem cells in the 1990s, many of the mammalian genes involved in circadian regulation were discovered and characterized, hence providing mechanistic evidence for the molecular mechanisms of the mammalian circadian clock (further detail will be provided in the "*SCN molecular genetics*" section).

Interestingly, the "eukaryotic-only" dogma of circadian clocks was not challenged until 1993, when the simplest form of a circadian clock was elegantly shown in the prokaryote *Synechococcus elongatus* (cyanobacteria) using a luciferase reporter transgene in the *psbAI* gene (16) . This report shows that cyanobacteria possess the three key properties of circadian clocks: 1) persistence in constant conditions with a period near 24-hrs; 2) phase resetting by light/dark signals (i.e. entrainment); and 3) temperature compensation of the period. Currently, it is recognized that most organisms on earth possess circadian timekeeping systems, ranging from cyanobacteria and fungi to plants, worms, flies, and mammals.

iii. Organization of the circadian system

a. The suprachiasmatic nucleus, the master pacemaker

The suprachiasmatic nucleus (SCN) of the anterior hypothalamus is the dominant pacemaker in the mammalian brain controlling a wide variety of physiological processes, including endocrine functions, hence providing a strong foundation for the appropriate elaboration and coordination of mammalian physiology. The role of the SCN in circadian function was not elucidated until the 1970s when various studies established that SCN

lesions resulte in the abnormal phenotypic expression or complete loss of circadian function (17-19). Subsequent neuronal firing studies *in vivo* (20,21) and *in vitro* (22) provided evidence that SCN neurons function in an unimodal fashion to provide rhythmicity to other brain areas. Nevertheless, it was not until the seminal work of Michael Menaker and colleagues in 1990 that the SCN was unequivocally shown to be the master locus of circadian rhythms in mammals (23). The authors performed neural transplantation experiments and showed that small neural grafts from the suprachiasmatic region restored circadian rhythms of locomotor activity to arrhythmic animals whose SCN had been previously lesioned (23). Most importantly, this report shows that the restored rhythms always exhibited the period of the donor genotype regardless of the host's genotype.

Mechanistically, a basic circadian system has a minimum of three main components, including photoreceptors, a pacemaker and a rhythmic output. The entrainment pathways transduce information between the photoreceptive elements and the pacemaker. In turn, the coupling pathways (i.e. the efferent pathways) are necessary as a link between the pacemaker and the multiple effectors. Hence, the effector outputs are the overt rhythms of behaviour that allow chronobiologists to study the properties of the central pacemaker (e.g. locomotor rhythms controlled via the SCN). Nevertheless, there may be multiple photoreceptors, clocks or overt rhythms. In fact, evidence suggests that each mammalian organ has a clock, but all are tightly governed from the SCN via endocrine communication (see 24 for review). Therefore, it is assumed that these components may interact in a variety of ways.

b. The retinohypothalamic tract

In 1991, Foster, Provencio and Menaker reported non-rod, non-cone photoreceptor perikarya that were immunoreactive for cone opsins in the eyes of retinally-degenerated mice. They classified it as an unrecognized class of photoreceptive cell type within the mammalian retina and cleverly showed that they were involved in the mediation of circadian rhythmicity (25). In 1998, Provencio and colleagues identified these perikarya as a class of retinal ganglion cells (RGCs) sparsely distributed throughout the retina, similar to the type III glanglion cells of the rat, that project monosynaptically to the SCN (Figure 1; 26). The authors proposed these cells to be specialized retinal ganglion cells involved in the integration of environmental irradiance without compromising the spatial resolution required for vision (26). Then, in 2002, Provencio and colleagues reported that these specialized retinal ganglion cells form a photoreceptive "net" in the mouse inner retina and express the photopigment melatonin (27). A few months later, Berson and Yau confirmed these findings in mouse and human tissue (28,29).

c. *Light-induced clock entrainment*

The RHT is responsible for transducing photic information from the eyes to SCN neurons (Figure 1). Several studies have shown that lights triggers the pre-synaptic release of glutamate and pituitary adenylate cyclase activating peptide (PACAP) from RHT nerve terminals, resulting in postsynaptic activation of ionotropic N-methyl-D-aspartate (NMDA) receptors and PACAP type 1 (PAC1) receptors, respectively (Figure 1; 30-32). In turn, these excitatory signals activate various kinase signaling pathways, such as the p42/p44 Mitogen-Activated Protein Kinase (MAPK) and Protein Kinase C (PKC) pathways, amongst others (33-35). A large body of evidence indicates that activation of the MAPK pathway and CREB-dependent transcription following exposure to a resetting

FIGURE 1

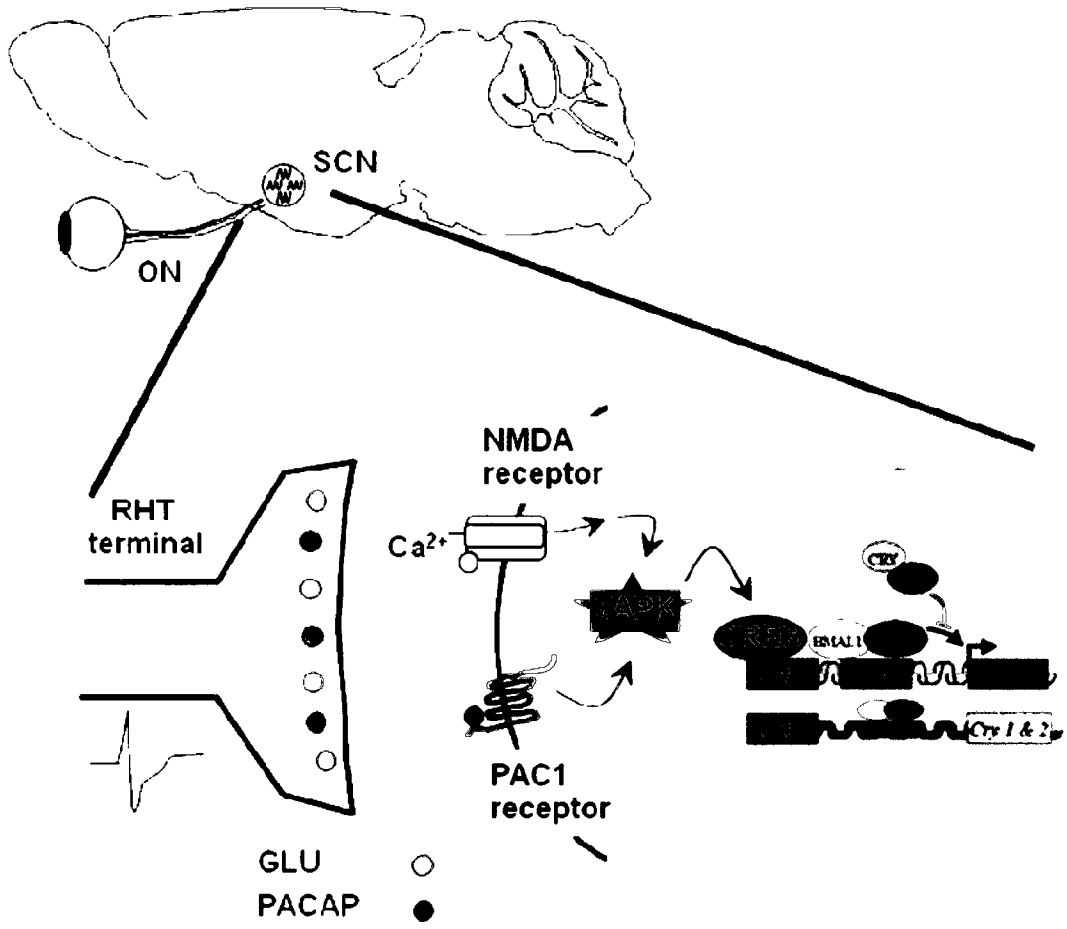

Figure 1. Cellular mechanisms that underlie photic entrainment of the circadian clock.

A light stimulus activates specialized retinal ganglion cells in the eye, which send their projections to the suprachiasmatic nuclei (SCN) via a branch of the optic nerve (ON) known as the retinohypothalamic tract (RHT). RHT nerve terminals co-store the neurotransmitter, glutamate (GLU, yellow circles) and the neuropeptide pituitary adenylate cyclase activating peptide (PACAP, blue circles). Activity-dependent release of GLU and PACAP from RHT terminals triggers post-synaptic activation of NMDA and PAC1 receptors, respectively, in the SCN. Receptor stimulation leads to the activation of a number of intracellular signaling cascades, most notably the p42/p44 mitogen-activated protein kinase (MAPK) pathway. MAPK activation is coupled to CREB activation, which induces the transcription of immediate early genes (such as *c-fos*) as well as the *Per1* and *Per2* genes. Light-induced *Per1* and *Per2* expression, accompanies (and mediates) light-induced phase shifts of behavioural rhythms in various mammalian species. Diagram and legend taken with permission from Dr. Hai-Ying Mary Cheng's 2010 CIHR grant.

light pulse during the subjective night are required for light-induced clock resetting (33). Moreover, a number of core clock genes (including *Per1* and *Per2*) possess CRE sites in their promoter regions and are potential targets of light-induced activation by CREB. In summary, light triggers activation of gene transcription, immediate early gene expression and cAMP response element binding protein (CREB)-dependent signaling, amongst others, resulting in the final induction of the *per1* and *per2* genes, which may be regarded as key modulator proteins of the rhythmically based light-entrainment process (Figure 1 & Figure 2; 36-38).

d. SCN neuroanatomy

In the mouse, the SCN is composed of ~20,000 neurons (~10,000 neurons per nucleus), divided into two nuclei via the third ventricle and positioned on top of the optic chiasm (Figure 3; 39-40). The SCN arises from the ventral diencephalon germinal epithelium as a component of periventricular cell bodies (40,41). In rodents, the SCN first appears in the anterior hypothalamus as a small cluster of compacted neurons dorsal to the optic chiasm (40,41). It expands caudally and is medially divided by a thin lamina of periventricular hypothalamic neurons.

It is now understood that the SCN is composed of two functional subdivisions, designated the *core* and the *shell* (43). The shell surrounds the core, which sits on top of the optic chiasm (Figure 1B). SCN core neurons predominantly express VIP or GRP, and smaller populations express NT or SP. Today it is widely accepted that RHT terminals projecting onto the SCN are exclusively in the core, overlapping VIP and GRP immunoreactive cells.

FIGURE 2

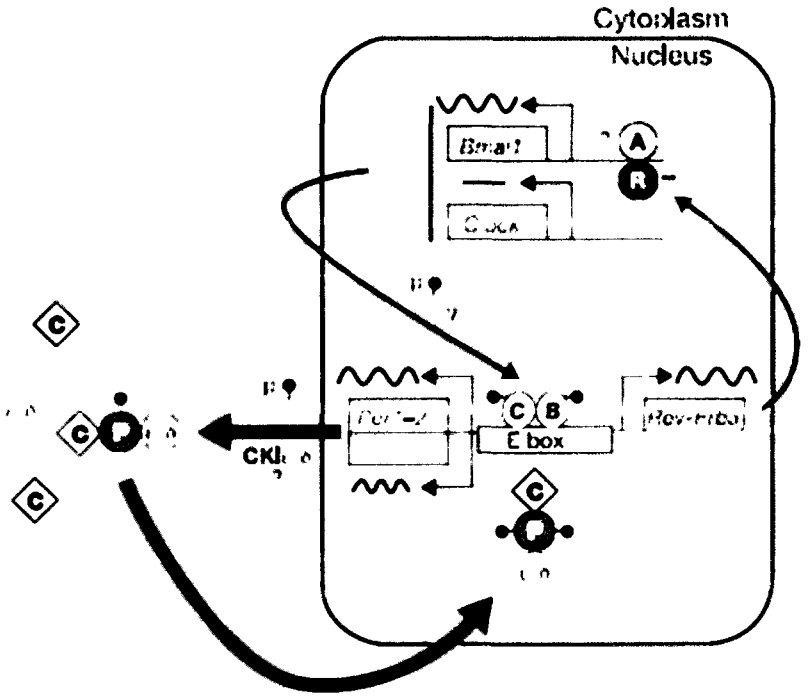

Figure 2. The mammalian circadian machinery is regulated via transcriptional/translational negative and positive feedback loops.
A simplified model of the mammalian clockwork machinery. Mechanistically, the clock is composed of negative (red arrows) and positive (green arrows) feedback loops. CLOCK (C, yellow circle) and BMAL1 (B, yellow circle) proteins heterodimerize and drive the transcriptional activation of *Per, Cry* and *Rev-erbα* genes through E-box sequences. PER (P, blue circles) proteins accumulate in the cytoplasm and bind to CRY proteins (C, orange diamond) which are then phosphorylated (small p) by CK1ε and CK1δ complexes (ε/δ white circles). Within the nucleus, CRY-PER-CK1 ε/δ complexes interact with CLOCK/BMAL1 heterodimers to inhibit transcription, resulting in a negative feedback loop of regulation. On the positive arm, REV-ERBα (R, red circle) proteins interact with *Bmal1* regulatory elements to inhibit *Bmal1* transcription. Furthermore, CRY-mediated inhibition of CLOCK/BMAL1-mediated transcription results in the activation of *Bmal1* transcription, due to inhibition of REV-ERBα-mediated repression. It is also hypothesized that an activator protein (A, grey circle) may be involved in the positive regulation of *Bmal1* transcription (?). Recent work has also identified that the B-TrCP1 and FBXL3 E3 ubiquitin ligase complexes target PER and CRY proteins for degradation (not shown; 76-77). Figure taken with permission from reference 197 (see appendix II).

FIGURE 3

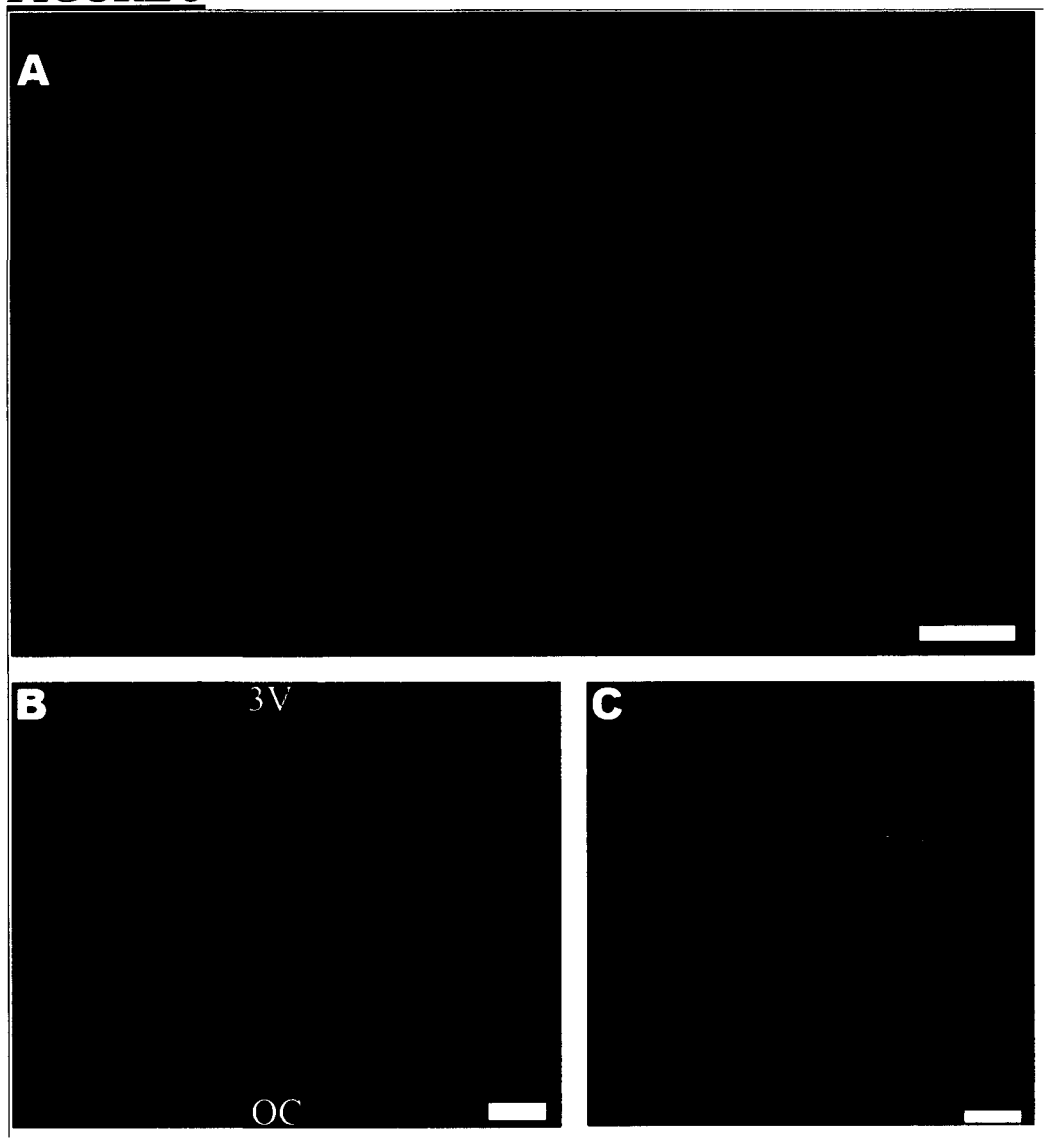

Figure 3. The suprachiasmatic nucleus is the master pacemaker.
(A) Coronal indirect ECFP immunoflurorescence in order to visualize the SCN and forebrain regions in a miR-132 transgenic mouse brain. **(B)** Higher power (20X) magnification of the SCN from the same brain section (boxed region in (A)). Note the bilateral nature of the SCN. **(C)** Merged DsRED (red) expression driven by the *mPer2* promoter (146) and DAPI (blue) to visualize the sagittal SCN in the adult mouse brain. (A) scale bar = 1mm; (B-C) scale bar = 50μm. 3V: third ventricle; OC: optic chiasm. All images captured via confocal microscopy on a single focal plane. HYMC designed and generated the miR-132 and *mPer2*-DsRED transgenic mice at Ohio State University. Tissue harvesting performed jointly by MAS & HYMC. Confocal imaging, compilation of images and figure design performed by MAS.

Furthermore, the intergeniculate leaftlet (IGL) has been shown to project onto the SCN via the geniculohypothalamic tract (GHT). The median raphe nucleus also projects onto the SCN (50) and dense afferents to the shell also arise from other hypothalamic nuclei, as well as the paraventricular nucleus, basal forebrain, limbic cortex, septal area and brainstem (50). The SCN projects efferently onto the hypothalamus, basal forebrain, midline thalamus, IGL and periaqueductal gray (51). Retrograde experiments have elegantly shown that these efferent projections arise differentially from the core and the shell subdivisions (51-53). Current evidence suggests that the SCN functions via the coupling of individual neuronal oscillators to form a network that serves as the pillar of the pacemaker. Current research in various laboratories investigates whether there are specific SCN neuronal subsets responsible for this coupling function.

iv. SCN molecular genetics

a. The PAS domain

The PAS (PER-ARNT-SIM) domain is found in a vast number of proteins. The term PAS arose from the first letter of each of the three founding members of the family: **P**eriod (PER), the product of the *dPer* gene; the AHR (aryl hydrocarbon receptor) nuclear translocator (**A**RNT), originally identified as a protein essential for signal transduction by the AHR; and the *Drosophila Single-minded* locus (**S**IM), a regulator of midline cell lineage (55-58). The PAS domain may be briefly described as a region of homology to these three founding member. It contains 250-300 amino acids and a pair of highly degenerate 50 amino acids subdomains defined as the A and B repeats (56-58). Biologically, the PAS domain has been characterized as a signature of proteins involved in environmental adaptation and cell signaling via protein-protein interaction modules.

Interestingly, The PAS domain is highly conserved in the molecules that regulate circadian rhythmicity. Invertebrates and vertebrates employ orthologues of a number of PAS proteins to regulate transcription of circadian rhythms.

The first PAS protein identified was the product of the Drosophila *Period (dPer)* locus. It is interesting to note that one of the original mutations described in the *Per* locus of *Drosophila* ($dPer_1$) resides within the PAS domain, whereas the other two mutations reside immediately adjacent to the C-terminal of the PAS domain (7,54,55). It has been shown that the PAS domain of PER can act as a dimerization surface to support interactions with other PAS domain-containing proteins (59). Furthermore, it was shown that constitutive overexpression of PER inhibited the cycling of its own mRNA (60), hence leading to the hypothesis that PER was a dominant-negative inhibitor of its own transcription, most likely by inhibiting another bHLH-PAS protein pair (61).This model of regulation is now defined to be a transcription-translation negative-feedback loop that drives the rhythmic expression of the PERIOD proteins (and CRY proteins; 64), as well as other components, that in unison regulate the circadian behaviour of mammalian organisms (Figure 2; 59,62-64).

b. The E-box motif

A key observation that allowed for the decoding of the circadian clock pathway was the discovery that a 69-bp region upstream of the *dPer* promoter was sufficient to drive the *in-vivo* cycling of heterologous reporters in flies (65). Further sequence analysis revealed that an element harboring the E-box core sequence CACGTG was necessary for the robust cycling amplitude (65). These observations were consistent with the hypothesis that the PER protein acts as an inhibitor of a CLOCK-bHLH-PAS heterodimer in both

Drosophila and mammals. Using two-hybrid screens, it was later determined that a heterodimer was formed between the mammalian MOP3 (Member of PAS superfamily 3; also known as ARNTL1 or BMAL1) and CLOCK proteins *in-vivo* (61,63,66). *Drosophila* homologues for these two proteins were also identified in screens for circadian rhythm mutants (67,68). Moreover, mutations in the *dCycle* and *dClock* loci were shown to result in a significant decrease in the expression of both PER and TIM, and both mutations resulted in arrhythmia as homozygous alleles (67,68). Sequence analysis of these two loci indicated that they were orthologues of mammalian *Mop3* and *Clock*, respectively. In summary, all of these reports provided the biochemical and genetic evidence that *Mop3* and *Clock* (*Cycle* in *Drosophila*) were key components of the circadian clock in various species and that the mammalian and fly circadian core mechanism is functionally similar.

In 1998, it was demonstrated that the E-Box element motif was also present in the mammalian *Per1* promoter and that the CLOCK/MOP3 heterodimer was capable of driving transcription of luciferase promoters harboring this motif (66). It was also demonstrated that *dClock* activates *dPer* transcription through sequences harboring the E-box motif (63). In addition, it was also demonstrated that PER and TIM could inhibit CLOCK/CYCLE-induced transcription of their own messages (63). As a group, these reports support the feedback inhibition model of the PER proteins and provide a role for two additional b-HLH-PAS containing proteins in the regulation of circadian rhythmicity in flies, mice and humans.

c. The molecular clock

The circadian clock mechanism involves a cell-autonomous transcription-translation feedback loop composed of core genes that are highly conserved amongst animals (Figure 2; see 69 for review). In mammals, the circadian clock is composed of a primary negative-feedback loop involving the genes *Clock* and its paralogue *Npas2* (Neuronal PAS domain protein 2), *Bmal1* (ARNTL-Like protein 1, Brain and Muscle; also known as aryl hydrocarbon receptor nuclear translocator-like [*Arntl]*), *Per1, Per2, Cry1* (Cryptochrome 1) and *Cry2* (Cryptochrome 2). During daytime, the bHLH-PAS domain-containing transcription factor CLOCK (or NPAS2) interacts with BMAL1 to activate transcription of the *Per* and *Cry* genes, resulting in accumulation of these transcripts. The mammalian CRY proteins have been characterized as interaction partners with the PER proteins and involved in nuclear translocation (64). Once translated, PER and CRY proteins heterodimerize and translocate into the nucleus, where they interact with CLOCK/BMAL1 heterodimers to inhibit their own transcription (71). During nighttime, the PER-CRY repressor complex is degraded, and the CLOCK/BMAL1 heterodimer can then activate a new round of transcription. This cycle has a periodicity of ~24-hrs. In addition to this primary feedback loop, there is a second negative-feedback loop that involves the nuclear hormone receptor *Rev-erbα*, a direct target of CLOCK/BMAL1, which has been shown to strongly repress *Bmal1* transcription (72). It has been hypothesized that this secondary loops adds robustness to the molecular clock, since is not essential for circadian rhythm generation in mice (72).

Recent studies have shown that post-translational modifications and degradation of clock proteins also play roles in the regulation of circadian rhythmicity (73). PER1 and PER2 proteins are progressively phosphorylated as they accumulate during the late

afternoon as well as night by Casein Kinase 1 delta (*CK1δ*) and Casein Kinase 1 epsilon (*CK1ε*) (74). One of the roles for phosphorylation of the PER proteins is to target them for polyubiquitylation and degradation by the 26S proteosomal pathway (75). In addition, *in-vitro* studies have suggested that β-TrCP1 (beta-Transducin repeat-Containing Protein 1) and FBXL3 (F-Box and Leucine-rich repeat protein 3) E3 ubiquitin ligase complexes directly target the PER and CRY proteins, respectively, for degradation (76,77). These results have been confirmed in *Fbxl3* mutant mice that have a long-period circadian phenotype, due to a defect in targeting CRY1 and CRY2 for degradation (78,79).

Furthermore, a recent study has shown that circadian transcription of CLOCK/BMAL1 target genes is accompanied by circadian changes in Histone 3 (H3) acetylation and chromatin remodeling (80). It has also been shown that circadian transcription of the mouse D-site albumin promoter Binding Protein (*Dbp*) gene is accompanied by rhythmic binding of CLOCK/BMAL1 to E-box *cis*-regulatory elements, acetylation of H3 at lysine 9, trimethylation of H3 at lysine 4 and a reduction in histone density (81). In addition, the CLOCK protein has recently been shown to have histone acetyltransferase (HAT) activity and can acetylate its partner, BMAL1 (82,83). Moreover, the histone deacetylase Sirtuin 1 (SIRT1) interacts with CLOCK and can deacetylate BMAL1 as well as H3 at lysine 9 and 14 (84). *Sirt1* has also been shown to be expressed in a circadian fashion in the liver and regulates the circadian expression of *Bmal1, Rorc* (RAR-related orphan receptor gamma), *Per2* and *Cry1* through interactions with CLOCK/BMAL1 and via deacetylation and degradation of PER2 (85). The cumulative data suggest that the core clock autoregulatory feedback loops as well as its downstream targets are tightly regulated via rapid biochemical kinetics of chromatin

remodeling and translational control events. The responsive nature of the SCN provides an exemplary model to study these events. The precise biochemical kinetics of these molecular interactions remains to be determined.

d. Human genetics

The daily cycle of sleep and wakefulness is a key circadian rhythm of behaviour in humans. Sleep regulation has been hypothesized to be regulated via two processes: 1) a sleep homeostatic process that regulates the rise of sleep propensity during wakefulness and its dissipation during sleep; and 2) a circadian process that determines the change between sleep and wakefulness (86). A wide variety of sleep disorders have been identified in humans and have been linked to circadian alterations in the timing of sleep. These disorders include, but are not limited to, familial advanced sleep-phase syndrome (FASPS), delayed sleep phase syndrome (DSPD), non-24-hour sleep-wake syndrome and irregular sleep-wake pattern (87-89).

Currently, FASPS in the only established Mendelian-inherited circadian rhythms disorder in humans (88,89). FASPS is inherited in an autosomal dominant fashion and is characterized by persistent 3-4 hour advanced sleep onsets and awakening times relative to conventional schedules (88,89). FASPS is thought to arise from an abnormal phase of the circadian cycle relative to the desired sleep-wake schedule. Interestingly, Toh and colleagues found that a missense mutation in human *PER2* co-segregated with FASPS and found that the mutation occurs in a phosphorylation site within a CK1-binding domain of PER2 (90). In addition, Xu and colleagues identified a mutation in *CK1δ* in FASPS patients (91). These two mutations are important examples in how core circadian clock gene-associated mutations may lead to a circadian phenotype, affecting human

health. Furthermore, a related condition known as delayed sleep phase syndrome has been associated with a polymorphism in the human PERIOD3 gene, in which patients suffer from sleep-onset insomnias (92). In summary, the molecular insights on core clock mechanisms gathered over the past few decades have to be put into the context of human physiology, thereby allowing an effective application and possible treatments of circadian mechanisms onto real life.

v. Chromatin remodeling and translational control of the clock

Chromatin remodeling is defined as the process of disruption and re-assembly of histone–DNA interactions. The epigenetics field emerged from the observations that chromatin can be altered by covalently modifying histone proteins. These modifications include phosphorylation, ubiquitination, ADP-ribosylation, methylation and acetylation (93,94). The effect of chromatin remodeling is dependent on the context of nucleosomes at a given promoter and can result in 1) transcriptional activation or (2) transcriptional repression. Various epigenetic mechanisms that alter the architecture of chromatin, for example, DNA methylation and histone modification, have been implicated in clock timing processes. The rhythms of *Per* and *Cry* expression in the liver coincide with rhythmic H3 acetylation (considered a mark of active transcription) at their gene promoters (80). CLOCK has been demonstrated to possess histone acetyltransferase activity (95). EZH2, a polycomb group protein with histone methyltransferase activity, interacts with CLOCK-BMAL1 complexes and is recruited to the *mPer1* and *mPer2* promoters, where it catalyzes the methylation of histone H3 at lysine 27, considered a mark of transcriptional repression (155). Most recently, it has also been shown that NCOR1 (Nuclear receptor Corepressor 1) and HDAC3 (Histone Deacetylase 3) interact

in order to regulate oscillatory metabolic gene transcription (96).

Cells also regulate gene expression via translational control. This level of regulation provides a rapid response to growth and proliferation stimuli and plays a key role in controlling feedback mechanisms in the cell. For example, in systems with little or no transcriptional control (e.g. reticulocytes and oocytes) (97), translation is the predominant key regulator of gene expression. Recent studies highlight the importance of mechanisms that influence the steady-state levels of proteins in the control of the circadian clock. For example, phosphorylation of PER1 and PER2 by CKIε results in targeting of the PER proteins by ßTrCP, an F-box protein that comprises the SCF (Skp1-Cul1-F-box protein) ubiquitin ligase, to the ubiquitin-proteasome degradation pathway (76,98). On the other hand, mechanisms that regulate *de novo* protein synthesis are also likely to influence circadian clock processes since expression of nocturnin, a deadenylase that controls mRNA decay by shortening of the poly(A) tail, is rhythmic in multiple murine tissues and is induced by mitogenic signals (99). Additionally, the mTOR signaling pathway, a key regulator of translation, has also been shown to be activated by light in the SCN (100), suggesting an important role of translational regulation in photic entrainment.

vi. microRNAs and the clock

a. microRNA biogenesis

Many primary-miRNA (pri-miRNA) transcripts have been cloned and characterized (119-121). The current consensus is that all of pri-miRNA transcripts are capped and polyadenylated and are hence transcribed by RNA polymerase II and share structural and mechanistic properties with messenger RNA (mRNA). pri-miRNAs are processed into

hairpin precursors designated pre-miRNA and then into mature miRNAs. Mature miRNAs are then loaded into an effector complex that impacts target gene expression via mRNA cleavage, translational repression or both (101-104).

pri-miRNA processing is catalyzed by two RNAseIII enzymes, Drosha and Dicer. These enzymes are highly conserved among all phyla and have been shown to be dsRNA-specific and to regulate RNA metabolism. Drosha is thought to be involved in protein-protein interactions as well as RNA-binding and cleaves pri-miRNAs to pre-miRNAs of ~60-nucleotides. DGCR8, a protein containing two dsRNA-binding domains (dsRBD) and a WW domain, is also necessary for pri-miRNA processing and interacts with Drosha in the microprocessor complex (102-104). pre-miRNA transport from the nucleus to the cytoplasm is mediated by exportin-5 in a Ran-GTP (Ras-related Nuclear protein-Guanosine-5'-Triphosphate) dependent manner (105-108). Cytoplasmic Dicer is then responsible for cleaving the loop sequence of the pre-miRNA yielding the mature miRNA duplex. Subsequently, the mature single-stranded miRNAs are loaded into effector complexes designated as miRNP (miRNA ribonucleoprotein) and RISC (RNA-induced silencing complex) complexes. Dicer has a helicase domain and may be involved in mature miRNA duplex unwinding, although it has not yet been demonstrated experimentally. The incorporation of one of the strands of the duplex into RISC is not random and has been hypothesized to be regulated by the free energy between the two ends of the duplex. Whichever strand presents the weaker base-pairing on the 5'-end is thought to be loaded onto RISC and the other strand degraded (109,110). Once loaded, a single-stranded small RNA guides distinct modes of silencing (see 111 for review).

b. microRNA regulatory functions

miRNA function has been primarily based on the original findings of *let-7* and *lin-4* guided silencing in *C. elegans* (112-118). Mature miRNAs bind to the 3'-UTR (untranslated region) of their target mRNAs with imperfect complementarity leading to translation repression. Therefore, it is widely accepted that miRNAs are gene regulators (or as this thesis will define, modulators or orchestrators) that base-pair to their target mRNAs.

Since the first publications of miRNA sequences (119-121), target identification has been the most challenging problem in the miRNA field and researchers have developed *in-silico* approaches to identify these interactions, which then need to be validated in cell culture or animal models in order to elucidate their biological significance. Bioinformatics tools have been developed that are based upon the following criteria: 1) miRNA binding sites are mainly located within the 3'-UTR of target mRNA; 2) base-pairing to the target is asymmetrically weighted along the miRNA, since it has been shown that perfect base-pairing on the miRNA 5'-end is crucial for the ability of the miRNA to repress a target and that G:U wobble base-pairing disrupts this regulation (122-125); and 3) miRNA binding sites are conserved among orthologous genes of different species and the conservation criteria reduces the predicted number of false positive predicted targets (126-129).

It is interesting to highlight that the targets and biological functions of only a small number of miRNAs have been elucidated experimentally in model organisms. Furthermore, most studies report the identification of only one or a few targets per miRNA and fail to observe target regulation in a broader, tissue-specific physiological content.

c. *microRNAs in chronobiology*

In summary, genetic studies have established that circadian rhythms are generated by cellular oscillators that drive rhythmic expression of core clock genes via a series of interlocked positive and negative transcriptional-translational feedback loops. Clock timing processes have also been shown to be regulated at the post-translational level. Most recently, a few reports have provided evidence that a new level of regulation of the biological timing process exists, that is, translational control via miRNA regulation (130, 131).

Via serial analysis of chromatin occupancy (SACO) of miRNAs that target CREB, Cheng and colleagues identified miR-132 and miR-219 as being bound to *Creb* (130, 132). The authors further showed that miR-219 physically interacts with *Clock* nd that it is transcriptionally activated by CLOCK/BMAL1 heterodimers. On the other hand, miR-132 is activated by CREB. They further mapped 5' CRE sites at both miRNA gene loci and an additional E-box motif in miR-219. In this same report, they provide *in-vivo* evidence that mature miR-219 exhibits robust circadian rhythmicity, whereas mature miR-132 is strongly induced by nocturnal light exposure in the SCN. Behaviourally, silencing of endogenous miR-132 in the SCN via intracerebroventricular infusions of synthetic antagomirs enhanced light-induced clock resetting, whereas circadian period length is increased upon miR-219 silencing. Nevertheless, the downstream *in-vivo* targets that miR-132 and miR-219 regulate and their role in circadian biology have not yet been elucidated.

For peripheral oscillators, miR-122, a hepatocyte-specific miRNA, has been shown to be expressed in a circadian manner in the mouse liver. It was further shown that

miR-122 was transcriptionally regulated by *Rev-erbα*. Moreover, *Smarcd1l/Baf60a,* a component of the SWI/SNF chromatin remodeling complex, was identified as a direct miR-122 target. It was further shown that the Pparβ/δ protein was upregulated upon miR-122 silencing in the liver. The authors proposed that miR-122 interacts with perixosome proliferator-activated receptors (PPARs) to coordinate hepatic lipid metabolism (131).

RATIONALE & HYPOTHESIS

It is estimated that up to one-third of mammalian genes are regulated by miRNAs and that our genome encodes hundreds of miRNAs which are likely to regulate thousands of genes (133,134). Many brain-specific miRNAs have been cloned and sequenced, but their gene targets and function in neural physiology remain unknown (135-141). miR-132 has recently been shown to be involved in the SCN-modulated light-entrainment process (130). Nevertheless, the downstream targets that miR-132 regulates and their roles in the clock entrainment process have not yet been elucidated.

Using an array of mouse transgenic technology, bioinformatics, biochemistry, molecular biology, cell culture, *in-vivo* knockdown and confocal imaging, I have identified five *in-vivo* targets of miR-132 and validated their predicted 3'-UTR microRNA-response elements (MREs). Furthermore, via photic behavioural paradigms combined with molecular biology and biochemistry, the roles of these targets in the light-induced clock entrainment process were elucidated. Via a bioinformatics approach, I further show that miR-132 preferentially targets genes involved in chromatin remodeling- and translational control-associated functions. This study provides a novel paradigm in miR-132-dependent regulation of circadian clock entrainment, in which miR-132 fine-tunes the expression of gene clusters involved in chromatin remodeling and translation control. I further propose a model supported by the data presented in this thesis in which light induces a cascade of molecular waves that lead to tightly coordinated intracellular events that in unison function to ensure optimal light-entrainment of the mammalian circadian clock. In this model, miR-132 is light-activated in order to serve a fundamental role in the direct post-transcriptional regulation of light-activated transcripts, such as

Mecp2, Paip2 and Btg2, which in turn modulate light-activated *Per1* and *Per2* gene expression. I further hypothesize that the ability of one miRNA to fine-tune the expression of functionally related genes is not confined to miR-132, but that miRNAs in general are present in genomes to orchestrate gene expression. This is supported by the evidence of this thesis showing that miR-132 regulates specific gene clusters, i.e. chromatin remodeling- and translational control-associated genes. Future studies will undoubtedly identify novel gene clusters that are under the regulation of other miRNAs and whether these processes may be regulated via a single miRNA and/or as functional miRNA clusters.

MATERIALS & METHODS

(Some of the methodology section has been adapted from the manuscript Alvarez-Saavedra et al, circa November 2009).

Generation of ECFP-pBI-pre-miR132 transgene construct

The following steps were taken to generate the ECFP-pBI-pre-miR132 construct (generated by Dr. Hai-Ying Mary Cheng). First, the XbaI site (position 7705) of the pBI-G Tet vector (Clontech, Mountain View, CA) was mutagenized to a NheI using the QuickChange® II XL Site-Directed Mutagenesis Kit (Stratagene, La Jolla, CA) with the following primers:

SEQUENCE	**FORWARD OLIGONUCLEOTIDE**
pBI-G Tet	5'-CATGTCTGGATCCGCTAGCACTAGGTCGACGCGG-3'
	REVERSE OLIGONUCLEOTIDE
pBI-G Tet	5'-CCGCGT CGACCTAGTGCTAGCGGATCCAGACATG-3'

Subsequently, the *LacZ* gene cassette was excised from the mutagenized pBI-G Tet vector using the flanking XbaI sites and the backbone vector was religated to generate the pBI*-Tet vector. The mouse ornithine decarboxylase PEST sequence was amplified by PCR from the pTAL-d2EGFP vector (Clontech) using the following primers:

SEQUENCE	**FORWARD OLIGONUCLEOTIDE**
PEST	5'-CGTGTACAGCCATGGCTTCCCGCCGGAG-3'
	REVERSE OLIGONUCLEOTIDE
PEST	5'-CGTGTACACTACACATTGATCCTA GCAGAAG-3'

and cloned into the BsrGI site of the pCX-ECFP vector (generous gift of Andras Nagy). The entire ECFP-PEST gene cassette was amplified by PCR using the following primers:

GENE	**FORWARD OLIGONUCLEOTIDE**
ECFP-PEST	5'-CGTCTAGACGCCACCATGGTGAGCAAGGG-3'
	REVERSE OLIGONUCLEOTIDE

ECFP-PEST	5'-CGTCTAGACTACACATTGATCCTAGCAGAAG-3'

and cloned into the XbaI site of the pBI* Tet vector to generate the ECFP-pBI-Tet vector. To introduce additional SalI and NotI sites upstream of the pre-miR132 sequence of the pCAAGS-pre-miR132 vector (142), the palindromic oligodeoxynucleotide denoted by the sequence: 5'-CTAGTGTCGACGCGGCCGCGTCGACA-3' was self-annealed and cloned into the SpeI site. The pre-miR132 sequence was subsequently excised from the modified pCAAGS-pre-miR132 vector using the flanking NotI sites, and cloned into the NotI site of the ECFP-pBI-Tet vector to generate the final ECFP-pBI-miR132 vector. The final construct was confirmed by sequencing. All oligonucleotides were obtained from Invitrogen (Carlsbad, CA, USA).

Generation of transgenic mice and animal husbandry

ECFP-pBI-pre-miR132 DNA was linearized, purified and injected into the pronuclei of oocytes from FVB/N mice at the Ohio State University Transgenic Facility. Founders were identified by PCR genotyping using the following primers:

GENE NAME	**FORWARD OLIGONUCLEOTIDE**
pre-miR132 genotyping	5'-GGAAGGAGAGCAAACACAGC-3'
	REVERSE OLIGONUCLEOTIDE
pre-miR132 genotyping	5'-CGTCTAGACTACACATTGATCCTAGCAGAAG-3'

Founders were backcrossed for 3-4 generations onto a C57BL/6J background prior to analysis. Mice were maintained at the animal facility of the University of Ottawa in accordance with institutional guidelines. All animal handling and experimental procedures were approved by the Animal Welfare Committee of the University of Ottawa. Oligonucleotides were obtained from Invitrogen.

Vector construction

The full-length 3'-UTRs for each of the following genes were amplified by PCR from mouse bacterial artificial chromosome (BAC) constructs (BACPAC Resources, Oakland, USA) using the following primer sets:

GENE NAME	FORWARD OLIGONUCLEOTIDE
Ep300	5'-CGCTCTAGAGAATTCAGACACCTTGTAGTATTTTGG-3'
Jarid1a	5'-CGCCCCGGGACTGGGTACAGTGTGATGGTG-3'
Btg2	5'-CGCTCTAGAAAGCTTATAGGAGCCACCCGACCCTGGC-3'
Paip2a	5'-CGCTCTAGAGAATTCCATGTCTGAGCAGCCGGCCG-3'
	REVERSE OLIGONUCLEOTIDE
Ep300	5'-CGCTCTAGATCAGGTGTCTGTCTCACACAG-3'
Jarid1a	5'-CGCCTCGAGCCTGGTTAAAAGTGGCTCCTG-3'
Btg2	5'-CGCTCTAGACAGTCGCATCGAGTGCACTGGTGTGC-3'
Paip2a	5'-CGCTCTAGATCGGTTCTACTATCATTTAT-3'

The 3'-UTRs were first cloned into pBluescript (Clontech), mutagenized and then sub-cloned into the CMV-pGL3-Control vector (Promega, Madison, WI), between the luciferase (*luc+*) gene and the SV40 late poly(A) signal. For the mouse *Mecp2* gene, the following sequential steps were taken: a ~12kb fragment encompassing the entire 3'-UTR was excised with *XmaI* from a BAC construct (Clone ID number RP23-396E2; BACPAC Resources Center) and sub-cloned into pBluescript (Clontech). A ~9.6 kb fragment encompassing the *Mecp2* 3'-UTR which harbors the miR-132 MRE was excised with *XmaI-AleI*. This fragment was inserted into a pGL3-CT$^{(AleI\text{-}linker)}$ vector that had previously been modified as follows: an *XmaI* site was removed via *SmaI-BglII* digestion, re-filled with Klenow polymerase (Invitrogen) and re-ligated with T4 DNA ligase (Takara, Shiga, Japan) Then, 3'-*XmaI* and 5'-*AleI* sites were inserted by self-annealing the palindromic oligodeoxynucleotide:

5'-CTAGACCCGGGTTAATTAAGGGCCCGTT-3' and cloned into the XmaI/HpaI sites between the *luc*+ gene and the SV40 poly(A) signal. Site-directed mutagenesis of the predicted MREs of the all the wild-type 3'UTRs was performed using the QuikChange® Site-Directed Mutagenesis Kit (Stratagene) with the following primers:

GENE NAME	**FORWARD OLIGONUCLEOTIDE**
Ep300$^{\Delta 7}$	5'ATTACTTATAAATATGAACTTTGGATCACTGTATAAAATTTGATTTCTTATTACCTAT
Jarid1a $^{\Delta 7\text{-site1}}$	5'TTTACTTTTTTCTAAATGTCTCTGACTACTCTATAGATTATTTTTCCTTTTTTGATATA
Jarid1a $^{\Delta 7\text{-site2}}$	5'GATATACATATATGAATATAGATATATATATATATATTTACCAGCAGCGTATGATAC
Mecp2$^{\Delta 7}$	5'-TGACCAAATATCACCAGACTCAACGTGTGCCGAG-3'
Btg2$^{\Delta 7}$	5'-CAAACCCTAGAGCTGGAGCAGGCCTGTCTC-3'
Paip2a$^{\Delta 2}$	5'TCTGAAGTAGTGGGTTTTGATTGAGTTTTTAAAAAACTGTTTGGATTTTAATT-3'
	REVERSE OLIGONUCLEOTIDE
Ep300$^{\Delta 7}$	5'GTTTATTTAACAATAGGTAATAAGAAATCAAATTTTATACAGTGATCCAAAGTTCAT 3'
Jarid1a$^{\Delta 7\text{-site1}}$	5'GTATATCAAAAAAGGAAAAATAATCTATAGAGTAGTCAGAGACATTTAGAAAAAAC
Jarid1a$^{\Delta 7\text{-site2}}$	5'CTCTATCATACGCTGCTGGTAAATATATATATATATATCTATATTCATATATGTATAT
Mecp2$^{\Delta 7}$	5'-CTCGGCACACGTTGAGTCTGGTGATATTTGGTCA-3'
Btg2$^{\Delta 7}$	5'-GAGACAGGCCTGCTCCAGCTCTAGGGTTTG-3'
Paip2a$^{\Delta 2}$	5'-ATGCTTAATAAAAGTGCTGAGAGTCTTACTAAGTAAGGAGCTGTCAC 3'

All primers were obtained from Invitrogen and pre-screened clones were verified by DNA sequencing at The Centre for Applied Genomics (TCAG), The Hospital for Sick Children, Toronto, Canada.

Behavioural and Photic Stimulation Paradigms

Mice were individually housed in polycarbonate cages equipped with a running wheel in ventilated cabinets with timer-controlled lighting (white LED lighting ~ 100 lux at cage level). To monitor wheel-running activity, cages were equipped with magnetic switches, and switch closures were recorded with the ClockLab® software (Coulbourn Instruments, Whitehall, Pennsylvania). Beginning at 6-8 weeks of age, adult male mice were singly housed in the wheel-running cages and stably entrained to a 12 hr:12 hr light:dark (LD)

cycle for at least 14 days prior to release into constant darkness (DD). After 12-14 days in DD, mice received a brief light pulse of medium light intensity (40 lux) for 15 min at CT 15. Light pulses were administered by removing the cage from the cabinet and placing it in a secondary containment chamber with controlled white LED lighting. Immediately after the light pulse, cages were returned to the behavioural cabinet and remained in DD for an additional 12-14 days. Subsequently, mice received a second light pulse of high light intensity (400 lux) for 15 min at CT 15, and afterwards returned to DD for 12-14 days.

For the doxycycline reversal experiments, mice were fed *ad libitum* rodent chow containing doxycycline (6 mg/g food; Bio-Serv, Frenchtown, NJ) for 4 weeks while being maintained in wheel running cages, in a fixed 12 hr:12 hr LD cycle. After 3 weeks of Dox feeding, mice were released into DD conditions, and 5-7 days thereafter, mice received a single light pulse (40 lux, 15 min) at CT 15. Light-induced phase shifts were determined by measuring the displacement between two regression lines drawn through the daily activity onsets 10 days before and 10 days after the light pulse. Using the ClockLab® Analysis software (Coulbourn Instruments), period length was determined by drawing a regression line through the onsets of daily activity during the first 10-14 days in DD. Data are presented as the mean $\pm$ SEM. Statistical significance was measured using the Student's t-test. Significance was accepted for $p < 0.05$.

Tissue Harvesting

Mice that had been stably entrained to a 12:12 LD cycle (100 lux) for a minimum of 2 weeks were dark adapted (DD) for 2 days prior to tissue harvest at designated circadian times as described below. For photic stimulation experiments, mice were exposed to light

(15 min) at designated circadian times and light intensity levels, returned to DD for a prescribed length of time, and processed for tissue. For these experiments, circadian time was estimated based on the prior light-dark cycle, where *ZT12* (i.e. lights off) was used to define circadian time 12 (CT12) up to 3 days in DD.

For immunolabeling, mice were killed via cervical dislocation, and their brains were removed rapidly under red dim light. Brains were immersed in chilled oxygenated physiological saline, cut into 600-μm coronal sections with an oscillating tissue slicer, and fixed (6 hrs, room temperature) in a 4% (w/v) formaldehyde/100mM phosphate-buffered saline (PBS) solution, pH 7.4. Tissue was cryoprotected in 30% sucrose (w/v) overnight, and then cut into thin (40 μm) sections using a freezing microtome. For RNA isolation, mice were killed in the dark and their eyes covered with black tape. Brains were removed and the SCN dissected in RNAse-free conditions under a dissecting microscope with the optic chiasm facing up. The SCN was rapidly frozen on dry ice and stored until processing.

Immunofluorescent and immunohistochemical detection

For immunofluorescent labeling, 40 μm brain sections were washed five times in PBST (100mM PBS, 0.1% Triton X-100), blocked (1 hr, room temperature) in 10% horse serum-PBST, and incubated (overnight, 4 °C) in primary antibodies. The following primary antibodies were used: rabbit anti-GFP (1:2000; Eusera, Edmonton, Alberta), goat anti-GFP (1:2000; Eusera), mouse anti-GFAP (1:1000; Molecular Probes, Eugene, OR), rabbit anti-MeCP2 (1:150; Millipore, Billerica, MA), rabbit anti-MeCP2 pS421 (1:3000; generous gift of Z. Zhou), rabbit anti-BTG2 (1:400; Aviva Systems Biology, San Diego, CA), rabbit anti-Histone H3-tri methyl K4 (1:500, Abcam, Cambridge, MA), sheep anti-

H2.AZ-K4-K7-K11 (1:300, Abcam), and rabbit anti-PAIP2A (1:1200, Sigma-Aldrich, St. Louis, MO). The following day, sections were washed five times in PBST and incubated (2 hrs, room temperature) with Alexa Fluor® 488- and/or Alexa Fluor® 594-conjugated secondary antibodies (1:1000; Molecular Probes) against the primary antibodies. In some experiments, sections were counterstained with the nuclear marker DRAQ5™ (1:2000; Biostatus Ltd., Shepshed, Leicestershire, UK). Sections were mounted on slides with Dako Fluorescence Mounting Medium (Dako Canada, Inc., Mississauga, Ontario).

For immunohistochemical detection, brain sections were washed five times with PBST, treated with 0.3% hydrogen peroxide in PBS for 20 min, blocked (1 hr, room temperature) in 10% horse serum/PBST, and incubated (overnight, 4 °C) in primary antibodies. The following primary antibodies were used: rabbit anti-p300 (C-20) (1:1000; Santa Cruz Biotechnology, Inc., Santa Cruz, CA), rabbit anti-JARID1A (1:600, Abcam), rabbit anti-PER1 (1:4000; generous gift of S. Reppert), rabbit anti-PER2 (1:10,000; generous gift of D. Weaver), rabbit anti-CLOCK 1:5000 (gift of D. Weaver), rabbit anti-BMAL1 1:5000 (gift of D. Weaver), rabbit anti-MeCP2 (1:1000; Millipore), rabbit anti-H3-K56 (1:50,000; Abcam), anti-p300/Lys1499 1:10,000 (Cell Signaling, Danvers, MA, USA) and anti-SIRT1 1:1000 (Millipore). Sections were washed five times in PBST and incubated (2 hrs, room temperature) with biotinylated anti-rabbit IgG(H+L) secondary antibodies (1:300; Vector Laboratories, Burlingame, CA). Immunodetection was accomplished using the HRP-ABC technique (Vector Laboratories) according the manufacturer's instructions.

Cell Culture and Transfection

HEK293, Neuro-2a (N2A) and 3T3 cells were obtained from ATCC (American Type Culture Collection, Manassas, VA, USA) and were grown in Dulbecco's Modified Eagle Medium (DMEM; Invitrogen), supplemented with 10% fetal bovine serum (Wisent, Quebec, Canada) and 1% penicillin/streptomycin (Wisent). To examine the effects of miR-132 knockdown on target gene expression, N2A cells were grown on 6-well plates and transfected with 3 μg of miRIDIAN® mmu-miR-132 Hairpin Inhibitor (Dharmacon, Inc., Lafayette, CO) or miRIdIAN® microRNA Hairpin Inhibitor Negative Control #1 (Dharmacon, Inc.), and 1 μg of pCS-Venus vector per well to monitor transfection efficiencies (generous gift of A. Miyawaki), using Lipofectamine 2000 (Invitrogen) according to manufacturer's protocols.

To examine the effects of MeCP2 overexpression on endogenous PER1 and PER2 levels, N2A cells were grown on 6-well plates and transfected with 1.5 μg of pcDNA3.1-hMeCP2-e1-myc (generous gift of B. Minassian) in combination with 2 μg of pCMV-KCREB (Clontech) and 0.5 μg of pCS-Venus. Thirty-six hours post-transfection, lysates were prepared and analyzed via Western blotting.

Luciferase Assays

HEK293 and N2A cells were grown on 24-well plates and transfected with 12.5 ng of the pRL-TK vector (Promega), 200 ng of the CMV-pGL3 construct containing the 3'UTRs of the respective genes, and 25 pmol of miRIDIAN® mmu-miR-132 Mimic or miRIDIAN® microRNA Mimic negative control #1 (Dharmacon) using Lipofectamine 2000. For the determination of luciferase activity, cell lysates were prepared 24-hrs post-transfection and processed using the Dual Glo® Luciferase Assay System (Promega).

Readings were acquired using the GloMax 96 Plate Luminometer with the automated dual injection system (Promega).

Western blotting

Brain tissue was homogenized in ice-cold RIPA buffer supplemented with protease inhibitor cocktail, homogenized and incubated for 20 min on ice with gentle mixing. Two adult SCNs per genotype were pooled, yielding ~100µg of total protein lysate. After pre-clearing by centrifugation (15 min at 17,000 x g), proteins were quantitated via the Bradford method using the Coomassie Plus™ Protein Assay Reagent (Fisher Scientific Canada, Whitby, ON) at 595nm wavelength. Protein samples were resolved on sodium dodecyl sulfate polyacrylamide gels under denaturing conditions, and blotted onto PVDF membranes (Bio-Rad, Hercules, CA, USA) by wet transfer for 2 hr at 80 V for low molecular weight proteins (such as BTG2, PAIP2A, MeCP2) or overnight (~16 hr) at 35 V for high molecular weight proteins (such as p300 (300kDa) or JARID1A (185kDa). Membranes were blocked (45 min, room temperature) with 5% skim milk in TBST (Tris-buffered saline, 0.05% Triton X-100), and incubated (4°C, overnight) with the following antibodies: rabbit anti-BTG2 (1:3000), rabbit anti-PAIP2A (1:6000), rabbit anti-p300 (1:1000), rabbit anti-JARID1A (1:2000), mouse anti-MeCP2 (1:2000, Sigma-Aldrich), rabbit anti-PER1 (1:2000, Abcam), rabbit anti-PER2 (1:10,000), rabbit anti-PAIP2B (1:1000), rabbit anti-PABP (1:1000, Cell Signaling), rabbit anti-pCREB (1:2500; Cell Signaling), rabbit anti-SIRT1 (1:1000; Millipore) and rabbit anti-actin (1:30,000, Sigma-Aldrich). Membranes were incubated (2 hr, room temperature) with ImmunoPure® HRP-conjugated goat anti-rabbit or anti-mouse IgG(H+L) secondary antibody (1:250,000; Pierce, Rockford, IL). Membranes were washed 5 x 5 min in TBST after antibody

incubations, and the signal was detected by chemiluminescence using the SuperSignal® West Femto Maximum Sensitivity Substrate (Pierce). All western blot quantitations were performed with ImageJ software (http://rsbweb.nih.gov/ij/) on grayscale images.

Chromatin Immunoprecipitation (ChIP)

3T3 cells (~$2x10^7$) were transiently transfected with 48 μg of pcDNA3.1-hMeCP2-e1-myc and 6 μg of pCS-Venus to monitor transfection efficiency. Thirty-six hrs post-transfection, cells were crosslinked with 1% formaldehyde w/v for 15 min at room temperature (RT) and quenched for 5 min at RT with 125 mM glycine. After quenching, cells were immediately placed on ice and rinsed twice with 5ml of ice-cold 100mM PBS, pH 7.4 containing protease inhibitor cocktail (Sigma-Aldrich). Cells were scraped in ice-cold 100mM PBS with protease inhibitor cocktail, and centrifuged for 10 min at 1000 x *g*. Cell pellets were then resuspended in 50 mM HEPES-KOH, pH 7.5, 140 mM NaCl, 1 mM EDTA, 1% Triton X-100, 0.1% sodium deoxycholate, 0.1% SDS with protease inhibitor cocktail and incubated on ice for ~30 min. Cells were then sonicated for 80 cycles (30 sec pulse, 90 sec rest intervals) to an average size of ~800bp using a 4°C sonicator (Bioruptor® UCD-200, Diagenode, Inc., Sparta, NJ). After sonication, cell debris was pelleted by centrifuging 2 min, 4°C at 8000 x *g*. Supernatant was collected and a 20 μl input sample was analyzed on a 2% agarose gel to verify chromatin size. Additionally, 100 μl of recovered chromatin was used for DNA quantitation and as qPCR positive control. GammaBind Plus Sepharose Beads (GE Healthcare, Piscataway, NJ, USA) were blocked with BSA (100 ng/μl beads; New England Biolabs, Ipswich, MA) and salmon sperm DNA (100 ng/μl beads; Invitrogen) for 30 min at RT. Beads were washed 3 times with RIPA buffer (50 mM Tris-Cl, pH 8, 150 mM NaCl, 2 mM EDTA,

pH 8, 1% NP-40, 0.5% sodium deoxycholate, 0.1% SDS with protease inhibitor cocktail) and resuspended in 2 volumes of RIPA. Pre-clearing of recovered chromatin was performed by incubating with 100 µl of blocked GammaBind Plus Sepharose bead slurry for 1 hr at 4°C. Beads were centrifuged for 2 min, 4°C at 8000 x *g* and pre-cleared chromatin was recovered and further diluted 1:10 in RIPA for immunoprecipitation. Immunoprecipitation was performed overnight at 4°C by incubating 50 µg of pre-cleared chromatin with 5 µg mouse anti-c-myc (Sigma-Aldrich), 5 µg rabbit anti-MeCP2 (Abcam), 3 µg rabbit anti-H3 (Abcam), 5 µg rabbit anti-H3K4Me3 (Millipore) and 5 µg anti-rabbit IgG (Jackson Immunoresearch, West Grove, PA). Immune complexes were captured with 120 µl of blocked GammaBind Plus Sepharose Bead slurry for 2 hrs at 4°C. Beads were then collected by centrifuging for 2 min at 8000 x *g*. Beads were washed three times with 20 mM Tris-Cl, pH 8, 150 mM NaCl, 0.1% SDS, 1% Triton X-100 and 2 mM EDTA, pH 8, and once with 20 mM Tris-Cl, pH 8, 500 mM NaCl, 0.1% SDS, 1% Triton X-100 and 2 mM EDTA, pH 8. DNA was eluted with 150 µl of elution buffer (1% SDS, 100 mM $NaHCO_3$) for 15 min at RT. Eluted DNA was further diluted in 2 volumes of elution buffer and incubated overnight at 55°C with 100 µg of proteinase K (Invitrogen) for cross-link reversal. The DNA was then phenol-chloroform extracted and resuspended in 100 µl of TE, pH 8 (10 mM Tris-Cl, 1 mM EDTA, pH 8). 2 µl ($1/50^{th}$) of DNA was used per reaction for quantitative PCR (qPCR) analysis.

Reverse Transcription of miRNAs

SCN tissue was pooled from 3 mice of the same genotype and total RNA was isolated using the *mir*Vana™ miRNA Isolation Kit (Applied Biosystems, Foster City, CA) according to the manufacturer's instructions. Total RNA (10 ng) was reverse transcribed

using the TaqMan® MicroRNA Reverse Transcription Kit (Applied Biosystems) and miR-132- or miR-219-specific stem-loop primers according to manufacturer's protocol.

Quantitative Real-Time PCR

Real-time PCR for mature miR-132 and miR-219 was performed using TaqMan® microRNA assay (Applied Biosystems) according to manufacturer's instructions, using the Rotor-Gene 6000 Real-Time Rotary Analyzer (Corbett Life Science, Concorde, New Zealand). For Reverse-Transcriptase-qPCR (RT-qPCR) analysis of *Mecp2* and *Gapdh* transcript levels in SCN tissue from *Mecp2*$^{Floxed/y}$ mice, miR-132 transgenics and non-transgenic controls, total RNA was isolated using Trizol (Invitrogen) from 2 SCN pools. 500ng of total RNA was used for cDNA synthesis using SuperScript III RT (Invitrogen) according to manufacturer's instructions. qPCR analysis was carried out using the ABsolute™ Blue QPCR SYBR® Green Mix (ABgene, Ltd., Rockford, IL, USA), using the Rotor-Gene 6000 Real-Time Rotary Analyzer (Corbett Life Science) under the following conditions: one cycle at 95°C for 15 min; and 50 cycles at 95°C for 15 sec, 60°C for 30 sec, and 72°C for 30 sec. Primer specificity was always analyzed after each run with melting curves. The following primers were used;

GENE	FORWARD OLIGONUCLEOTIDE	REVERSE OLIGONUCLEOTIDE
Mecp2	5'-CTCCATAAAATACAGACTCACCAGT-3'	5'-CTTAAACTTCAGTGGCTTGTCT-3'

For qPCR analysis of ChIP DNA, PCRs were also performed using the ABsolute™ Blue QPCR SYBR® Green Mix (Abgene) under the following conditions: one cycle at 95°C for 15 min; and 50 cycles at 95°C for 15 sec, 60°C for 30 sec, and 72°C for 30 sec. Primer specificity was always analyzed after each run with melting curves. The following primers were used to analyze ChIP'ed DNA:

GENE	FORWARD OLIGONUCLEOTIDE
mPer1-CRE	5'-TTTGACGTCACCTCCCTCTC-3'
mPer1-Ebox1	5'-TGACGGTGTGAGACATCCTG-3'
mPer1-Ebox2	5'-GGCTTCCTGGAGACCTTTTC-3'
mPer1-Ebox3	5'-GGTCTGTGTCCCAGCATTTC-3'
mPer1-CpG #1	5'-GGGGTAGGCTCCCTAAACAC-3'
mPer1-CpG #2	5'-GGCGTCTCTGAGCCAATAAG-3'
mPer2-CRE1	5'-CCAGGTGGATGAGCTGTGTA-3'
mPer2-CRE2	5'-GAACCTCTGAGGGAACCACA-3'
mPer2-E-Boxes	5'-GTGCCAGGTGAATGGAAGTC-3'
mPer2-Ebox#1	5'-GCGGTCACGTTTTCCACTAT-3'
mPer2-CpG	5'-ACGTCGTCGCAGGTGATAG-3'
	REVERSE OLIGONUCLEOTIDE
mPer1-CRE	5'-GCCCACTTCCCTATCTGTCA-3'
mPer1-Ebox1	5'-TCTTCCTGGCATCTGATTGG-3'
mPer1-Ebox2	5'-TGAGAGAAGGGCAATTGAGG-3'
mPer1-Ebox3	5'-CTTCCCTGCAAACGTAGGTG-3'
mPer1-CpG #1	5'-CCCATTCCTATTTTCGAGCA-3'
mPer1-CpG #2	5'-AGTTCGACGGCTCCAGAGTA-3
mPer2-CRE1	5'-AGCACCTCTGGTTCCTCTGA-3'
mPer2-CRE2	5'-GTGCTCCCCATGTCTTGAGT-3'
mPer2-E-Boxes	5'-CTCATCAATTGGTGGAGACG-3'
mPer2-Ebox#1	5'-CCGGTTACGTAAG ACGACCA-3'
mPer2-CpG	5'-CGAGTAGGCTCGTCCACTTC-3'

All primers were obtained from Invitrogen.

Image acquisition and processing

Immunohistochemistry images were acquired using 20X and 40X oil objectives with a Zeiss Axiovert Observer Z1 epifluorescent/light microscope equipped with an AxioCam MRm cooled-color camera (Oberkochen, Germany). Immunofluorescent tissue sections were examined and images were captured with 20X, 40X oil and 63X oil objectives using a Zeiss 510 laser scanning confocal microscope with argon (488nm), helium/neon (546nm) and helium/neon (633nm) lasers. All fluorescent image quantitations were performed with Zen 2008 (Zeiss). PER1 and PER2 rhythms, originally in grayscale, were

quantitated using ImageJ software. Each unilateral SCN was measured individually by the sum of all grayscale values from 0-255 divided by the total number of pixels within the region of interest. Background values were obtained from non-immunoreactive tissue in the lateral hypothalamus and subtracted from SCN mean gray values. Only central SCN were included in the quantitation. For PER1 and PER2 light induction experiments, a different method for quantitation was used given the subanatomical nature (i.e. core vs. shell) of light-dependent light induction. First, images were assigned a minimal threshold using a grayscale threshold value between 0-100 to 0-120. Summation of all particles within the area of interest yielded a total area of immunoreactive cells within the SCN. Only particle areas of more than 50 pixels were included in the calculation of immunoreactive cells (50 pixels was experimentally determined to be above non-specific DAB staining). Total area was divided by an average cell size of 120 pixels to yield a cell count estimate. Only central SCN sections were quantitated. Final representative images were further processed with Adobe Photoshop CS2 for Mac. Only the contrast function was manipulated to reduce background noise.

RESULTS

(Some of the results section has been adapted from the manuscript Alvarez-Saavedra et al, circa November 2009).

i. Generation & characterization of microRNA-132 transgenic mice

As a first step in order to identify potential miR-132 targets in the SCN and characterize their role in circadian biology, a novel, tetracycline (Tet)-inducible miR-132 transgenic

mouse strain was developed in the laboratory (hereon referred to as miR-132 mice or tTA::miR-132 mice; mice were generated by Dr. Hai-Ying Mary Cheng). The sequence of the rat miR-132 precursor hairpin (pre-miR-132; Table 1), which is highly conserved in multiple metazoan species (Figure 4A, top), was cloned into a bidirectional Tet-responsive promoter, along with a destabilized ECFP version (Enhanced Cyan Fluorescent Protein containing a PEST domain; 145,146), as a second transgene (Figure 4A, bottom). This transgenic strain was crossed with the *Camk2α*-tTA activator line (147) to produce *Camk2α*-tTA::miR-132 double transgenic mice (i.e. tTA::miR-132 mice). Under doxycycline-free conditions, the expression pattern of the ECFP reporter is restricted to the forebrain due to *Camk2α*-tTA-driven expression (Figure 4B), as detected via immunolabeling and analyzed via confocal microscopy. The ECFP transgene is expressed in the majority of SCN neurons (>90%; Figure 4C) and it is excluded from glia, since the ECFP transgene does not co-localize with GFAP, a marker of the glial lineage (Figure 4C). In order to further characterize the miR-132 transgenic founder lines, a detailed ECFP expression characterization of lines #2550, #2561 and #2570 was performed. Confocal imaging revealed that lines #2570 and #2561 are the highest expressors, followed by line #2550 in which ECFP labeling is modest (Figure 5). Due to

TABLE 1

mmu-microRNA-132/microRNA-212 genomic sequence from mouse chromosome 11 (Ensembl 2008; http://uswest.ensembl.org/index.html). Sequence below corresponds to mouse chromosome 11, Ensembl coordinates #7498**6567**-7498**7867**.

Note the following sequence motifs:
pre-microRNA-212.
pre-microRNA-132.
TGACGTCA: CRE putative binding sites.

TABLE 1

mmu-microRNA-132/microRNA-212 genomic sequence from mouse chromosome 11 (Ensembl 2008; http://uswest.ensembl.org/index.html). Sequence below corresponds to mouse chromosome 11, Ensembl coordinates #7498**6567**-7498**7867**.

Note the following sequence motifs:
pre-microRNA-212.
pre-microRNA-132.
TGACGTCA: CRE putative binding sites.
Underlined Sequence: pre-microRNA-132 transgene (note that the transgene was amplified from the rat genome).
Bold: Mismatches to rat sequence.

5'TCCACACACGCCCCTTCCCTGTCCCGTCCCTTCCCGTCCGGTCCCGTCCCGT
CCCATCGGACTGTCCCACTGAGCTCAGGACTTCCCGCCTCTGCAAGCGGAGC
TGTCCTCTCGGACCAGGCGGGGGCGGGGCTTCGATCAGGCCGCCCCGCCCTA
CCCCCACCGCTCCCCACCGCCGGAAATGCCTCCCCGCTGGGACATCTTTGACG
TCACAGGACTCTGACGTCACGGTCGCGTGTCTGTCCGCGCGCGCTTGGGAGG
AGGTGGGGGGGCCTGAGAAGCAGCAGCACTCTCAACTGCGGGCGACGGGAT
ATCCCCGCCCGGGCAGCGCGCCGGCACCTTGGCTCTAGACTGCTTACTGCCC
GGGCCGCCTTCAGTAACAGTCTCCAGTCACGGCCACCGACGCCTGGCCCCGC
CCCAGGACCGCCGACCCCCGGCCCCTCCACGCCTCCCTGCGCCGCTGTCCGC
GGTGCTGATGCAGTGCAAGCGCCTCCCTCGGGCACGCCTGTTCAAGGTCCCT
GTGGGTTGCGGTGGGCGCAGGCCCCGCAGACACTCGCGCACCCCCGCCGCCC
GCGGTGCTGACGTCAGCCTGCAAGCCCCGCCCCCGCGTCTCCAGGGCAACCG
TGGCTTTCGATTGTTACTGTGGGAACCGGAGGTAACAGTCTACAGCCATGGTC
GCCCCGCAGCACGCCCACGCTCCCCACCACTCCCGAGTTCTGCCAGCCTGGG
TTTGGGCAGATACAGAGCAAGAGGAGGCGGGGCGGCGACGCAACATTCGAT
GTGTCTGCGGAGGTGGCAAGAGGTGTGCTCAGAAAGGCGGCCTTTCAGGCTG
CTGTGCATCTACCTCGGTGCAGAAGCAAGATCCGCGGAGTGTCTGAACATCC
TCCTCAGAGACTCTCCTGTCTTCCTAGTCGAGGTATCGCTGCCTAAGGTGGCG
AGAAAATGGGTGGTTCTGCGATAAGGATTCTTATCTCATGAGTGGTGAACCG
ATGGGATCAGGAGTCCTGTGAGAAGGAAGAAGTCACTTTTGCCAGCAGAAAG
CTGAAGGGGGAGGAGAAGGAAGTTTTATCACACCTTTCTTCCAGAAAACCCT
AGGTGAGCAGGTAGAGGGGAAAGGGCAAAGAATCCCTTTCCTGATAGAGCC
ATAACTCTGTCCCCCAACTTTCTCCTGGGCCATCATTAAAAGGGTCCTTAACA
CAGCAAGAAGCTGGCAGGCTAGTGAAATTCACCTGGCCCCTAATTCATTGTC
TGAAGGTATCAGCCAGCAGTCTTCCCTCAACTGGTCTGTAAGTAATGCAT-3'

FIGURE 4

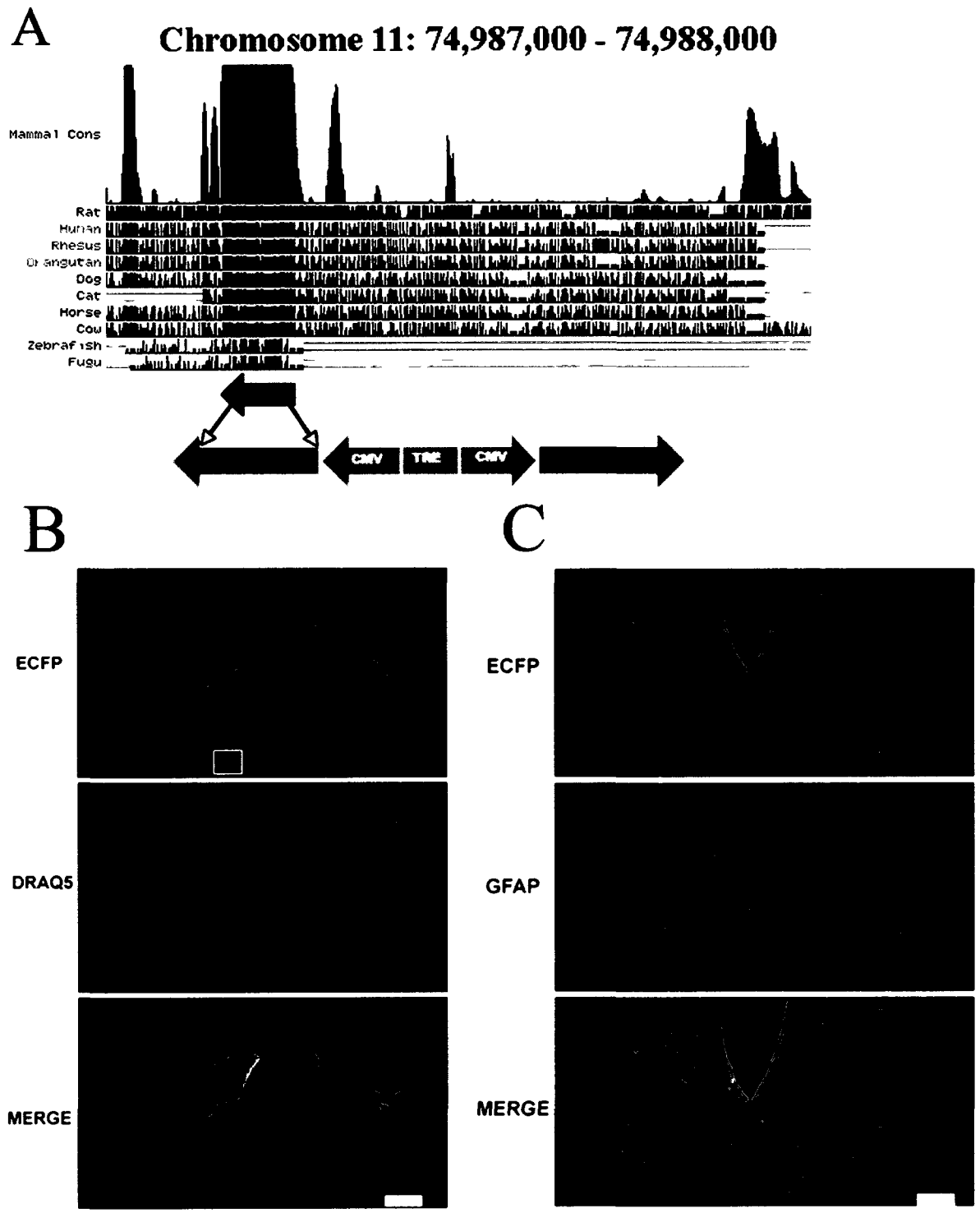
A
Chromosome 11: 74,987,000 - 74,988,000
Mammal Cons
Rat
Human
Rhesus
Orangutan
Dog
Cat
Horse
Cow
Zebrafish
Fugu
CMV
TRE
CMV
B
ECFP
DRAQ5
MERGE
C
ECFP
GFAP
MERGE

(A, top) Conservation of miR-132 across species: Genomic position of mouse pre-miR-132 on chromosome 11 (alignment scores are indicated by green bars in the conservation track of the species listed) using the UCSC Genome Browser (July 2007 assembly). Red arrow immediately below the conservation tracks indicates the position of the miR-132 stem-loop precursor sequence. **(A, bottom)** Transgene design: the pre-miR-132 sequence (green arrow) and the ECFP-PEST cassette (blue arrow) were cloned in opposite orientations flanking a bidirectional Tet-responsive promoter. CMV: minimal CMV promoter; TRE: Tet-responsive element. **(B,C)** ECFP transgene expression in the brains of *Camk2α*-tTA::miR-132 transgenic mice. **(B)** Sagittal and **(C)** coronal SCN sections were processed for ECFP immunoreactivity using a polyclonal anti-GFP (green) antibody. In (B), sections were counterstained with the nuclear marker, DRAQ5 (pseudocolored in red). Scale bar = 1 mm. In (C), sections were co-labeled for GFAP immunoreactivity (red). Note the lack of co-localization between GFAP and ECFP. Scale bar = 50 μm. n = 3 mice per genotype. All images were captured via confocal microscopy on a single focal plane with (B) 10X and (C) 20X objectives. This figure and figure legend are reproduced from the manuscript Alvarez-Saavedra et al, circa November 2009. Tissue harvesting performed jointly by MAS & HYMC. Bioinformatics, confocal imaging, compilation of images and figure design performed by MAS.

FIGURE 5

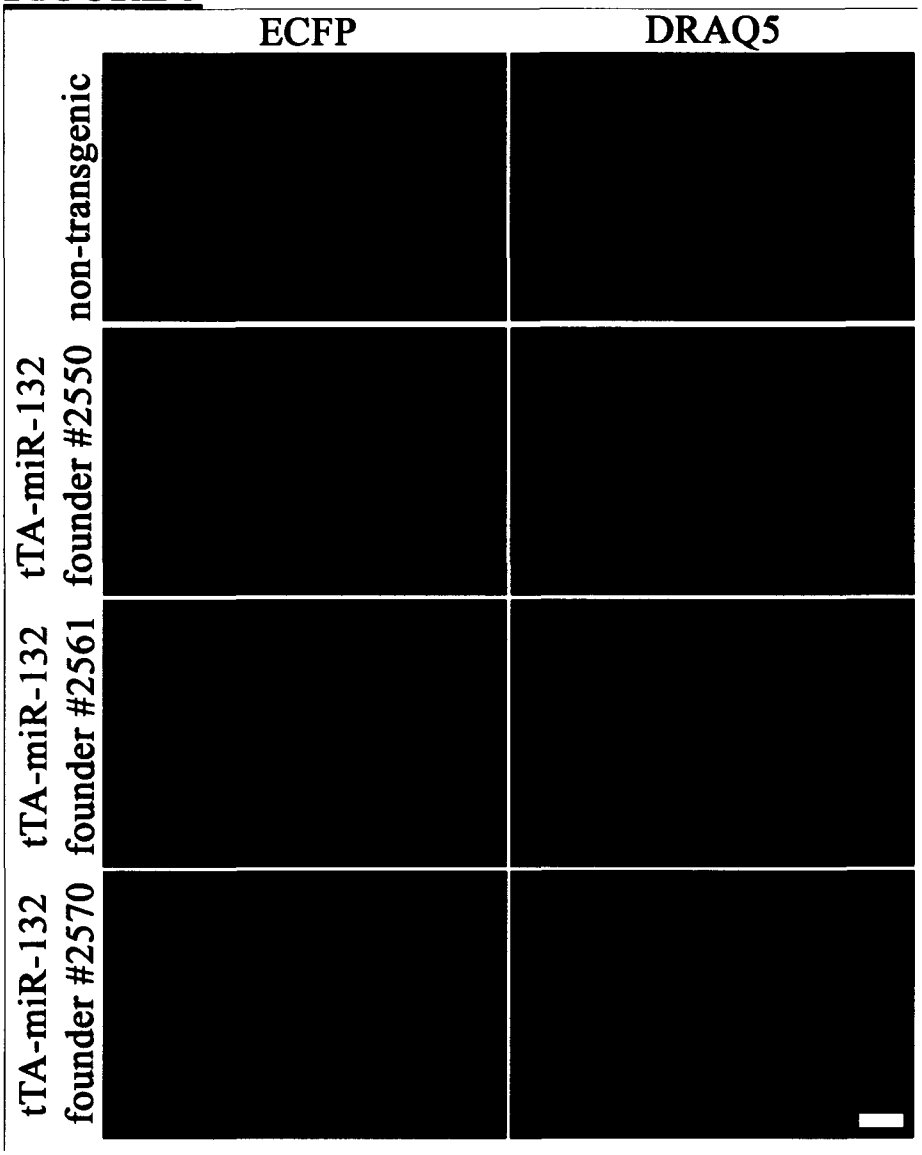

Figure 5. Characterization of tTA::miR-132 transgenic founder lines.
(A) ECFP transgene expression in the brains of *Camk2α*-tTA::miR-132 transgenic lines #2550, #2561 and #2570. Coronal SCN sections were processed for ECFP immunoreactivity using a polyclonal anti-GFP antibody (green; left panels). Sections were counterstained with the nuclear marker, DRAQ5 (pseudocolored in red; right panels). Note the lack of ECFP labeling in non-transgenic littermate control mice opposed to weak ECFP expression in founder line #2550 and higher ECFP expression in founder lines #2561 and #2570. n = 3 mice per genotype. All images were captured via confocal microscopy on a single focal plane with a 10X objective. Scale bar = 1mm. Tissue harvesting performed jointly by MAS & HYMC. Confocal imaging, compilation of images and figure design performed by MAS.

these results, all subsequent experiments involving the miR-132 transgenic strain were performed with founder lines #2561 and #2570. No qualitative differences were found between these two founder lines in all subsequent results obtained.

Via Reverse Transcriptase quantitative PCR (RT-qPCR), I confirmed that the abundance of mature miR-132 is upregulated in the SCN of founder lines #2561 and #2570 at CT10 from 2.7- to 7.5-fold relative to non-transgenic controls, respectively (Figure 6A). As a control, no difference was detected for mature miR-219, an endogenous miRNA that is also expressed in the SCN, between transgenic and non-transgenic controls (Figure 6B). These results suggest that the miRNA machinery is not perturbed in the presence of excess levels of pre-miR-132.

ii. Behavioural analyses of microRNA-132 transgenic mice

The next step was to analyze the *in-vivo* functional role of miR-132 in the regulation of circadian behaviour. Both non-transgenic and tTA::miR-132 mice were able to entrain stably to a full photoperiod of 12-hr light:12-hr dark (LD 12:12) and both strains remained rhythmic upon subsequent release into conditions of constant darkness (DD) for 2 weeks (Figure 7A). The mean circadian period length was statistically indistinguishable between the two genotypes (period [hrs] of non-transgenic vs. tTA::miR-132 mice: 23.5 ± 0.07 vs. 23.6 ± 0.05 hrs, $p>0.05$). These data indicate that transgene overexpression of miR-132 does not compromise the generation and maintenance of circadian rhythms, period length determination and stable entrainment to a full photoperiod. Since miR-132 *in-vivo* knockdown in the SCN has previously been shown to potentiate (i.e. enhance) phase delays upon nocturnal light treatment (130), I examined the role of miR-132 in light-induced clock entrainment using a paradigm that gauges the responsiveness and/or

FIGURE 6

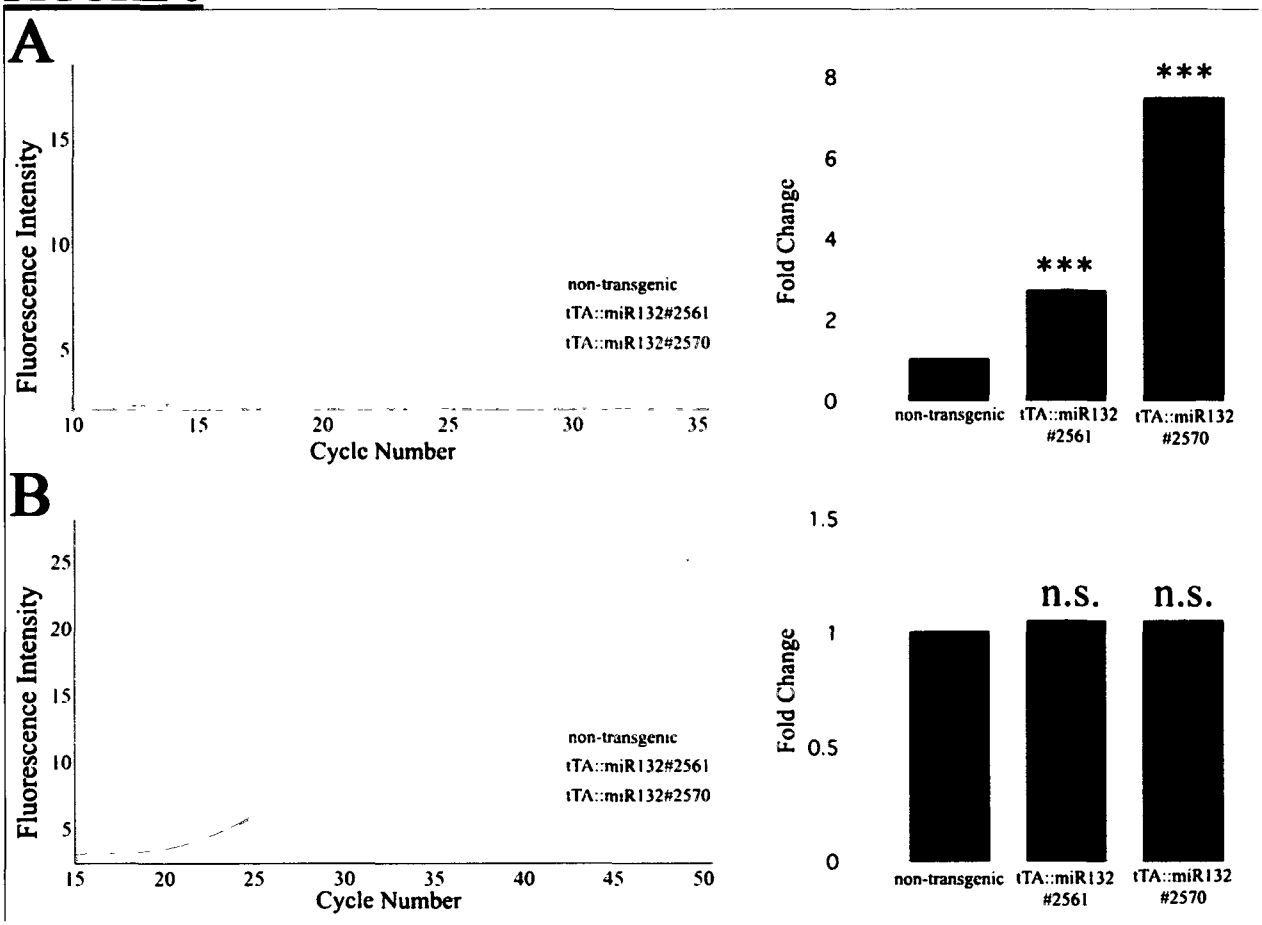

Figure 6. miR-132 is robustly expressed in miR-132 founder lines #2561 and #2570 and does not misregulate the expression of other miRNAs.

(A,B) The abundance of **(A)** mature miR-132 and **(B)** mature miR-219 in the SCN of non-transgenic (black lines) and tTA::miR-132 transgenic (green and red lines) mice was determined via ABI Taqman® miRNA qPCR analysis. Raw data are presented as fluorescence intensity vs. number of PCR cycles. Two independent miR-132 founder lines, #2561 and #2570, were examined. SCN tissues from 3 mice were pooled for each sample, from which quadruplicate determinations were made. Quantitation of (*top right*) mature miR-132 and (*bottom right*) mature miR-219 abundance from (A) and (B), respectively. Data are quantitated and presented as relative fold change, in which values for non-transgenic controls are set arbitrarily as 1. Error bars denote SEM of quadruplicate determinations. ***$p<0.001$. n.s. = non-significant vs. non-transgenic control (one-way ANOVA). This figure and figure legend are reproduced from the manuscript Alvarez-Saavedra et al, circa November 2009. Tissue harvesting performed jointly by MAS & HYMC. Statistical analysis, compilation of images and figure design performed by MAS.

FIGURE 7

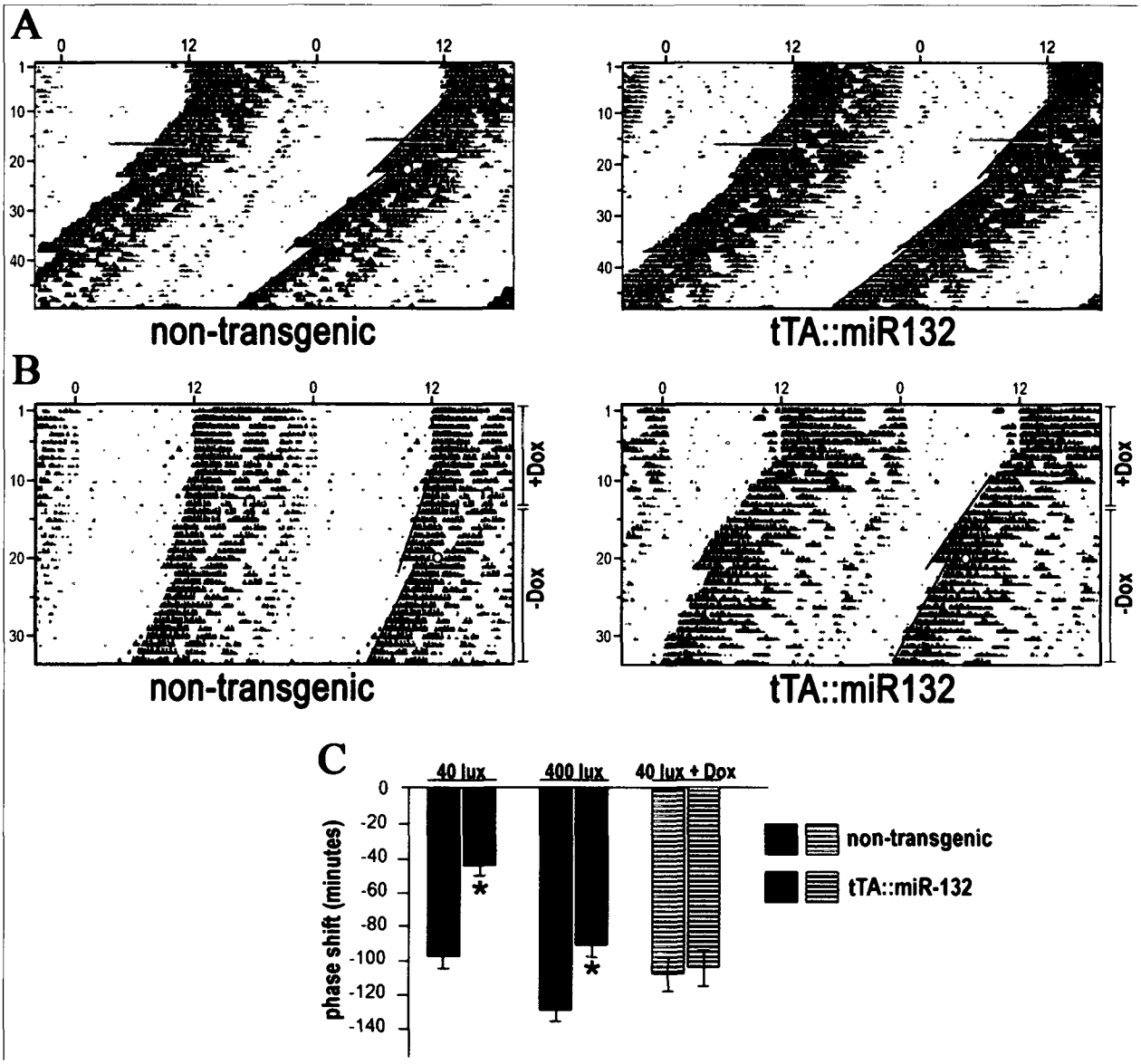

Figure 7. Light-induced clock resetting is attenuated in miR-132 transgenic mice.
(A) Representative double-plotted actograms of wheel-running activity of non-transgenic *(left)* and tTA::miR-132 transgenic *(right)* mice maintained under doxycycline-free conditions. Mice were stably entrained to a fixed 12h:12h light-dark (LD) cycle prior to release into constant darkness (DD). After 2 weeks in DD, mice received a single, 15-min light pulse of 40 lux intensity (yellow circles) at CT 15, and returned to DD. After 15 days in DD, mice received a second light pulse of higher intensity (red circle: 15 min, 400 lux) at CT 15, and returned to DD for an additional 2 weeks. Note that tTA::miR-132 transgenic mice exhibit smaller light-induced phase shifts at both light intensities,

transgenic mice exhibit smaller light-induced phase shifts at both light intensities, compared with non-transgenic controls. Periods of darkness are shaded in gray. Activity onsets are indicated by blue lines. The x-axis indicates the *Zeitgeber* (ZT) time of the initial 12h:12h light-dark cycle (100 lux during the L portion). The y-axis indicates the n^{th} day of study. Missing activity data on day 17 (green bars) were due to computer malfunction. It should be noted that single transgenic mice, either tTA or miR-132 alone, were phenotypically indistinguishable from the non-transgenic mice. **B)** Representative double-plotted actograms of non-transgenic *(left)* and tTA::miR-132 transgenic *(right)* mice that had been maintained on a Dox diet (6 mg/g body weight) during adulthood for 4 weeks in order to "turn off" miR-132 transgene expression. Mice were returned to regular, Dox-free rodent chow 1 week prior to exposure to a single, 15-min light pulse of 40 lux intensity (yellow circle) at CT 15. Note that doxycycline treatment restored the magnitude of light-induced phase shifts of tTA::miR-132 transgenic mice to the level of non-transgenic controls. +Dox: Period of Dox feeding; -Dox: Dox-free conditions. **(C)** Quantitation of the effects of miR-132 transgene expression and doxycycline treatment on CT 15 light-induced phase shifts. Values are presented as mean ± SEM phase shift (in min). Negative values indicate phase delays. n = 10-14 per group. $*p< 0.05$ vs. same-treated non-transgenic control (two-tailed Student's t-test). This figure and figure legend are reproduced from the manuscript Alvarez-Saavedra et al, circa November 2009. Experimental design and execution, statistical analysis and figure jointly compiled by MAS & HYMC.

sensitivity of the clock to light administered during the subjective night. After 2 weeks in DD, mice received a 15-min light pulse of medium intensity (40 lux) in the early night (CT15) (Figure 7A, yellow circles). In non-transgenic mice, this light treatment resulted in a mean phase delay of -98 ± 7.7 minutes (Figure 7A, left actogram & Figure 7C). Interestingly, light (40 lux)-induced phase delays were greatly reduced in tTA::miR-132 mice (-45 ± 5.8 minutes, $p<0.01$; Figure 7A, right actogram & Figure 7C). The attenuated phase-delaying response exhibited by tTA::miR-132 mice was not due to reduced sensitivity of the clock to light, since a second light pulse (15 min, CT 15) of higher intensity (400 lux, red circles), administered 2 weeks later, also resulted in a diminished phase-shifting response in tTA::miR-132 mice compared with non-transgenic controls (phase delay (minutes) of non-transgenic vs. tTA::miR-132 mice to 400 lux light pulse: -130 ± 6.9 minutes vs. -92 ± 6.7 minutes, $p<0.05$; Figure 7A, right and left actograms & Figure 7C). Moreover, the circadian behaviour of *Camk2α*-tTA and miR-132 single transgenic mice were indistinguishable from that of non-transgenic controls, arguing against the possibility that tTA expression alone or potential miR-132 transgene insertional effects was the cause for the reduced phase-shifting effects of light in tTA::miR-132 mice.

I have previously shown that the *Camk2α-tTA* transgenic line is active during mouse embryogenesis as early as 12.5 days post-coitum (dpc; 149). Therefore, I decided to analyze ECFP expression during mouse brain development in miR-132 transgenic mice. miR-132 transgenic embryos from founder line #2570 expressed ECFP in the forebrain as early as 16.5 dpc (Figure 8A, top). No ECFP expression was detected in non-transgenic littermate controls (Figure 8A, bottom). Therefore, in order to rule out the possibility that

FIGURE 8

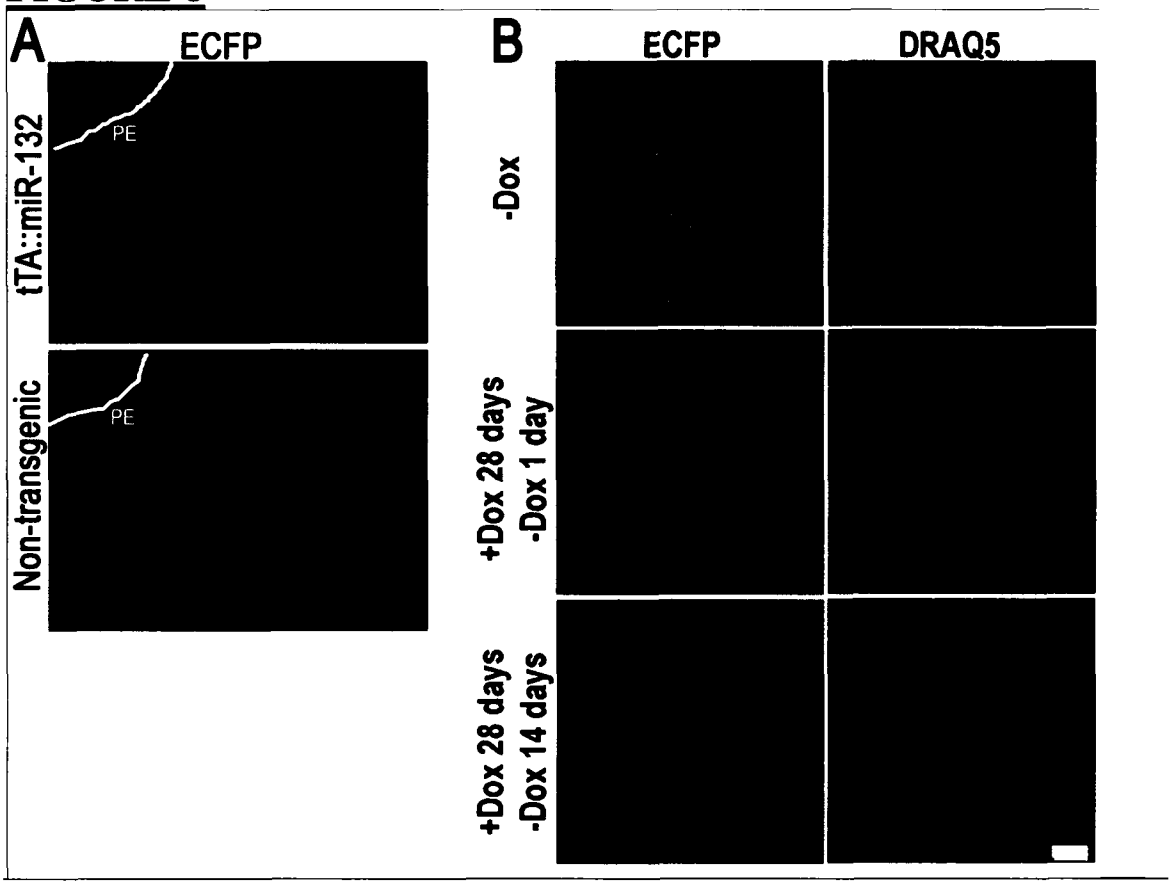

Figure 8. Dox-treatment turns off transgene expression in most SCN neurons.
A) tTA-miR-132 transgene expression can be detected via ECFP direct fluorescence during embryonic development as early as 16.5 dpc in the forebrain. Note the lack of ECFP fluorescence on non-transgenic littermate control embryos. **(B)** Assessment of Dox-mediated transgene silencing in tTA::miR-132 adult mice. Mice were fed Dox-containing rodent chow (6 mg/g food) for 28 days and then returned to a regular diet lacking Dox for an additional 14 days. Three treatment groups were examined for ECFP transgene expression: *(top rows)* Dox-naïve mice (-Dox) and Dox-fed mice that were killed *(middle rows)* 1 day after cessation of Dox treatment (+Dox 28 days/-Dox 1 day) or *(bottom rows)* 14 days after cessation of Dox treatment (+Dox 28 days/-Dox 14 days). Brain sections were processed for ECFP immunoreactivity (green, left panels) and counterstained with DRAQ5 (pseudocolored in red, right panels). Note that only a few SCN neurons have re-activated transgene expression 14 days after Dox-treatment cessation. Scale bar = 100 μm. n = 3 mice per condition. PE: pigmented epithelium of the eye. Images captured using an epifluorescent microscope (A) and via confocal microscopy on a single focal plane with a 20X objective (B). Experimental design and execution fort Panel A performed by MAS. Panel B reproduced from the manuscript Alvarez-Saavedra et al, circa November 2009. Tissue harvesting, doxycycline experimental paradigms, confocal imaging, compilation of images and figure design performed by MAS.

the reduced phase delays exhibited by tTA::miR-132 mice resulted from an irreversible effect of miR-132 overexpression during mouse development, I fed miR-132 transgenic and non-transgenic adult mice a Dox-containing diet (6 mg/g rodent chow) *ad libitum* for 4 weeks to silence transgene expression. During this time, mice were maintained in wheel cages under a fixed LD schedule. After the third week of Dox feeding, mice were released into DD, and a week after returned to regular rodent chow (no Dox). Mice were then treated with a brief light pulse (15 min, 40 lux, yellow circles) at CT 15 (Figure 7B, right and left actograms). Importantly, non-transgenic as well as tTA::miR-132 mice that were both fed a Dox diet showed light-induced phase delays that were statistically indistinguishable (phase delay (minutes) of non-transgenic vs. tTA::miR-132 mice: -109 ± 10.1 minutes vs. -106 ± 10.5 minutes, $p>0.05$; Figure 7B & Figure 7C). Furthermore, via immunofluorescent labeling, I verified that the 4-week Dox regimen completely turned off ECFP transgene expression in the SCN of tTA::miR-132 mice and that 2 weeks after return to *ad libitum* feeding on regular rodent chow, transgene expression in the SCN had not as yet reactivated, except for a few isolated cells (Figure 8B).

Collectively, the data indicate that upregulation of miR-132 expression in the SCN of adult mice attenuates light-induced resetting of behavioural rhythms. In addition, the data exclude the possibility that transgene overexpression during development (of ECFP or miR-132) are the cause for the phase-delaying phenotype. Moreover, these data are consistent with the previous report showing that knockdown of endogenous miR-132 expression in the SCN potentiates light-induced phase-shifting (130), consistent with the opposite in the overexpression model (this thesis). In summary, I have validated the

utility of these transgenic mouse models to probe the function of endogenous miR-132 and to further characterize the role of miR-132 in light-induced clock resetting.

iii. Bioinformatics analysis of predicted microRNA-132 targets

Once the behavioral analysis of the miR-132 transgenic mice was performed, I turned my focus on the identification of a short-list of candidate miR-132 target genes that may account for the effects of miR-132 on light-induced clock entrainment. I decided to interrogate three target prediction algorithms, TargetScan (www.targetscan.org; 150); miRanda (www.microrna.org; 151), and PicTar (pictar.mdcberlin.de; 152), based upon the criterion that the miR-132 MRE must be conserved across most vertebrate species. Preliminary studies identified more than 400 potential miR-132 targets (Table 2). At the time of analysis, MeCP2, an epigenetic modulator, was the only reported miR-132 target in neuronal primary cultures (148). Due to my previous experience in the MecP2 field and the fact that Rett Syndrome patients (caused by human *MECP2* mutations) show abnormal sleep patterns, I decided to investigate whether other chromatin remodeling factors were predicted to be miR-132 targets. Unexpectedly, I observed that many other chromatin-associated remodeling proteins were also predicted to be miR-132 targets, such as *Ep300*, *Jarid1a*, *H3f3b*, *H2A.Z*, *Sirt1* and *Dnmt3a* (Table 2).

This "miR-132-specific chromatin-associated gene cluster" led me to further investigate whether other functional clusters are predicted to be miR-132 targets. Indeed, I also observed that proteins involved in mRNA turnover/translational control were also potential miR-132 targets, such as *Btg2*, *Paip2a*, *Eif4a2*, *Eif5a2* and *Papola* (Table 2). A

After these preliminary observations, a more strict and detailed computational analysis was performed upon the functional annotations of the predicted targets, to

TABLE 2

Preliminary human microRNA-132 target prediction analysis using the miRecords (http://mirecords.biolead.org/) software (196). miRecords is a free web-resource for animal miRNA-target interactions which consists of two components. The *Validated Targets* component is a large, high-quality database of experimentally validated miRNA targets resulting from meticulous literature curation. The *Predicted Targets* component of miRecords is an integration of predicted miRNA targets produced by 11 established miRNA target prediction programs. I'm only showing the results for 6 selected prediction softwares. Note that this list was obtained in November 2008. Refseq: reference sequence number; Symbol: gene name; 1: interaction predicted; 0: no interaction predicted.

Refseq	Symbol	miranda	mirtarget2	pictar	pita	rnahybrid	targetscan
NM_001219	CALU	1	1	1	1	1	1
NM_001387	DPYSL3	1	1	1	1	1	1
NM_001429	EP300	1	1	1	1	1	1
NM_001945	HBEGF	1	1	1	1	1	1
NM_001967	EIF4A2	1	1	1	1	1	1
NM_002106	H2AFZ	1	1	1	1	1	1
NM_002235	KCNA6	1	1	1	1	1	1
NM_002515	NOVA1	1	1	1	1	1	1
NM_002687	PNN	1	1	1	1	1	1
NM_002719	PPP2R5C	1	1	1	1	1	1
NM_002787	PSMA2	1	1	1	1	1	1
NM_003042	SLC6A1	1	1	1	1	1	1
NM_003375	VDAC2	1	1	1	1	1	1
NM_004496	FOXA1	1	1	1	1	1	1
NM_004735	LRRFIP1	1	1	1	1	1	1
NM_004772	C5orf13	1	1	1	1	1	1
NM_005776	CNIH	1	1	1	1	1	1
NM_005841	SPRY1	1	1	1	1	1	1
NM_006305	ANP32A	1	1	1	1	1	1
NM_033030	BOLL	1	1	1	1	1	1
NM_080604	TJAP1	1	1	1	1	1	1
NM_139015	UNQ1887	1	1	1	1	1	1
NM_173475	DCUN1D3	1	1	1	1	1	1
NM_012238	SIRT1	1	1	1	1	1	1
NM_012460	TIMM9	1	1	1	1	1	1
NM_014279	OLFM1	1	1	1	1	1	1
NM_014764	DAZAP2	1	1	1	1	1	1
NM_015039	NMNAT2	1	1	1	1	1	1
NM_015057	MYCBP2	1	1	1	1	1	1

NM_015379	BRI3	1	1	1	1	1	1
NM_198859	PRICKLE2	1	1	1	1	1	1
NM_016018	PHF20L1	1	1	1	1	1	1
NM_016620	ZNF644	1	1	1	1	1	1
NM_016626	MEX3C	1	1	1	1	1	1
NM_017893	SEMA4G	1	1	1	1	1	1
NM_020177	FEM1C	1	1	1	1	1	1
NM_021012	KCNJ12	1	1	1	1	1	1
NM_021190	PTBP2	1	1	1	1	1	1
NM_021914	CFL2	1	1	1	1	1	1
NM_024659	GTDC1	1	1	1	1	1	1
NM_024920	DNAJB14	1	1	1	1	1	1
NM_020796	SEMA6A	0	1	1	1	1	1
NM_021705	NFYA	1	1	1	1	1	0
NM_022758	C6orf106	1	0	1	1	1	1
NM_024595	C1orf108	1	0	1	1	1	1
NM_024632	SAP30L	0	1	1	1	1	1
NM_031283	TCF7L1	1	0	1	1	1	1
NM_032186	ZNF644	1	1	1	1	1	0
NM_032246	MEX3B	1	0	1	1	1	1
NM_006599	NFAT5	1	0	1	1	1	1
NM_006763	BTG2	1	0	1	1	1	1
NM_006922	SCN3A	1	1	1	1	1	0
NM_006924	SFRS1	1	0	1	1	1	1
NM_006940	SOX5	0	1	1	1	1	1
NM_007038	ADAMTS5	1	0	1	1	1	1
NM_007294	BRCA1	1	0	1	1	1	1
NM_012247	SEPHS1	1	0	1	1	1	1
NM_012395	PFTK1	1	0	1	1	1	1
NM_012479	YWHAG	0	1	1	1	1	1
NM_013257	SGK3	1	1	1	1	1	0
NM_014217	KCNK2	1	1	1	1	1	0
NM_014250	HMG2L1	1	1	1	1	1	0
NM_014715	RICS	1	0	1	1	1	1
NM_014731	ProSAPiP1	1	0	1	1	1	1
NM_014784	ARHGEF11	1	0	1	1	1	1
NM_014795	ZEB2	0	1	1	1	1	1
NM_014850	SRGAP3	1	1	1	1	1	0
NM_014997	KIAA0265	1	0	1	1	1	1
NM_015059	TLN2	1	0	1	1	1	1
NM_015076	CDC2L6	0	1	1	1	1	1
NM_015094	HIC2	1	0	1	1	1	1

NM_015265	SATB2	1	0	1	1	1	1
NM_015271	TRIM2	1	0	1	1	1	1
NM_004036	ADCY3	1	0	1	1	1	1
NM_004470	FKBP2	1	0	1	1	1	1
NM_004501	HNRNPU	1	0	1	1	1	1
NM_004737	LARGE	1	0	1	1	1	1
NM_004992	MECP2	1	0	1	1	1	1
NM_005324	H3F3B	1	1	0	1	1	1
NM_005880	DNAJA2	1	0	1	1	1	1
NM_005941	MMP16	1	0	1	1	1	1
NM_006016	CD164	1	0	1	1	1	1
NM_006141	DYNC1LI2	0	1	1	1	1	1
NM_006186	NR4A2	1	0	1	1	1	1
NM_006315	PCGF3	1	0	1	1	1	1
NM_006352	ZNF238	1	0	1	1	1	1
NM_001029875	RGS7BP	1	1	0	1	1	1
NM_001033059	AMD1	1	1	0	1	1	1
NM_001033117	SRGAP3	1	1	0	1	1	1
NM_001033561	PHF12	1	1	0	1	1	1
NM_001033578	SGK3	1	1	0	1	1	1
NM_001039590	USP9X	1	1	0	1	1	1
NM_001040624	NCALD	1	1	0	1	1	1
NM_001043318	C14orf43	1	1	0	1	1	1
NM_001081676	SCN3A	1	1	0	1	1	1
NM_001395	DUSP9	1	0	1	1	1	1
NM_001455	FOXO3	1	0	1	1	1	1
NM_001634	AMD1	1	1	1	1	1	0
NM_002024	FMR1	1	0	1	1	1	1
NM_002505	NFYA	0	1	1	1	1	1
NM_002707	PPM1G	1	0	1	1	1	1
NM_002742	PRKD1	1	0	1	1	1	1
NM_002745	MAPK1	1	0	1	1	1	1
NM_002816	PSMD12	0	1	1	1	1	1
NM_002859	PXN	1	0	1	1	1	1
NM_002890	RASA1	0	1	1	1	1	1
NM_003106	SOX2	1	0	1	1	1	1
NM_003107	SOX4	1	0	1	1	1	1
NM_003108	SOX11	1	1	0	1	1	1
NM_003185	TAF4	1	0	1	1	1	1
NM_003262	SEC62	1	0	1	1	1	1
NM_003483	HMGA2	1	0	1	1	1	1
NM_003768	PEA15	1	0	1	1	1	1

NM_152556	FLJ31818	1	0	1	1	1	1
NM_152594	SPRED1	1	0	1	1	1	1
NM_152641	ARID2	1	1	0	1	1	1
NM_170706	NMNAT2	1	1	1	1	1	0
NM_170709	SGK3	1	1	1	1	1	0
NM_173491	LSM11	1	0	1	1	1	1
NM_178010	SOX5	1	1	1	1	1	0
NM_178830	C19orf47	1	0	1	1	1	1
NM_032632	PAPOLA	1	0	1	1	1	1
NM_032961	PCDH10	0	1	1	1	1	1
NM_033224	PURB	1	0	1	1	1	1
NM_033389	SSH2	1	0	1	1	1	1
NM_138288	C14orf147	1	0	1	1	1	1
NM_144664	FAM76B	0	1	1	1	1	1
NM_145043	NEIL2	0	1	1	1	1	1
NM_145239	PRRT2	1	0	1	1	1	1
NM_016076	FAM152A	1	0	1	1	1	1
NM_016185	HN1	1	1	1	1	1	0
NM_016396	CTDSPL2	1	0	1	1	1	1
NM_016480	PAIP2	1	1	1	1	1	0
NM_016577	RAB6B	1	0	1	1	1	1
NM_017508	SOX6	1	1	0	1	1	1
NM_017545	HAO1	1	0	1	1	1	1
NM_017637	BNC2	1	1	0	1	1	1
NM_017778	WHSC1L1	1	0	1	1	1	1
NM_017964	SLC30A6	1	0	1	1	1	1
NM_018638	ETNK1	1	1	0	1	1	1
NM_018945	PDE7B	1	0	1	1	1	1
NM_019606	MEPCE	1	0	1	1	1	1
NM_000891	KCNJ2	1	0	1	1	1	1
NM_001001433	STX16	1	0	1	1	1	1
NM_001002032	HN1	0	1	1	1	1	1
NM_001002033	HN1	1	1	1	1	1	0
NM_001003681	HMG2L1	0	1	1	1	1	1
NM_001003712	OSBPL8	0	1	1	1	1	1
NM_001004317	LIN28B	1	0	1	1	1	1
NM_001005210	LRRC55	1	0	1	1	1	1
NM_001009881	ZCCHC11	1	1	0	1	1	1
NM_001011666	CREB5	1	1	0	1	1	1
NM_194278	C14orf43	1	1	1	1	1	0
NM_198686	RAB15	1	0	1	1	1	1
NM_199327	SPRY1	1	1	1	1	1	0

NM_201269	ZNF644	1	1	1	1	1	0
NM_207362	C2orf55	1	0	1	1	1	1
NM_182688	UBE2G2	1	1	0	1	1	0
NM_182898	CREB5	1	1	0	1	1	0
NM_182899	CREB5	1	1	0	1	1	0
NM_183075	CYP2U1	1	1	0	1	1	0
NM_183238	ZNF605	1	1	0	1	1	0
NM_194328	RNF38	1	1	0	1	1	0
NM_194329	RNF38	1	1	0	1	1	0
NM_194330	RNF38	1	1	0	1	1	0
NM_194332	RNF38	1	1	0	1	1	0
NM_197941	ADAMTS6	0	0	1	1	1	1
NM_197970	BOLL	0	1	1	1	1	0
NM_198236	ARHGEF11	1	0	1	1	1	0
NM_198427	BCAN	1	0	0	1	1	1
NM_198551	MIA3	1	1	0	1	1	0
NM_199246	CCNG1	1	1	0	1	1	0
NM_199282	ARHGAP27	0	0	1	1	1	1
NM_199478	PLP1	1	1	0	1	1	0
NM_205768	ZNF238	1	0	1	1	1	0
NM_206594	ESRRG	1	1	0	1	1	0
NM_206595	ESRRG	1	1	0	1	1	0
NM_206840	NVL	1	1	0	1	1	0
NM_206854	QKI	0	0	1	1	1	1
NM_206855	QKI	1	0	1	1	1	0
NM_207174	ABCG1	1	1	0	1	1	0
NM_207363	NAP5	1	1	0	1	1	0
NM_207413	FAM150A	1	1	0	1	1	0
NM_207429	FLJ45803	0	0	1	1	1	1
NM_207481	NAP5	1	1	0	1	1	0
NM_207491	MGC48628	1	1	0	1	1	0
NM_207628	ABCG1	1	1	0	1	1	0
NM_207645	LOC399947	1	1	0	1	1	0
NM_212554	METTL10	1	1	0	1	1	0
NM_212558	TMEM215	0	0	1	1	1	1
NM_145893	A2BP1	0	0	1	1	1	1
NM_148174	AZIN1	1	1	0	1	1	0
NM_152330	FRMD6	1	1	0	1	1	0
NM_152332	TC2N	1	1	0	1	1	0
NM_152538	IGSF11	1	1	0	1	1	0
NM_152989	SOX5	0	1	1	1	1	0
NM_153207	AEBP2	0	0	1	1	1	1

NM_153828	RTN4	1	0	1	1	1	0
NM_172020	POM121	0	0	1	1	1	1
NM_172070	UBR3	0	0	1	1	1	1
NM_173083	LIN9	0	0	1	1	1	1
NM_173171	NR4A2	1	0	1	1	1	0
NM_173172	NR4A2	1	0	1	1	1	0
NM_173214	NFAT5	1	0	1	1	1	0
NM_173505	ANKRD29	1	1	0	1	1	0
NM_173536	GABRG1	1	1	0	1	1	0
NM_173561	UNC5CL	1	1	0	1	1	0
NM_173598	KSR2	1	0	0	1	1	1
NM_176815	DHFRL1	1	1	0	1	1	0
NM_177983	PPM1G	1	0	1	1	1	0
NM_178426	ARNT	1	1	0	1	1	0
NM_178586	PPP2R5C	0	1	1	1	1	0
NM_178864	NPAS4	0	0	1	1	1	1
NM_181742	ORC4L	1	1	0	1	1	0
NM_181861	APAF1	1	1	0	1	1	0
NM_181868	APAF1	1	1	0	1	1	0
NM_181869	APAF1	1	1	0	1	1	0
NM_003828	MTMR1	1	1	0	1	1	0
NM_003902	FUBP1	1	0	0	1	1	1
NM_003913	PRPF4B	0	1	0	1	1	1
NM_003930	SKAP2	1	1	0	1	1	0
NM_003972	BTAF1	1	1	0	1	1	0
NM_004124	GMFB	0	1	0	1	1	1
NM_004300	ACP1	1	1	0	1	1	0
NM_004330	BNIP2	0	0	1	1	1	1
NM_004392	DACH1	0	0	1	1	1	1
NM_004393	DAG1	0	0	1	1	1	1
NM_004458	ACSL4	0	0	1	1	1	1
NM_004609	TCF15	1	1	0	1	1	0
NM_004654	USP9Y	1	1	0	1	1	0
NM_004717	DGKI	1	1	0	1	1	0
NM_004726	REPS2	1	1	0	1	1	0
NM_004815	ARHGAP29	1	1	0	1	1	0
NM_004866	SCAMP1	1	1	0	1	1	0
NM_004904	CREB5	1	1	0	1	1	0
NM_005000	NDUFA5	1	1	0	1	1	0
NM_005197	FOXN3	1	0	1	1	1	0
NM_005316	GTF2H1	1	1	0	1	1	0
NM_005482	PIGK	1	1	0	1	1	0

NM_005487	HMG2L1	0	1	1	1	1	0
NM_005520	HNRNPH1	0	0	1	1	1	1
NM_005596	NFIB	1	0	0	1	1	1
NM_005605	PPP3CC	1	1	0	1	1	0
NM_005648	TCEB1	0	0	1	1	1	1
NM_005677	COLQ	1	0	1	1	1	0
NM_005722	ACTR2	1	1	0	1	1	0
NM_005808	CTDSPL	1	0	1	1	1	0
NM_005863	NET1	1	0	1	1	1	0
NM_005898	CAPRIN1	1	1	0	1	1	0
NM_005966	NAB1	1	1	0	1	1	0
NM_005968	HNRNPM	0	0	1	1	1	1
NM_006073	TRDN	1	1	0	1	1	0
NM_006079	CITED2	0	0	1	1	1	1
NM_006134	TMEM50B	1	1	0	1	1	0
NM_006164	NFE2L2	1	1	0	1	1	0
NM_006306	SMC1A	1	1	0	1	1	0
NM_006313	USP15	0	0	1	1	1	1
NM_006469	IVNS1ABP	1	1	0	1	1	0
NM_006489	NOVA1	0	1	1	1	1	0
NM_020774	MIB1	1	0	0	1	1	1
NM_020824	ARHGAP21	0	0	1	1	1	1
NM_020841	OSBPL8	0	1	1	1	1	0
NM_021260	ZFYVE1	0	0	1	1	1	1
NM_021643	TRIB2	0	0	1	1	1	1
NM_021965	PGM5	1	1	0	1	1	0
NM_021982	SEC24A	1	0	0	1	1	1
NM_022075	LASS2	0	0	1	1	1	1
NM_022138	SMOC2	1	1	0	1	1	0
NM_022367	SEMA4A	1	1	0	1	1	0
NM_022491	SUDS3	1	1	0	1	1	0
NM_022552	DNMT3A	0	0	1	1	1	1
NM_022650	RASA1	0	1	1	1	1	0
NM_022776	OSBPL11	0	0	1	1	1	1
NM_022781	RNF38	1	1	0	1	1	0
NM_024039	MIS12	1	1	0	1	1	0
NM_024294	C6orf106	1	0	1	1	1	0
NM_024311	MFSD11	1	1	0	1	1	0
NM_024345	WDR32	1	1	0	1	1	0
NM_024424	WT1	1	0	1	1	1	0
NM_024425	WT1	1	0	1	1	1	0
NM_024426	WT1	1	0	1	1	1	0

NM_024512	LRRC2	1	1	0	1	1	0
NM_024700	SNIP1	1	1	0	1	1	0
NM_024743	UGT2A3	1	1	0	1	1	0
NM_024945	RMI1	1	1	0	1	1	0
NM_025195	TRIB1	1	1	0	1	1	0
NM_025203	C2orf44	1	1	0	1	1	0
NM_030627	CPEB4	0	0	1	1	1	1
NM_030756	TCF7L2	0	0	1	1	1	1
NM_030895	ZNF696	1	1	0	1	1	0
NM_031203	HNRNPM	1	0	1	1	1	0
NM_031282	FCRL4	1	1	0	1	1	0
NM_031844	HNRNPU	1	0	1	1	1	0
NM_032041	NCALD	0	1	1	1	1	0
NM_032042	FAM172A	1	1	0	1	1	0
NM_032169	ACAD11	1	1	0	1	1	0
NM_032199	ARID5B	1	0	0	1	1	1
NM_006516	SLC2A1	1	1	0	1	1	0
NM_006654	FRS2	1	1	0	1	1	0
NM_006688	C1QL1	0	0	1	1	1	1
NM_006807	CBX1	0	0	1	1	1	1
NM_006813	PNRC1	1	1	0	1	1	0
NM_006851	GLIPR1	1	1	0	1	1	0
NM_006912	RIT1	1	1	0	1	1	0
NM_006920	SCN1A	1	0	0	1	1	1
NM_006947	SRP72	1	1	0	1	1	0
NM_007008	RTN4	0	0	1	1	1	1
NM_007042	RPP14	1	1	0	1	1	0
NM_007099	ACP1	1	1	0	1	1	0
NM_007158	CSDE1	0	1	1	1	1	0
NM_007296	BRCA1	1	0	1	1	1	0
NM_007298	BRCA1	1	0	1	1	1	0
NM_007299	BRCA1	1	0	1	1	1	0
NM_007300	BRCA1	1	0	1	1	1	0
NM_007302	BRCA1	1	0	1	1	1	0
NM_007303	BRCA1	1	0	1	1	1	0
NM_007305	BRCA1	1	0	1	1	1	0
NM_007345	ZNF236	1	1	0	1	1	0
NM_007353	GNA12	0	0	1	1	1	1
NM_012141	INTS6	1	1	0	1	1	0
NM_012154	EIF2C2	0	0	1	1	1	1
NM_013229	APAF1	1	1	0	1	1	0
NM_013390	TMEM2	0	0	1	1	1	1

NM_013393	FTSJ2	1	1	0	1	1	0
NM_014034	ASF1A	1	1	0	1	1	0
NM_014035	SNX24	1	1	0	1	1	0
NM_014317	PDSS1	1	0	1	1	1	0
NM_014319	LEMD3	1	1	0	1	1	0
NM_014423	AFF4	1	0	0	1	1	1
NM_014682	ST18	0	0	1	1	1	1
NM_014705	DOCK4	1	0	0	1	1	1
NM_014791	MELK	1	1	0	1	1	0
NM_015002	FBXO21	1	1	0	1	1	0
NM_015103	PLXND1	0	0	1	1	1	1
NM_015247	CYLD	1	1	0	1	1	0
NM_015250	BICD2	0	0	1	1	1	1
NM_015269	ZCCHC11	1	1	0	1	1	0
NM_015286	DMN	1	1	0	1	1	0
NM_015326	SRGAP2	1	1	0	1	1	0
NM_015332	NUDCD3	1	1	0	1	1	0
NM_015349	KIAA0240	1	0	0	1	1	1
NM_015368	PANX1	1	1	0	1	1	0
NM_001106	ACVR2B	0	1	0	1	1	1
NM_001227	CASP7	1	1	0	1	1	0
NM_001270	CHD1	1	0	0	1	1	1
NM_001415	EIF2S3	1	1	0	1	1	0
NM_001438	ESRRG	1	1	0	1	1	0
NM_001537	HSBP1	1	1	0	1	1	0
NM_001668	ARNT	1	1	0	1	1	0
NM_001964	EGR1	1	1	0	1	1	0
NM_002030	FPR3	1	1	0	1	1	0
NM_002074	GNB1	0	0	1	1	1	1
NM_002202	ISL1	0	0	1	1	1	1
NM_002207	ITGA9	0	0	1	1	1	1
NM_002424	MMP8	1	1	0	1	1	0
NM_002480	PPP1R12A	0	0	1	1	1	1
NM_002552	ORC4L	1	1	0	1	1	0
NM_002657	PLAGL2	0	0	1	1	1	1
NM_002807	PSMD1	1	1	0	1	1	0
NM_002906	RDX	0	0	1	1	1	1
NM_002968	SALL1	0	1	0	1	1	1
NM_003045	SLC7A1	1	1	0	1	1	0
NM_003270	TSPAN6	1	1	0	1	1	0
NM_003298	NR2C2	1	1	0	1	1	0
NM_003318	TTK	1	1	0	1	1	0

NM_003325	HIRA	1	1	0	1	1	0
NM_003343	UBE2G2	1	1	0	1	1	0
NM_003588	CUL4B	1	1	0	1	1	0
NM_003649	DDO	1	1	0	1	1	0
NM_003663	CGGBP1	1	1	0	1	1	0
NM_003692	TMEFF1	0	0	1	1	1	1
NM_003763	STX16	1	0	1	1	1	0
NM_001015887	IGSF11	1	1	0	1	1	0
NM_001017424	KCNK2	0	1	0	1	1	1
NM_001017969	KIAA2026	1	0	0	1	1	1
NM_001024466	SOD2	1	1	0	1	1	0
NM_001029884	PLEKHG1	1	1	0	1	1	0
NM_001031623	ZNF451	1	1	0	1	1	0
NM_001031723	DNAJB14	1	1	0	1	1	0
NM_001031804	MAF	1	0	0	1	1	1
NM_001032999	CBFA2T2	1	0	0	1	1	1
NM_001033025	EXTL2	1	1	0	1	1	0
NM_001033112	PAIP2	0	1	0	1	1	1
NM_001037293	PALM2	1	0	0	1	1	1
NM_001039591	USP9X	1	1	0	1	1	0
NM_001039937	INTS6	1	1	0	1	1	0
NM_001040285	PAPD5	1	1	0	1	1	0
NM_001040625	NCALD	1	1	0	1	1	0
NM_001040626	NCALD	1	1	0	1	1	0
NM_001040627	NCALD	1	1	0	1	1	0
NM_001040628	NCALD	1	1	0	1	1	0
NM_001040629	NCALD	1	1	0	1	1	0
NM_001040630	NCALD	1	1	0	1	1	0
NM_001042355	CYLD	1	1	0	1	1	0
NM_001042412	CYLD	1	1	0	1	1	0
NM_001042481	FRMD6	1	1	0	1	1	0
NM_001042555	FRS2	1	1	0	1	1	0
NM_001042603	JARID1A	1	0	0	1	1	1
NM_001047160	NET1	1	0	0	1	1	1
NM_001076786	QSER1	1	1	0	1	1	0
NM_001077619	LOC137886	1	1	0	1	1	0
NM_001079867	PXMP3	1	1	0	1	1	0
NM_001079872	CUL4B	1	1	0	1	1	0
NM_001080393	GLT8D4	1	1	0	1	1	0
NM_001080517	SETD5	0	1	0	1	1	1
NM_001080975	REPS2	1	1	0	1	1	0
NM_001083	PDE5A	1	1	0	1	1	0

NM_000202	IDS	1	1	0	1	1	0
NM_000240	MAOA	1	1	0	1	1	0
NM_000264	PTCH1	0	0	1	1	1	1
NM_000318	PXMP3	1	1	0	1	1	0
NM_000332	ATXN1	0	0	1	1	1	1

investigate whether miR-132 preferentially targets chromatin- and translation-associated proteins, compared to other vertebrate miRNAs. Predicted miRNA targets were obtained from TargetScan (release 5.1, April 2009), which predicts biological targets of miRNAs upon the presence of conserved sites that match the seed region of the miRNA. The analysis was restricted to the set of miRNAs belonging to the same family as miR-132, i.e. conserved across most vertebrate species. From these, miRNAs with 50 or more predicted conserved targets were further interrogated. The Gene Ontology (GO) annotations from the Mouse Genome Informatics (MGI) database were used. For each miRNA, the frequency of its conserved targets that are annotated with GO terms "chromatin modification" (GO:0016568) and/or "chromatin assembly or disassembly" (GO:0006333) or any of their children terms in the ontology were analyzed. The results showed that miR-132 is highly enriched for conserved target genes that are involved in chromatin function (Figure 9A & Table 3), suggesting that miR-132 may be preferentially involved in the regulation of this physiological process via coordinated modulation of these targets. Out of 78 miRNAs analyzed, miR-132 had the third highest percentage of chromatin-related targets. Interestingly, miR-194, with the highest percentage of chromatin-related targets, shares a significant overlap of predicted targets with miR-132. An analogous study was carried out for occurrences of GO term "translation" (GO: 0006412) and its children terms in the ontology. miR-132 is ranked eighth amongst 78 miRNAs, indicating that translation-associated genes are more abundant than average for miR-132 (Figure 9B & Table 4), further suggesting that miR-132 may be preferentially involved in the regulation of this physiological process via coordinated modulation of these targets.

FIGURE 9

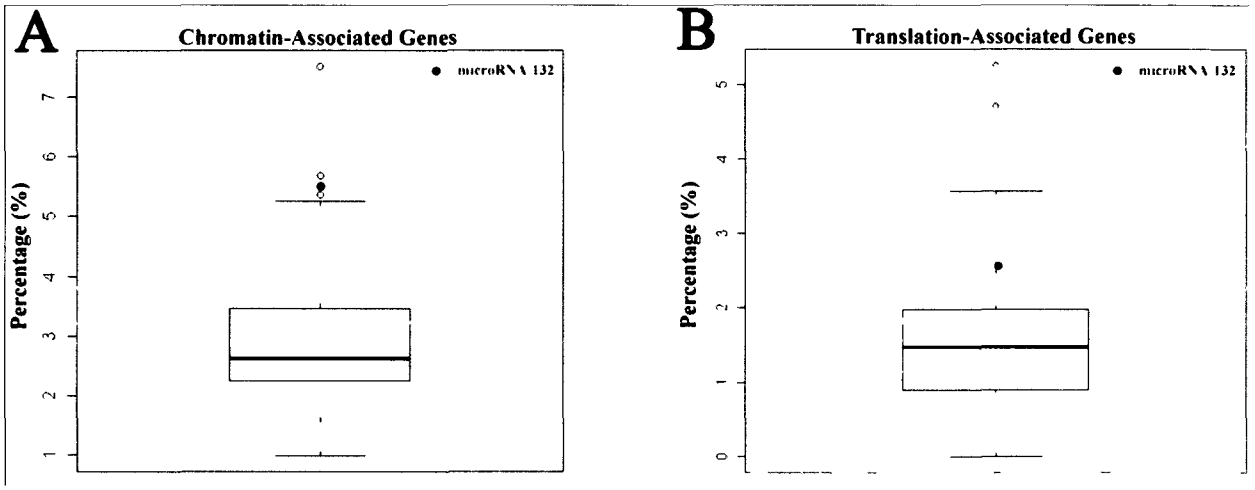

Figure 9. Computational analysis on the functional annotations of mmu-miR-132 predicted targets.

(A) Box plot of the percentage distribution of predicted miRNA targets with putative chromatin-related functionality. The red dot shows miR-132 (5.5%) as an extreme point (average = 2.97% ± 1.19). **(B)** Box plot of the percentage distribution of conserved miRNA targets that are involved in translational-related functionality. The red dot shows miR-132 (2.5%) well above the upper quartile (upper quartile = 1.96%; average = 1.54% ± 0.93). See Tables 1 and 2 for the complete lists of analyzed miRNAs and target percentage distribution. Dr. Carolina Perez-Iratxeta (Ottawa Health Research Institute; OHRI) designed and performed the computational analysis under the request of MAS & HYMC. CPI generated the figure and wrote the figure legend. This figure and figure legend are reproduced from the manuscript Alvarez-Saavedra et al, circa March 2010.

TABLE 3

Percentage of conserved miRNA target genes that are involved in chromatin-related functions for miRNAs of the same phylogenetic distribution as miR-132. The average percentage of chromatin-related genes among miRNA targets is equal to 2.97% ± 1.19. miR-132 is third on the list from 78 miRNAs with an abundance equal to 5.50%.

micro-RNA (miR)	# of conserved targets	# of chromatin-related targets	% abundance of chromatin-related targets
miR-194	173	13	7.51
miR-129/129-5p	229	13	5.68
miR-132/212	200	11	5.50
miR-216/216b	112	6	5.36
miR-22	228	12	5.26
miR-142-3p	200	10	5.00
miR-7/7ab	224	11	4.91
miR-192/215	65	3	4.62
miR-101	415	19	4.58
miR-193ab	110	5	4.55
miR-196ab	156	7	4.49
miR-365	134	6	4.48
miR-223	135	6	4.44
miR-140/140-5p/876-3p	158	7	4.43
miR-499/499-5p	148	6	4.05
miR-31	182	7	3.85
miR-150	106	4	3.77
miR-139-5p	167	6	3.59
miR-128	626	22	3.51
miR-425/489	86	3	3.49
miR-181	639	22	3.44
miR-130/301	498	17	3.41
miR-27ab	741	25	3.37
miR-29abc	664	21	3.16
miR-106/302	417	13	3.12
miR-26ab/1297	516	16	3.10
miR-30a/30a-5p/30b/30b-5p/30cde/384-5p	871	27	3.10
miR-218	564	17	3.01
miR-138	299	9	3.01
miR-1/206	436	13	2.98

miR-203	369	11	2.98
miR-144	439	13	2.96
miR-503	204	6	2.94
miR-383	69	2	2.90
miR-21/590-5p	143	4	2.80
miR-200bc/429	609	17	2.79
miR-103/107	324	9	2.78
miR-10	146	4	2.74
miR-24	304	8	2.63
miR-155	190	5	2.63
miR-141/200a	385	10	2.60
miR-143	155	4	2.58
miR-183	234	6	2.56
miR-9	742	19	2.56
miR-219/219-5p	237	6	2.53
miR-23ab	556	14	2.52
miR-205	202	5	2.48
miR-204/211	284	7	2.46
miR-15/16/195/424/497	690	17	2.46
miR-148/152	368	9	2.45
miR-214/761	291	7	2.41
miR-208/208ab	84	2	2.38
miR-137	678	16	2.36
miR-146	85	2	2.35
miR-133	384	9	2.34
miR-25/32/92/92ab/363/367	522	12	2.30
miR-135	395	9	2.28
miR-182	615	14	2.28
miR-153	451	10	2.22
miR-19	679	15	2.21
miR-338/338-3p	137	3	2.19
miR-34a/34b-5p/34c/34c-5p/449/449abc/699	324	7	2.16
miR-96/1271	605	13	2.15
miR-199/199-5p	245	5	2.04
miR-17-5p/20/93.mr/106/519.d	742	15	2.02
miR-217	149	3	2.01
miR-216/216a	102	2	1.96
miR-221/222	214	4	1.87
miR-124/506	1047	18	1.72

miR-125/351	472	8	1.69
miR-33/33ab	179	3	1.68
let-7/98	683	11	1.61
miR-18ab	125	2	1.60
miR-490/490-3p	68	1	1.47
miR-145	346	5	1.45
miR-190	76	1	1.32
miR-122	83	1	1.20
miR-375	101	1	0.99

TABLE 4

Percentage of conserved miRNA target genes that are involved in translational control-related functions for miRNAs of the same phylogenetic distribution as miR-132. The average percentage of translational control-related genes among miRNA targets is equal to 1.54% ± of 0.93. miR-132 is eighth from 78 miRNAs with an abundance equal to 2.50%.

micro-RNA (miR)	# of conserved targets	# of translation-related targets	% abundance of translation-related targets
miR-190	76	4	5.26
miR-146	85	4	4.71
miR-208/208ab	84	3	3.57
miR-22	228	7	3.07
miR-383	69	2	2.90
miR-21/590-5p	143	4	2.80
miR-7/7ab	224	6	2.68
miR-132/212	200	5	2.50
miR-205	202	5	2.48
miR-18ab	125	3	2.40
miR-139-5p	167	4	2.40
miR-221/222	214	5	2.34
miR-365	134	3	2.24
miR-223	135	3	2.22
miR-130/301	498	11	2.21
miR-148/152	368	8	2.17
miR-499/499-5p	148	3	2.03
miR-138	299	6	2.01
miR-153	451	9	2.00
miR-24	304	6	1.97
miR-196ab	156	3	1.92
miR-106/302	417	8	1.92
let-7/98	683	13	1.90
miR-150	106	2	1.89
miR-17-5p/20/93.mr/106/519.d	742	14	1.89
miR-144	439	8	1.82
miR-193ab	110	2	1.82
miR-96/1271	605	11	1.82
miR-204/211	284	5	1.76
miR-25/32/92/92ab/363/367	522	9	1.72
miR-101	415	7	1.69
miR-33/33ab	179	3	1.68

miR-31	182	3	1.65
miR-182	615	10	1.63
miR-137	678	11	1.62
miR-19	679	11	1.62
miR-128	626	10	1.60
miR-125/351	472	7	1.48
miR-200bc/429	609	9	1.48
miR-490/490-3p	68	1	1.47
miR-338/338-3p	137	2	1.46
miR-10	146	2	1.37
miR-27ab	741	10	1.35
miR-15/16/195/424/497	690	9	1.30
miR-133	384	5	1.30
miR-140/140-5p/876-3p	158	2	1.27
miR-219/219-5p	237	3	1.27
miR-181	639	8	1.25
miR-124/506	1047	13	1.24
miR-9	742	9	1.21
miR-26ab/1297	516	6	1.16
miR-30a/30a-5p/30b/30b-5p/30cde/384-5p	871	10	1.15
miR-1/206	436	5	1.15
miR-375	101	1	0.99
miR-216/216a	102	1	0.98
miR-503	204	2	0.98
miR-103/107	324	3	0.93
miR-29abc	664	6	0.90
miR-23ab	556	5	0.90
miR-129/129-5p	229	2	0.87
miR-145	346	3	0.87
miR-183	234	2	0.85
miR-203	369	3	0.81
miR-141/200a	385	3	0.78
miR-135	395	3	0.76
miR-218	564	4	0.71
miR-217	149	1	0.67
miR-143	155	1	0.65
miR-34a/34b-5p/34c/34c-5p/449/449abc/699	324	2	0.62
miR-194	173	1	0.58
miR-155	190	1	0.53
miR-142-3p	200	1	0.50
miR-199/199-5p	245	1	0.41
miR-214/761	291	1	0.34

miR-122	83	0	0.00
miR-192/215	65	0	0.00
miR-216/216b	112	0	0.00
miR-425/489	86	0	0.00

iv. In-vitro analysis of microRNA-132 MREs

In order to further determine whether these predicted chromatin- and translation-associated targets are indeed miR-132 targets, I analyzed the functionality of the predicted miR-132 response elements within the 3'UTRs of *Ep300*, *Jarid1a*, *Mecp2*, *Btg2* and *Paip2a* (Figure 10A). These targets were selected based on the published available data identifying 1) their brain expression; and 2) their potential roles in the clock timing process (further discussed below). In order to determine whether miR-132 regulates the expression of *Ep300*, *Jarid1a*, *Mecp2*, *Btg2* and *Paip2a* via their predicted miR-132 MREs, I designed and generated firefly luciferase reporter constructs bearing the full-length wild-type 3'UTR of the various genes, or a full-length mutant 3'UTR containing a 7-bp deletion of the seed sequence (Figure 10A). Except for *Paip2a*, a 2-nucleotide mismatch within the seed sequence was used, since the 7-bp deletion resulted in a significant deterioration of basal firefly luciferase activity relative to the wild-type construct. N2A cells were transfected with each of the reporter constructs in combination with a synthetic miR-132 "mimic" (double-stranded ~22-bp RNA oligonucleotides that mimics endogenous mature miRNA function) or a "microRNA negative control" (dsRNA oligonucleotides that have no complementarity to any known sequence in the human, rat or mouse genome). Co-transfection with the microRNA negative control had no discernible effect on luciferase activity, compared with cells that had been co-transfected with an equivalent amount of pcDNA3.1 empty vector. As an additional control, I transfected N2A cells with the backbone firefly luciferase construct pGL3-Control, which lacks a miR-132 MRE site, in combination with the miR-132 mimic or the miRNA

FIGURE 10

A

Gene	Conservation	3'-UTR Position	Target Site	Seed Match	Prediction Software
JARID1A	M/H/R/D/O	Site #1 1171-1177	5 AUGUCJCUGACUACU...C 3 (UTR) 3 GCUGGUACCGACAU CUGACAA U 5 (mmu-miR132)	7mer-m8	T/Z
JARID1A	M/H/R/D/O	Site #2 1240 1246	5'UAUAUAUAUAUAUUU...C 3' (UTR) 3 GCUGGUACCGACAU CUGACAA U 5 (mmu-miR132)	7mer 1A	T/Z
MeCP2	M/H/R/D/O	6949-6955	5'ACCAAAUAUCACCAG...3 (UTR) 3 GCUGGUACCGACAU CUGACAA U 5 (mmu-miR132)	8mer	T/Z/M/P
EP300	M/H/R/D/O	1034 1040	5 UUGGAUCA...UA...3 (UTR) 3 GCUGGUACC GACAU CUGACAA U 5 (mmu-miR132)	8mer	T/Z/M/P
BTG2	M/H/R/D/O	1834 1840	5 ACCCUAGA GCUG GACUGUU G 3 (UTR) 3 GCUGGUAC CGAC AU CUGACAA U 5 (mmu-miR132)	7mer-m8	T/Z/M/P
PAIP2A	M/H/R/D/O	148-154	5' UAAUAAAAGU A ...3' (UTR) 3 GCUGGUAC CGAC AU CUGACAA U 5 (mmu-miR132)	8mer	T/Z/M/P

B

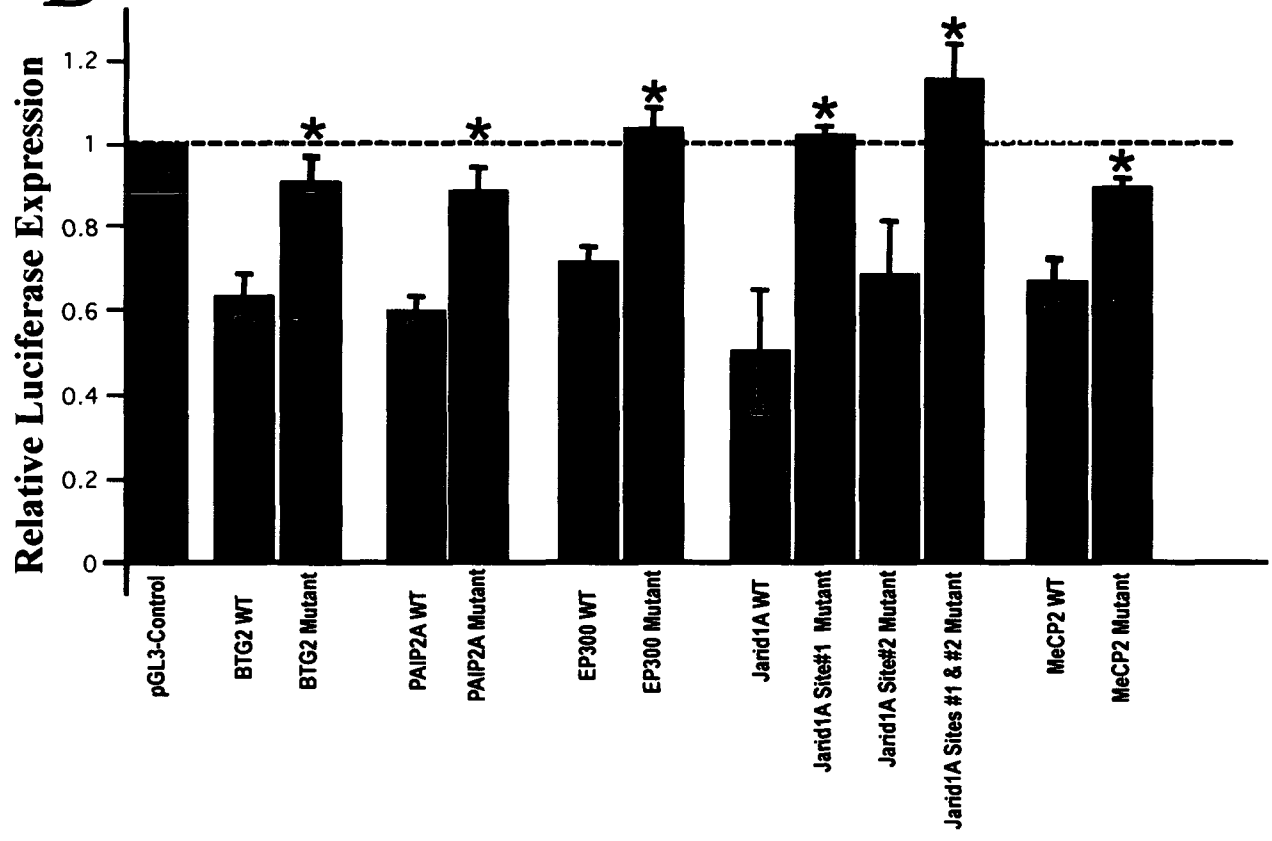

Figure 10. miR-132 response element (MRE) conservation across mammalian species of five selected mRNA targets and *in-vitro* validation of predicted mmu-miR-

132 MREs. **(A)** Table of miR-132 recognition elements (MREs) within the 3'UTRs of murine *Jarid1a*, *Mecp2*, *Ep300*, *Btg2* and *Paip2a*. *Conservation:* Seed site conservation across mammalian species (M, mouse; H, human; R, rat; D, dog; O, opossum). *3'-UTR Position:* Position of predicted miR-132 MREs within the 3'UTR (first nucleotide after the stop codon is denoted as position 1). *Target site:* alignment of the 3'UTR and miR-132. Nucleotides in purple (3'-UTR) and blue (miR-132) indicate complementarity. Mutant 3'UTRs were generated by deletion of the underlined nucleotides. For *Paip2a*, the underlined nucleotides were mutated via a C→G or G→C conversion. *Prediction software:* Predicted as a target of mmu-miR-132 based on the following target prediction algorithms (as of April 2009): T, TargetScan; Z, MirZ; M, miRanda; P, PicTar. **(B)** miR-132 mediates 3'UTR-dependent repression of luciferase reporter activity via specific miR-132 MREs. N2A cells were transfected with luciferase reporter constructs carrying the full-length wild-type (WT, red bars) or mutant 3'UTRs (mutant, blue bars) of *Btg2*, *Paip2a*, *Ep300*, *Jarid1a* and *Mecp2* in combination with synthetic miR-132 Mimic or a miRNA Mimic Negative Control. Renilla luciferase activity was used as an internal transfection control and was used to normalize raw firefly luciferase (FL) values. Control transfections using the backbone pGL3-Control (pGL3-CT) vector (no 3'-UTR) in combination with miR-132 Mimic, miRNA Mimic Negative Control or pcDNA3.1 empty vector were used to assess non-specific effects of miR-132 on a reporter construct that lacks a miR-132 target site, as well as potential effects of the Negative Control on luciferase activity. Values on the y-axis indicate relative luciferase activity = (UTR_{mimic}/UTR_{neg}) divided by ($pGL3\text{-}C_{mimic}/pGL3\text{-}CT_{neg}$), where UTR and pGL3-CT denote samples transfected with the 3'UTR reporter or the backbone pGL3-CT vector, respectively. Black bar denotes control transfection using pGL3-CT and is normalized to 1. Error bars represent the standard deviation from triplicate determinations of a single representative experiment. Consistent results were obtained from 3 independent experiments. In all cases, the relative luciferase activities of constructs bearing WT 3'UTRs were significantly reduced relative to control (black bar) and, with the exception of site #2 within the *Jarid1a* 3'UTR, mutation of the predicted target sites provided nearly complete rescue. $*p<0.05$ vs. WT 3'UTR (two-tailed Student's t-test and one-way ANOVA). This figure and figure legend are reproduced from the manuscript Alvarez-Saavedra et al, circa November 2009. Molecular cloning, luciferase assays and data analysis jointly performed by MAS & HYMC. Table and figure design performed by MAS.

Negative Control. In this case, co-transfection of the miR-132 mimic, but not the miRNA Negative Control, caused a subtle (~5-10%) reduction of luciferase activity, which was attributed as a non-sequence-specific effect of miR-132 overexpression *in-vitro*. Most importantly, the luciferase activity of the wild-type 3'UTR constructs of all genes examined was significantly repressed by the miR-132 mimic, with a range of repression between 28% and 50% (Figure 10B). In all cases except for *Jarid1a*, the effects of the miR-132 mimic were abolished by the mutation of the seed site (Figure 10B). For *Jarid1a*, which bears 2 putative miR-132 MREs within its 3'UTR, mutation of the first MRE (site 1), but not the second (site 2), abolished the repressive effects of the miR-132 mimic (Figure 10B). Collectively, the data indicate that all of the predicted *in-silico* targets of miR-132 reported herein can be repressed *in vitro* by miR-132 *via* specific miR-132 MRE sequences within their 3'UTRs.

v. In-vitro knockdown of microRNA-132

In order to further support the data that *Ep300*, *Jarid1a*, *Mecp2*, *Btg2* and *Paip2a* are miR-132 targets, endogenous mature miR-132 was inhibited in N2A cells with a mouse miR-132 hairpin inhibitor. 24-hrs post-transfection with the miR-132 inhibitor, all candidate target genes showed an upregulation at the protein level compared to cells transfected with a negative control inhibitor (i.e. an inhibitor with unmatched mouse, human or rat sequence; Figure 11) as well as mock-transfected cells. These data further argue that *Mecp2*, *Ep300*, *Jarid1a*, *Btg2* and *Paip2a* are indeed *bona fide* miR-132 targets.

vi. in-vivo knockdown of microRNA-132 in the mouse SCN

FIGURE 11

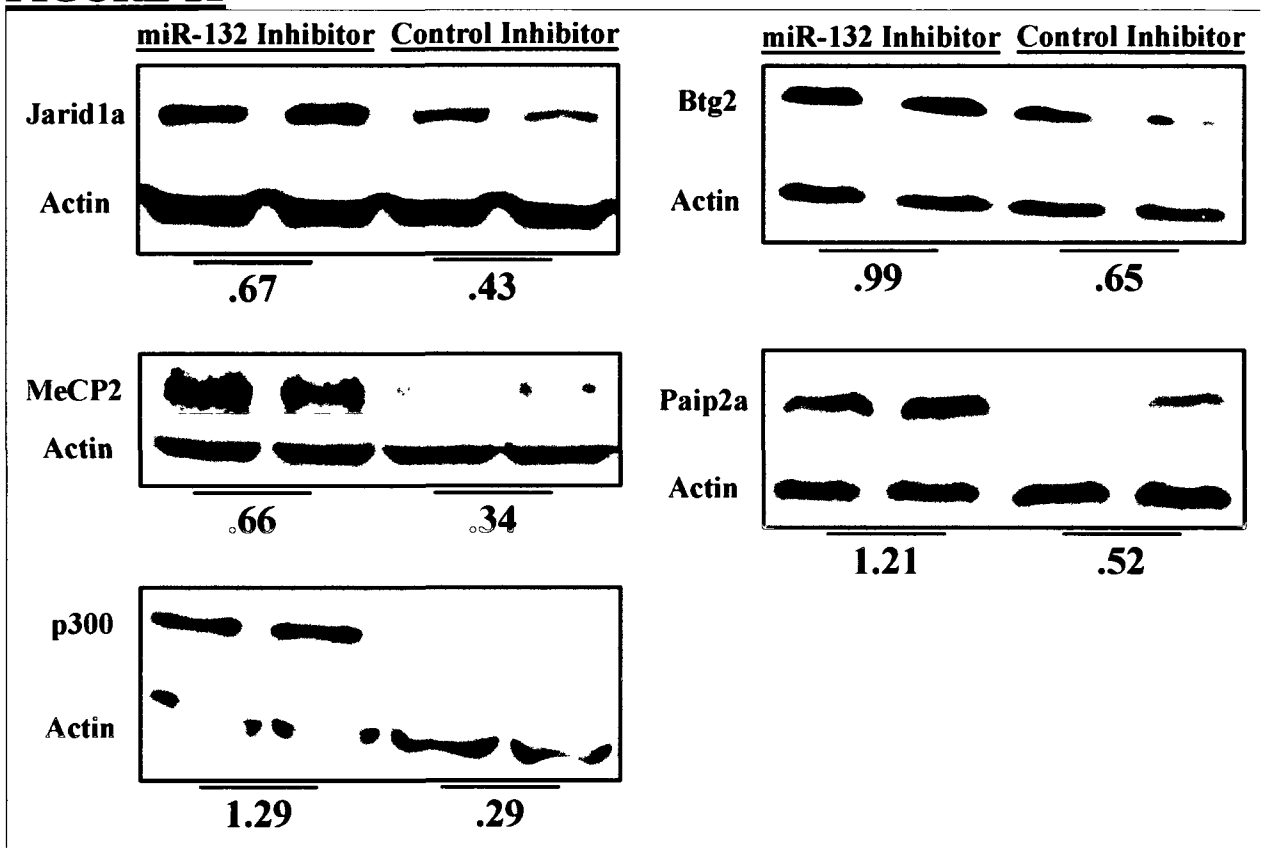

Figure 11. *in-vitro* miR-132 knockdown upregulates JARID1A, MeCP2, p300, BTG2 and PAIP2A protein levels.

JARID1A, MeCP2, p300, BTG2 and PAIP2A protein levels in N2A cells following transient knockdown of endogenous miR-132 expression as determined by Western blotting. N2A cells were transiently transfected with miR-132 hairpin inhibitors (lanes 1 and 2) to knock down miR-132 expression or a microRNA hairpin inhibitor negative control (lanes 3 and 4). Twenty-hour hours post-transfection, cells were harvested and analyzed via western blotting. β-actin expression served as loading control. Values presented below each blot represent the mean relative abundance of the protein examined, normalized to actin expression, for each transfection condition. Three independent experiments were performed, and similar results were obtained. Images quantitated on grayscale with ImageJ software. This figure and figure legend are reproduced from the manuscript Alvarez-Saavedra et al, circa March 2010. Experimental design and execution performed by MAS & HYMC. Quantitations and figure design performed by MAS.

Using an *in-vivo* knockdown approach, I further investigated whether *Ep300*, *Jarid1a*, *Mecp2*, *Btg2* and *Paip2a* are miR-132 targets in the mouse SCN. To this end, C57Bl/6 (wild-type) mice received an intracerebroventricular infusion of a miR-132 antagomir at CT 15 (Figure 12A), and 24-hrs later treated with a brief light pulse (15 min, 100 lux) at CT 15 in order to induce endogenous miR-132 expression (130). Target protein expression in the SCN 8-hrs post-light treatment was examined via western blotting. Compared with mice that had received infusions of either miR-219 or miR-1 antagomirs, or vehicle control, miR-132-infused mice exhibited an upregulation of all 5 proteins examined (Figure 12B). These data further support the *in-vitro* experiments suggesting that *Ep300*, *Jarid1a*, *Mecp2*, *Btg2* and *Paip2a* are indeed miR-132 targets in the mouse brain and further suggest that these targets themselves may play a role in light-induced clock resetting.

vii. microRNA-132 target analysis in microRNA-132 transgenic mice

As a last step to further support the *in-vitro* and *in-vivo* data suggesting that *Ep300, Jarid1a, Mecp2, Btg2* and *Paip2a* are indeed miR-132 targets in the mouse SCN, the expression of these 5 targets was analyzed via western blotting and immunolabeling in the SCN of tTA::miR-132 mice. To this end, I will briefly describe the known functional role(s) of each of these proteins.

The role of *EP300* (E1A-binding protein, 300kD) and its homolog, *CBP* (CREB-binding protein), in transcriptional regulation has been extensively documented (153 and references therein). These factors interact with a multitude of transcription factors, including CREB, as well as components of the general transcriptional machinery, to activate or repress gene transcription. Additionally, both p300 and CBP have been

FIGURE 12

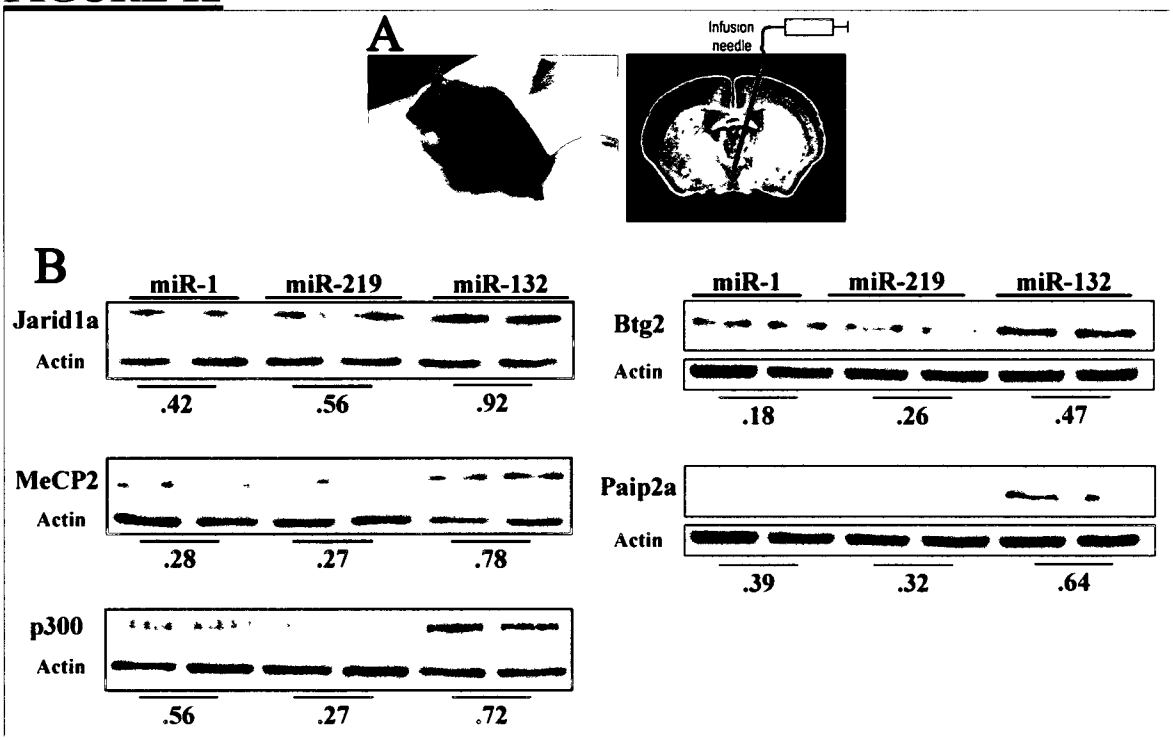

Figure 12. *in-vivo* miR-132 knockdown in the mouse SCN upregulates JARID1A, MeCP2, p300, BTG2 and PAIP2A protein levels.

(A) Photograph of post-surgery freely-moving cannulated mice (*left*) and schematic diagram illustrating stereotaxic-mediated antagomir infusions into the third ventricle of the mouse brain (*right*). **(B)** The effect of antagomir-mediated knockdown of endogenous miR-132 on the expression of JARID1A, MeCP2, p300, BTG2 and PAIP2A in the mouse SCN. C57Bl/6J mice were dark-adapted for 2 days and then infused with miR-132 antagomir (100 μM in 3 μl), miR-1 antagomir (100 μM in 3μl, miR-219 antagomir (100 μM in 3 μl) or saline (3 μl; data not shown) into the lateral ventricles at CT 15. The following day mice received a brief light pulse (15 min, 100 lux) at CT 15 to induce miR-132 endogenous expression, and 8 hours later (CT23) SCN tissue was harvested for analysis of protein expression via Western blotting. β-actin expression served as the loading control. Values presented below each blot represent the mean relative abundance of the protein examined, normalized to actin expression, for each genotype. n=10 mice per treatment condition, grouped in pools of 2. Images quantitated on grayscale with ImageJ software. Panel A borrowed from Dr. Hai-Ying Mary Cheng's lectures, 2010. Panel B and its corresponding legend are reproduced from the manuscript Alvarez-Saavedra et al, circa March 2010. For panel B, stereotaxic (surgical) cannulations were performed by Heather Dziema at Ohio State University, USA. Light treatment and dissection of SCN were performed jointly by Heather Dziema and Dr. Karl Obrietan. SCN tissue samples were shipped to Ottawa. Experimental paradigms designed jointly by MAS and HYMC. Western blots performed by MAS & HYMC. Quantitations and figure design performed by MAS.

implicated in chromatin remodeling, as they possess intrinsic acetyltransferase activity, and have been shown to acetylate histones as well as other proteins. The observation that p300 physically associates with CLOCK and promotes CLOCK/BMAL1-mediated transcription in the liver (80), together with evidence that the promoters of several core clock genes exhibit circadian rhythms in H3 acetylation, provide strong support for a role of p300 in circadian clock function in peripheral oscillators. Via western blotting and immunohistochemistry, a marked decrease in p300 protein levels was found in the SCN of tTA::miR-132 mice compared with non-transgenic controls at CT 16 via western blotting and immunohistochemistry (Figures 13 & Figure 14C), a time when endogenous miR-132 expression is at its nadir (130).

Jarid1A (jumonji, AT-rich interactive domain 1A) and other members of the *Jarid1* family are histone demethylases that specifically remove a methyl group from lysine 4 of the tri- (H3K4Me3)- and di (H3K4Me2)-methylated forms of H3 (154). As part of the "histone code" (155), the H3K4Me3 and H3K4Me2 marks are generally associated with sites of active transcription. H3K4Me3/Me2 may facilitate transcription by recruiting additional chromatin remodeling factors or histone modifying enzymes, or by impeding the binding of transcriptional repressors. While there are no reports that directly implicate *Jarid1a* in circadian clock processes, the promoter of the clock-regulated gene, *Dbp*, exhibits circadian rhythms in H3K4- trimethylation (81). As expected, overexpression of miR-132 resulted in diminished levels of JARID1A in the SCN of miR-132 mice as measured via western blotting and immunohistochemistry (Figures 13 & Figure 14D). Interestingly, decreased expression of JARID1A in the SCN of tTA::miR-132 transgenic mice was accompanied by a concomitant increase in H3K4Me3 immunoreactivity

FIGURE 13

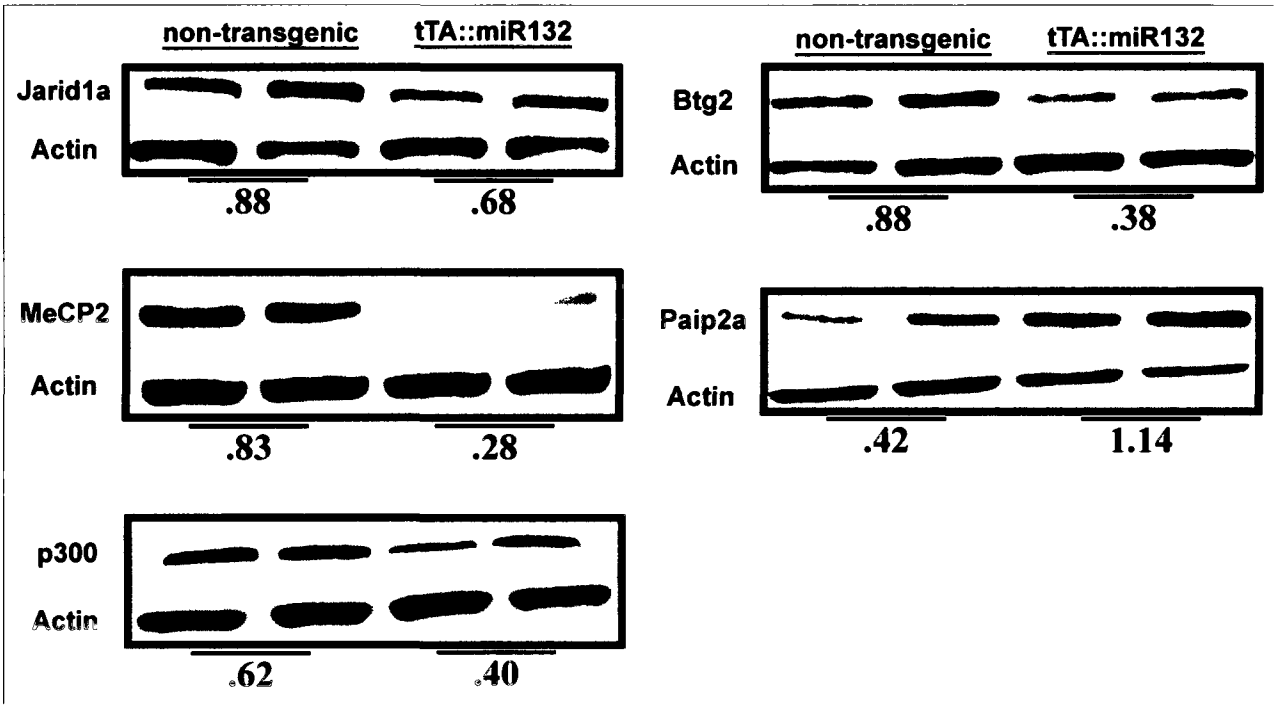

Figure 13. miR-132 overexpression in the SCN affects JARID1A, MeCP2, p300, BTG2 and PAIP2A protein levels.
JARID1A, MeCP2, p300, BTG2 and PAIP2A protein expression in the SCN of tTA::miR-132 transgenic mice (lanes 3 and 4) and non-transgenic controls (lanes 1 and 2) as determined by Western blotting. β-actin expression served as loading control. Values presented below each blot represent the mean relative abundance of the protein examined, normalized to actin expression, for each genotype. Note that PAIP2A levels are upregulated via miR-132 overexpression (see text for discussion). n = 4 mice per genotype, grouped in pools of 2. Images quantitated on grayscale with ImageJ software. This figure and figure legend are reproduced from the manuscript Alvarez-Saavedra et al, circa November 2009. Experimental design and tissue harvesting jointly performed by MAS & HYMC. Western blots performed by MAS. Quantitations and figure design performed by MAS.

FIGURE 14

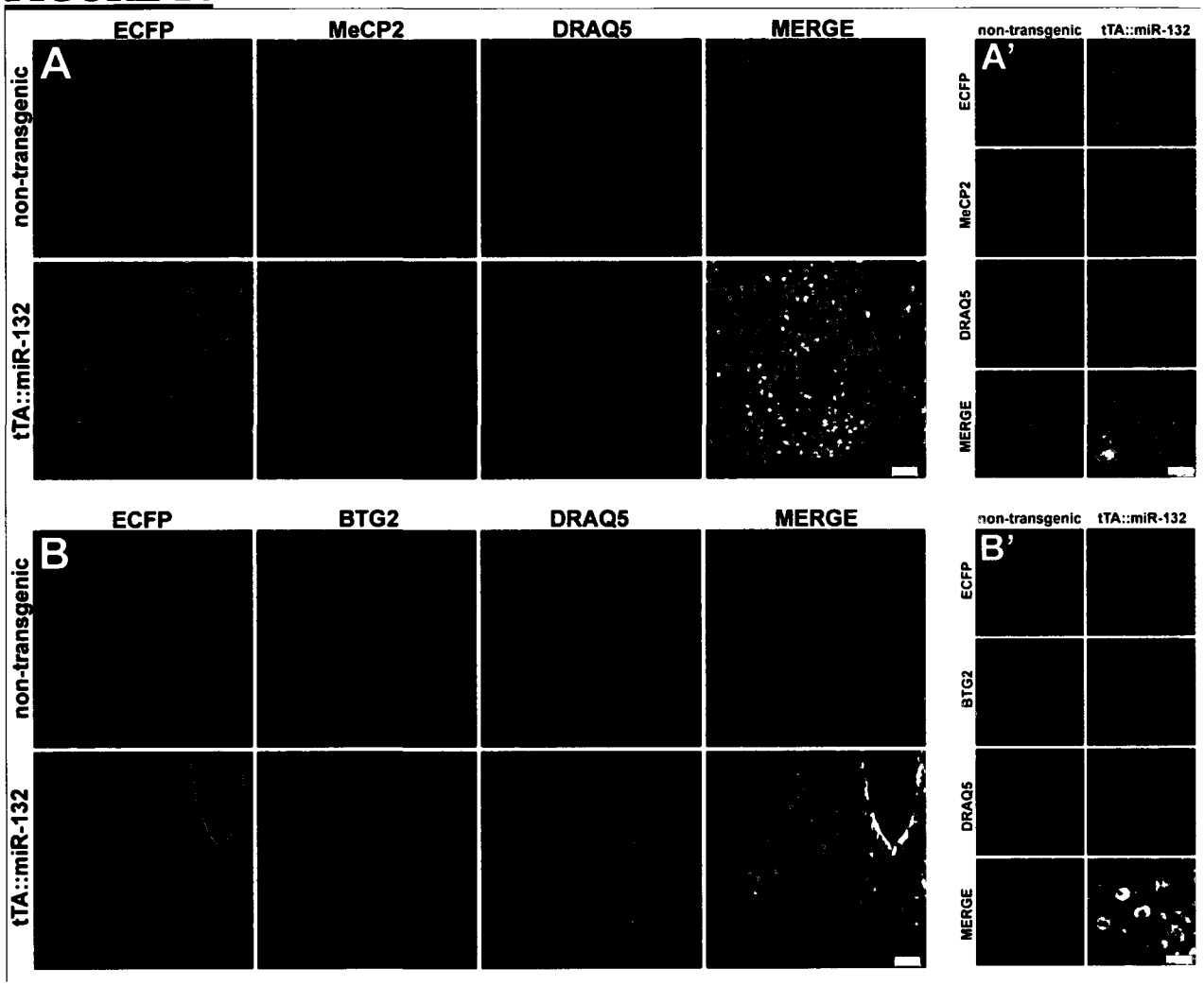
ECFP
MeCP2
DRAQ5
MERGE
A
non-transgenic
tTA::miR-132
non-transgenic
tTA::miR-132
A'
ECFP
MeCP2
DRAQ5
MERGE
ECFP
BTG2
DRAQ5
MERGE
B
non-transgenic
tTA::miR-132
non-transgenic
tTA::miR-132
B'
ECFP
BTG2
DRAQ5
MERGE

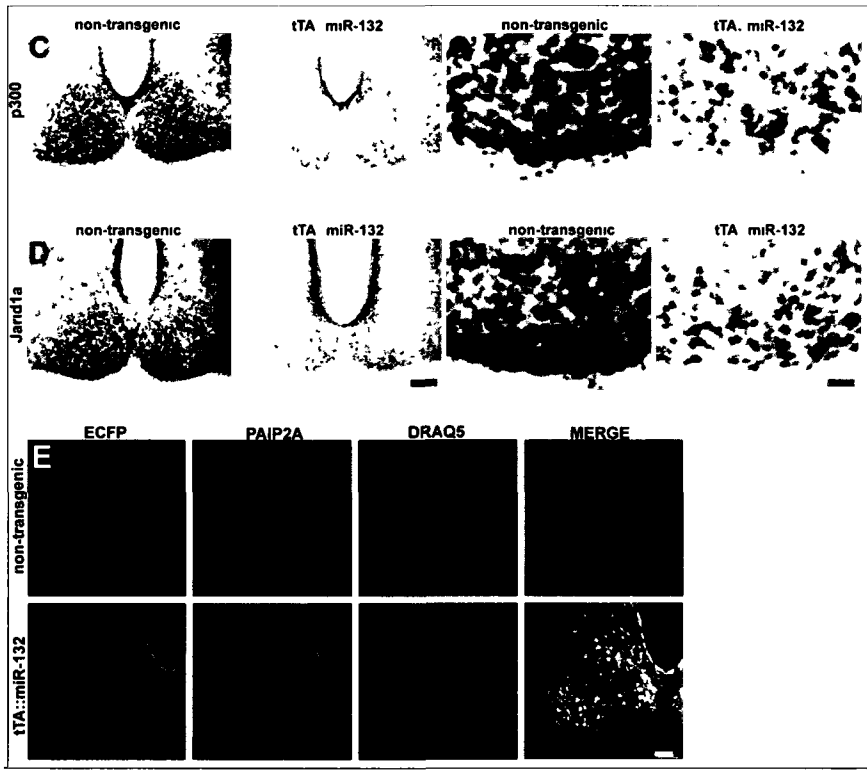

Figure 14. miR-132 regulates the expression of MeCP2, p300, JARID1A, BTG2 and PAIP2A in the SCN.

(A, B, E) MeCP2, BTG2 and PAIP2A protein expression in the SCN of tTA::miR-132 transgenic mice and non-transgenic controls at CT 16. SCN tissue from non-transgenic (top row) and tTA::miR-132 transgenic (bottom row) mice was harvested at CT 16 and analyzed for expression of **(A)** MeCP2, **(B)** BTG2 and **(E)** PAIP2A by indirect immunofluorescence (red). Transgene expression was confirmed by co-detection of ECFP (green). Sections were counterstained with the nuclear marker DRAQ5 (pseudocolored blue). Merged images are presented in the rightmost columns. Scale bars = 50μm. **(A', B')** Expression of **(A')** MeCP2 and **(B')** BTG2 in the retinorecipient region of the SCN, the ventrolateral aspect, is presented in higher magnification. Note the heterochromatic distribution of MeCP2 and the cytoplasmic distribution of BTG2. Scale bars = 5 μm. **(C, D)** Immunohistochemical detection of **(C)** p300 and **(D)** JARID1A protein expression in the SCN of tTA::miR-132 transgenic mice and non-transgenic controls at CT 16. Scale bars = 100μm. **(C', D')** Expression of **(C')** p300 and **(D')** JARID1A in the ventrolateral SCN is given in higher magnification images. Scale bars = 20 μm. n = 6 mice per genotype and representative images were chosen. Images captured using a Zeiss Axiovert Observer Z1 epifluorescent/light microscope (C-D) and via confocal microscopy on a single focal plane with a 40X objective (A-B & E) and with a 63X oil objective (A'-B'). Images quantitated with Zeiss "Zen" 2008 software, using the manual cursor command. This figure and figure legend are reproduced from the manuscript Alvarez-Saavedra et al, circa November 2009. Experimental design and tissue harvest jointly performed by MAS & HYMC. Confocal imaging, bright-field imaging and figure design performed by MAS.

(Figure 15A-E). Nevertheless, this heightened expression in H3K4Me3 within the SCN may be alternatively explained by an upregulation of histone methyltransferase activity in the transgenics. However, I examined the expression of two methyltransferases, DNMT3A and SMYD2, and found either no expression in the SCN of non-transgenic and tTA::miR-132 mice (in the case of DNMT3A; MAS & HYMC, unpublished), or comparable levels in the SCN regardless of genotype (in the case of SMYD2; MAS & HYMC, unpublished).

Mecp2 (methyl-CpG-binding protein 2) is a nuclear protein that was first characterized by its ability to bind methylated CpG dinucleotides. Early experiments suggested that MeCP2 functioned as a silencer of gene transcription (156-158), nevertheless novel insights suggest additional roles for MeCP2 within the nucleus, including chromatin compaction, alternative splicing and transcriptional activation (159-160). In addition, functional interactions between MeCP2 and CREB, a key intermediate in light-induced clock entrainment, have been reported (160). It is also important to note that patients suffering from the autism-spectrum disorder, Rett Syndrome (MIM #312750; http://www.ncbi.nlm.nih.gov/omim/312750), which is caused by mutations of the *MECP2* gene, exhibit disruptions in their circadian rhythms (161), suggesting a possible, direct link between MeCP2 and clock function. As expected, MeCP2 protein levels were highly reduced (~65%) in the SCN of tTa::miR-132 transgenic mice at CT16 as revealed via western blotting (Figure 13). MeCP2 immunoreactivity in the SCN of miR-132 transgenic mice in conjunction with confocal imaging revealed the hallmark heterochromatic localization of MeCP2, with reduced levels seen in heterochromatic foci of cells overexpressing the miR-132 transgene (Figure 14A & Figure 14A').

FIGURE 15

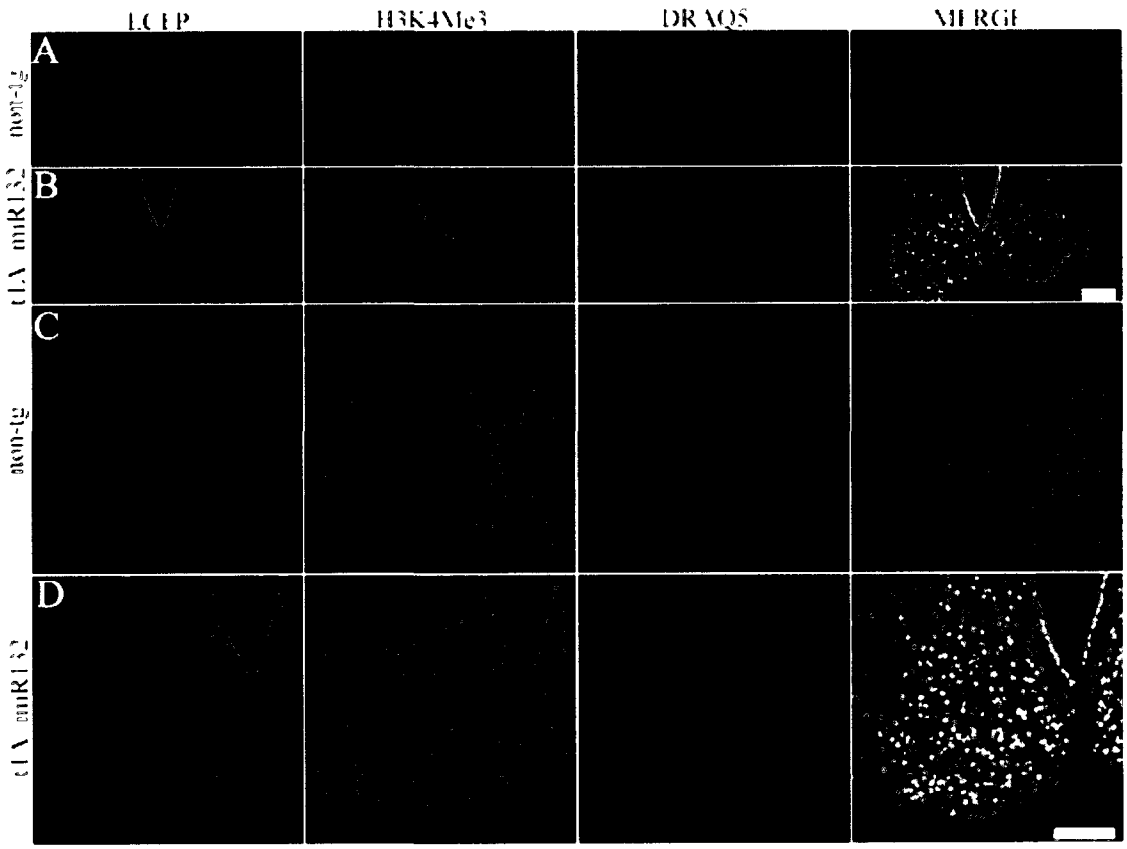
LCFP
H3K4Me3
DRAQ5
MERGE
A
B
C
D

E

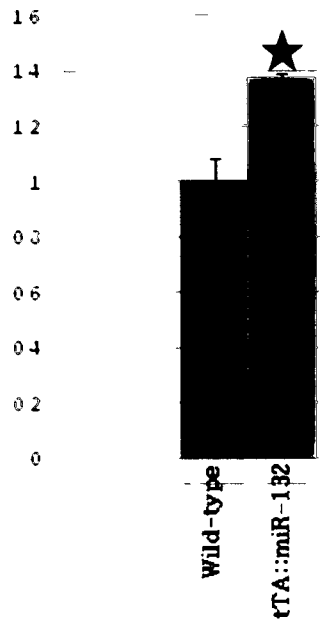
1.6
1.4
1.2
1
0.8
0.6
0.4
0.2
0
Wild-type
tTA::miR-132

Figure 15. Basal expression of H3K4Me3 in the SCN of tTA::miR-132 transgenic mice is upregulated.

(A-D) H3K4Me3 expression in the SCN of tTA::miR-132 transgenic mice and non-transgenic controls at CT 16. SCN tissue from **(A, C)** non-transgenic and **(B, D)** tTA::miR-132 transgenic mice was harvested at CT 16 and analyzed for expression of H3K4Me3 (red; second column). Transgene expression was confirmed by co-detection of ECFP (green; first column). Sections were counterstained with the nuclear marker DRAQ5 (pseudocolored blue; third column). Note co-localization of H3K4M3 and the nuclear marker DRAQ5 (merged; fourth column). Scale bars = 100μm (A-B) and 50 μm (C-D). n = 3 mice per genotype. Images captured via confocal microscopy on a single focal plane with a 20X objective (A-B) and with a 40X oil objective (C-D). **(E)** Quantitation of H3K4Me3 SCN basal expression in tTA::miR-132 mice vs. non-transgenic littermate controls. Values on the y-axis represent arbitrary mean fluorescence intensity for the unilateral SCN. Values are presented as mean ± SEM. n = 3 mice per condition. $*p<0.05$ vs. non-transgenic controls (two-tailed Student's t-test). Images quantitated with Zeiss "Zen" 2008 software, using the manual cursor command. This figure and figure legend are reproduced from the manuscript Alvarez-Saavedra et al, circa November 2009. Experimental design and tissue harvesting jointly performed by MAS & HYMC. Confocal imaging, quantitations and figure design performed by MAS.

Btg2 (B-cell translocation gene 2) was recently shown to bind to POP2/CAF1, a subunit of the CCR4/ POP2 deadenylase complex that is responsible for shortening of the poly(A) tail, the rate-limiting step in mRNA turnover (162). One study demonstrated that BTG2 induces mRNA decay by increasing the rate of POP2/CAF1-mediated deadenylation (162). Recent evidence suggesting the importance of mRNA degradation in modulating circadian rhythms of *mPer2* expression (163) raises the possibility for a role of BTG2 in circadian clock regulation. Via western blotting, BTG2 protein levels in the SCN were reduced 55% as compared to non-transgenic controls at CT16 (Figure 13). BTG2 immunoreactivity levels were also reduced in the SCN of tTA::miR-132 mice compared to non-transgenic controls (Figure 14B).

Paip2a (polyadenylate binding protein-interacting protein 2) is a potent suppressor of eukaryotic translation. EIF4G, a component of the translation initiation complex that binds to the 5'-cap of mRNA, interacts physically with PABP (polyadenylate binding protein) that is bound to the poly(A) tail, leading to circularization of the mRNA and enhanced translation efficacy (164). PAIP2A inhibits translation by disrupting the interaction between the poly(A) tail and PABP (165). Currently, there has been no characterization of PAIP2A in clock mechanisms. However, its functional partner, PABP-C1 (PABP, cytoplasmic 1), exhibits circadian rhythms of gene expression in the liver (166), and is a potential target of CREB transcription as it has been identified in a CREB-SACO library (132). In addition, a recent study showed that the mTOR signaling pathway, a key regulator of translation, is induced by light in the SCN (100), suggesting an important role of translational regulation in photic entrainment. Contrary to the results from the *in-vitro* and *in-vivo* knockdown experiments, an unexpected augmentation (2.7-

fold increase) of PAIP2A protein levels was observed in the SCN of tTA::miR-132 mice, relative to non-transgenic controls, at CT 16 via western blotting (Figure 13). These results were further corroborated via immunofluorescent labeling of PAIP2A in the miR-132 transgenic SCN (Figure 14E). One possibility is that constitutive and long-term overexpression of miR-132 in the SCN, within a certain cellular context, alters other gene regulatory networks that have secondary effects on *Paip2a* expression, for example, at the level of gene transcription. These secondary effects may mask the direct effects of miR-132 on *Paip2a* expression via the miR-132 MRE within the *Paip2a* 3'UTR. In support of this notion, a 2-fold increase was observed in PAIP2A protein levels in the SCN of mice infused with miR-132 antagomirs, compared to mice that had been infused with miR-219 or miR-1 antagomirs (Figure 12).

Thus, using a combination of 3'UTR reporter assays, *in-vitro* and *in-vivo* loss-of-function, as well as *in-vivo* gain-of-function, the data suggest that *Ep300*, *Jarid1a*, *Mecp2* and *Btg2* are *bona fide* targets of miR-132. In the case of 4 of these targets (*Paip2a* being the exception), this manifests in reduced steady-state levels of the target protein in the SCN of mice that overexpress miR-132. However, potential alterations in genetic networks in the transgenic SCN may secondarily influence the expression of the *Paip2a* gene, to an extent that these effects may mask the MRE-mediated effects of miR-132 on *Paip2a* expression.

viii. microRNA-132 target analysis in microRNA-219 transgenic mice

The *in vitro* and *in vivo* evidence suggests that *Ep300*, *Jarid1a*, *Mecp2*, *Btg2* and *Paip2a* are indeed miR-132 targets regulated via the characterized miR-132 MREs present on their respective 3'-UTRs. Nevertheless, in order to discard the possibility that these are

non-specific effects attributed to deregulation of the miRNA processing machinery due to miR-132 overexpression, I analyzed a *CamKIIα*-tTA::miR-219 transgenic mouse model in order to determine if overexpression of a miRNA deregulates the miRNA processing machinery. Briefly, the pre-miR-219 rat sequence was cloned into the same bidirectional Tet-responsive promoter used to generate the miR-132 transgene, making a miR-219-pBI-ECFP bi-directional construct (construct and mice generated by Dr. Hai-Ying Mary Cheng while at Ohio State University). This transgene was microinjected into FVB/N oocytes and four founder lines were further characterized. tTA::miR-219 transgenic lines #2665 and #2580 have a qualitatively similar expression pattern and levels compared to miR-132 transgenic lines #2561 and #2570 (Figures 16A & Figure 16B). Most importantly, overexpression of miR-219 in the SCN of tTA::miR-219 transgenic mice had no effect on the expression of JARID1A, MeCP2, p300, BTG2 and PAIP2A proteins as measured via western blotting at CT16 (Figure 17). This was expected since none of these transcripts bear predicted miR-219 MREs in their 3'UTRs. These data suggest that *in-vivo* pre-miRNA overexpression does not deregulate the miRNA processing machinery in the miR-132 and miR-219 transgenic mouse models.

ix. microRNA-132 target genes are activity-dependent

miR-132's regulatory role on light-induced clock resetting (130) suggests that its targets themselves are involved in the clock-resetting process. Hence, it is logical to hypothesize that these targets may be activity-dependent, and hence responsive to nocturnal photic stimulation, thereby playing roles in the molecular regulation of light entrainment. As a first step towards the characterization of their roles in the SCN and circadian biology, the light-dependent induction of *Ep300*, *Mecp2*, *Btg2* and *Paip2a* (measured via activation of

FIGURE 16

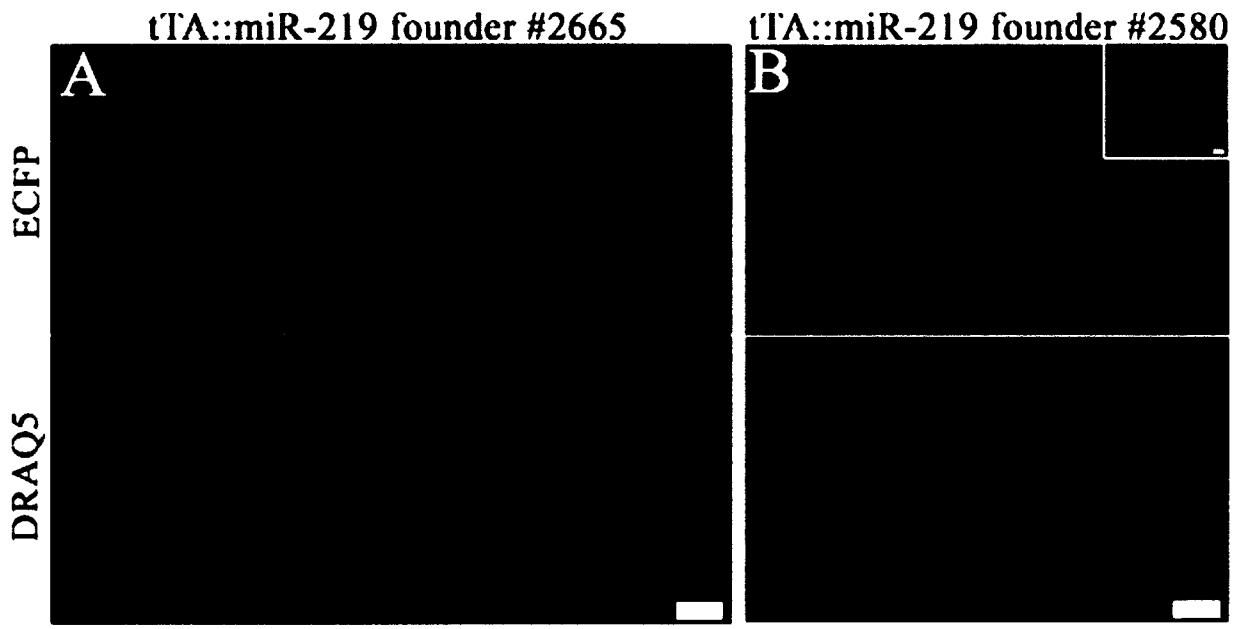

Figure 16. tTA::miR-219 transgene expression in the adult mouse brain.
(A,B) ECFP transgene expression in the brains of *Camk2α*-tTA::miR-219 transgenic mice. **(A)** Sagittal midbrain and **(B)** coronal SCN sections were processed for ECFP immunoreactivity. Sections were counterstained with the nuclear marker, DRAQ5 (pseudocolored in red (A); and blue (B)). Scale bars = 1 mm (A) and = 50μm (B). Images were captured via confocal microscopy on a single focal plane with 10X (A) and 20X (B) objectives. *INSET: ex-vivo* ECFP imaging of a 300μm SCN slice, highlighting the ventrolateral aspect, of tTA::miR-219 founder line #2580 at CT12. A 40X water immersion oil objective was used with a 458nm Argon laser to excite transgenic ECFP via confocal microscopy. SCN neuronal bodies are clearly visible. Scale bar = 50μm. miR-219 transgenic mice generated by Dr. Hai-Ying Mary Cheng while at Ohio State University, USA. Tissue harvesting performed jointly by MAS & HYMC. Confocal imaging, *ex-vivo* imaging, compilation of images and figure design performed by MAS.

FIGURE 17

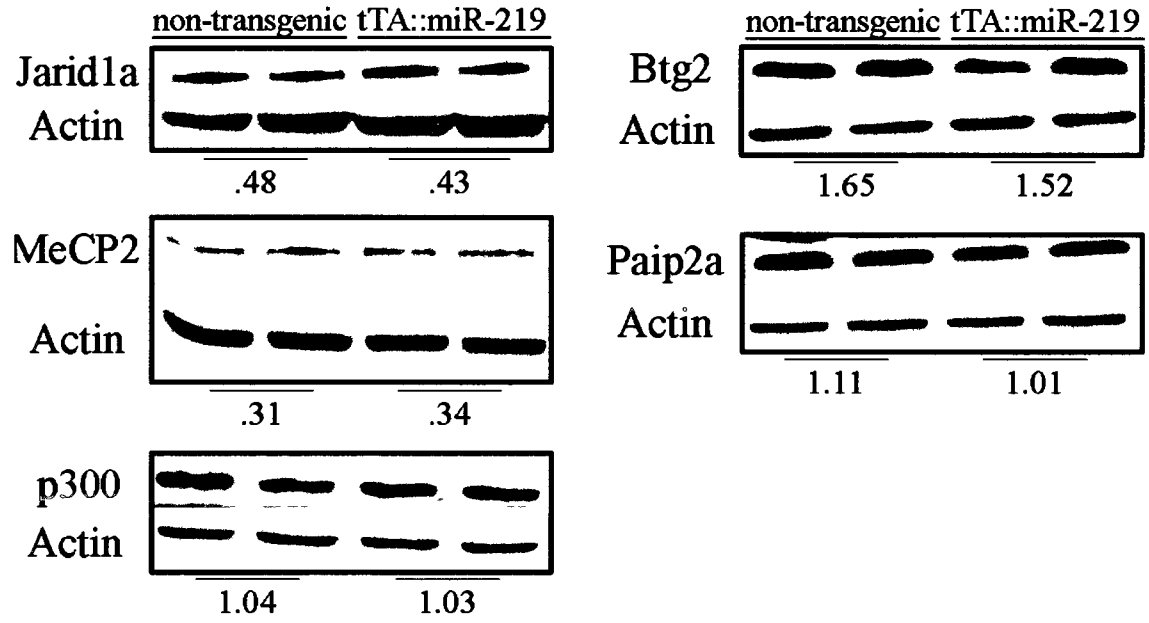

Figure 17. miR-219 overexpression in the SCN does not affect the expression of JARID1A, MeCP2, p300, BTG2 and PAIP2A proteins.
JARID1A, MeCP2, p300, BTG2 and PAIP2A protein expression in the SCN of tTA::miR-219 transgenic mice (lanes 3 and 4) and non-transgenic controls (lanes 1 and 2) at CT14 as determined by Western blotting. β-actin expression served as the loading control. Values presented below each blot represent the mean relative abundance of the protein examined, normalized to actin expression, for each genotype. Note that no significant differences between genotypes exist for all miR-132 predicted targets, despite robust upregulation of miR-219. n = 8 mice per genotype, grouped in pools of 2. Images quantitated on grayscale with ImageJ software. This figure and figure legend are reproduced from the manuscript Alvarez-Saavedra et al, circa March 2010. Experimental design, tissue harvest, quantitative analysis and compilation of images performed by MAS. Dr. Reynaldo Oliva-Hernández assisted with tissue harvesting.

post-translational modifications or total protein levels) was examined as well as the downstream effector of *Jaridla*, i.e. H3K4-trimethylation. Wild-type mice were subjected to a brief light pulse (15 min, 40 lux) at CT 15, and SCN tissue was harvested either 15 min or 2 hrs later to determine changes in post-translational modifications or total protein abundance, respectively.

p300/CBP transcriptional co-activator proteins play a central role in the coordination and integration of multiple signal-dependent cascades that regulate gene expression (167,168). These proteins serve as mediators of transcriptional activity in response to physiological cues. Interestingly, p300/CBP also contains histone acetyltransferase (HAT) activity, which endows the protein complex with the capacity to modulate chromatin activity. Autoacetylation at lysine-1499 of p300 has been shown to enhance its HAT activity and affect a wide variety of signaling events (169). It has also been shown that CaM kinase IV phosphorylates CBP at Ser302, which is required for CBP-dependent transcriptional activation in primary neurons (170). It is then reasonable to speculate that autoacetylation at lysine-1499 of p300 may be a light-activated residue involved in the clock-resetting response. Wild-type mice were subjected to a brief light pulse (15 minutes, 40 lux) at CT 15 and SCN tissue was harvested 15 minutes later. Immunolabelling did not detect any substantial changes in the light-pulses mice vs. dark-controls (data not available at the time of publication of this thesis). Due to the high basal level of expression detected, I reasoned that this post-translational modification may not be detectable via this immunohistochemical technique or that there are other residues that may be involved in the light-induced clock resetting response.

Phosphorylation of MeCP2 at serine 421 (pS421), has been shown to be induced by neuronal activity and is required for derepression of *Bdnf* transcription (171). Wild-type mice were treated with a brief light pulse (15 minutes, 40 lux) at CT 15 and SCN tissue was harvested 15 minutes later. Phosphorylation at serine 421 was robustly induced in the ventrolateral SCN (Figure 18A & Figure 18A') vs. non-treated mice. This suggests that MeCP2 may be involved in light-dependent modulation of target genes.

Wild-type mice were treated with a brief light pulse (15 minutes, 40 lux) at CT 15 and SCN tissue was harvested 15 minutes later in order to measure induction of H3K4Me3. Light elicited a pronounced elevation in the expression of H3K4Me3, the direct substrate of JARID1A, suggesting the possibility that light has an acute suppressive effect on JARID1A's demethylase activity (Figure 18B & Figure 18B'). Nevertheless, the possibility that a histone methylase is activated upon light treatment cannot be excluded. Thus, it appears that light evokes rapid changes in chromatin architecture within the SCN that in unison trigger a transcriptionally permissive state of target genes.

In addition, levels of BTG2 as well as PAIP2A proteins (Figures 18C-D') in the SCN were significantly induced 2-hrs following nocturnal photic stimulation at CT15. Collectively, these results indicate that the miR-132 targets examined, or the pathways that are directly regulated by the target, are themselves acutely induced in the SCN in response to light, arguing strongly that these targets play important roles in modulating light-induced clock resetting.

x. microRNA-132 overexpression's effects on core clock genes

FIGURE 18

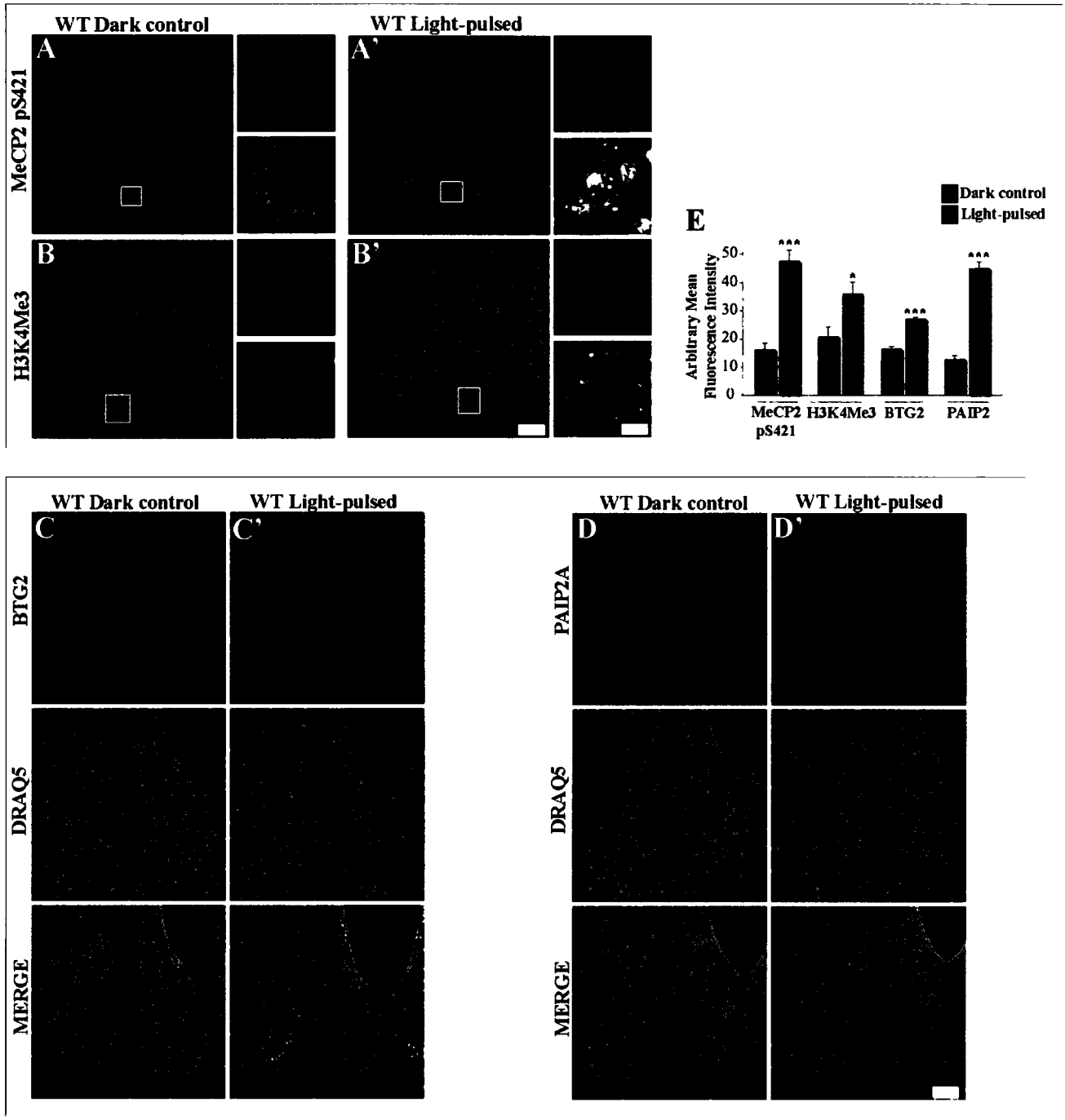

Figure 18. miR-132 targets and their downstream effectors are light-responsive. **(A, A', B, B')** A light stimulus acutely induces the phosphorylation of MeCP2 at Ser421 (pS421) and trimethylation of histone H3 at lysine 4 (H3K4Me3) in the SCN. C57Bl/6J (WT) mice received a brief light pulse (15 min, 40 lux) at CT 15. Tissue was harvested

(red) or **(B')** H3K4Me3 (red) by indirect immunofluorescence. Sections were counterstained with the nuclear marker DRAQ5 (pseudocolored in green). **(A, B)** Dark control mice were not exposed to light but were killed at the same circadian time. For each condition, the boxed region highlighting the ventrolateral SCN neurons in the left panel is presented in higher magnification in the right-most panels. Scale bar = 50 μm. *(Top right)* MeCP2 pS421 or H3K4Me3 immunoreactivity only; *(bottom right)* merged image of MeCP2 pS421 or H3K4Me3 immunoreactivity in combination with DRAQ5. Note upregulation in nuclear staining of both post-translational modifications. Scale bar = 5 μm. **(C, C', D, D')** BTG2 and PAIP2A protein levels in the SCN are induced in response to light. C57Bl/6J mice received a brief light pulse (15 min, 40 lux) at CT 15 and killed 2 hrs later for analysis of **(C')** BTG2 (red) and **(D')** PAIP2A expression by indirect immunofluorescence (red; top rows). **(C, D)** Dark control mice (DD) were not exposed to light but were killed at the same circadian time. Sections were counterstained with the nuclear marker DRAQ5 (pseudocolored in green; middle rows). Merged images highlight cytoplasmic labeling of both proteins (bottom rows). Scale bar = 50μm. **(E)** Quantitation of light-induced expression of pS421 MeCP2, H3K4Me3, BTG2 and PAIP2A in the SCN. Values on the y-axis represent arbitrary mean fluorescence intensity for individual cells (in the case of pS421 MeCP2 and H3K4Me3) or for the unilateral SCN (in the case of BTG2 and PAIP2A). Values are presented as mean ± SEM. n = 3 mice per condition. $*p<0.05$, $***p<0.001$ vs. dark control (two-tailed Student's t-test). Images captured via confocal microscopy on a single focal plane with a 40X objective (A-D') and with a 63X oil objective (boxed insets). Images quantitated with Zeiss "Zen" 2008 software, using the manual cursor command. This figure and figure legend are reproduced from the manuscript Alvarez-Saavedra et al, circa November 2009. Experimental design and tissue harvesting jointly performed by MAS & HYMC. Confocal imaging, statistical analysis, compilation of images and figure design performed by MAS.

The next logical step was to analyze the potential role that miR-132 plays in core clock timing mechanisms. I first examined the circadian profile of PER1 and PER2 protein

expression in the SCN of tTA::miR-132 mice and non-transgenic controls. Consistent with previous reports, the peak and nadir of PER1 and PER2 protein expression in the SCN of non-transgenic (i.e. wild-type) mice were reached during the early subjective night (CT 14) and late subjective night (CT 22)/early subjective day (CT 2), respectively (Figure 19A & Figure 19B). Compared with non-transgenic controls, tTA::miR-132 mice exhibited a marked reduction in the amplitude of PER1 rhythms in the SCN (Figure 19A & Figure 19C). The dampened rhythm was due largely to a decrement in PER1 abundance during the peak (CT 10 – 14), rather than elevated expression during the nadir (Figure 19C). The phasing of PER1 expression in the SCN was comparable between non-transgenic and tTA::miR-132 mice. In contrast, miR-132 overexpression in the SCN had no significant effect on PER2 protein rhythms (Figure 19B & Figure 19C).

Numerous studies have shown a strong correlation between phase-shifting of behavioural rhythms and induction of *Per1* and *Per2* expression in the SCN following nocturnal light exposure (13,173). To examine light-inducible expression of PER1 and PER2 in the SCN, tTA::miR-132 mice and non-transgenic controls were administered a brief light pulse (15 min, 40 lux) at CT 15 and killed 4 hours later for determination of PER1 and PER2 levels. Consistent with previous studies (174), light exposure during the early subjective night significantly increased the number of PER1- and PER2-immunoreactive cells in the SCN of non-transgenic (wild-type) mice relative to dark controls (Figures 20A-C). There was a modest but significant increase in the number of PER1-ir cells in tTA::miR-132 transgenic SCN in response to photic stimulation, relative

FIGURE 19

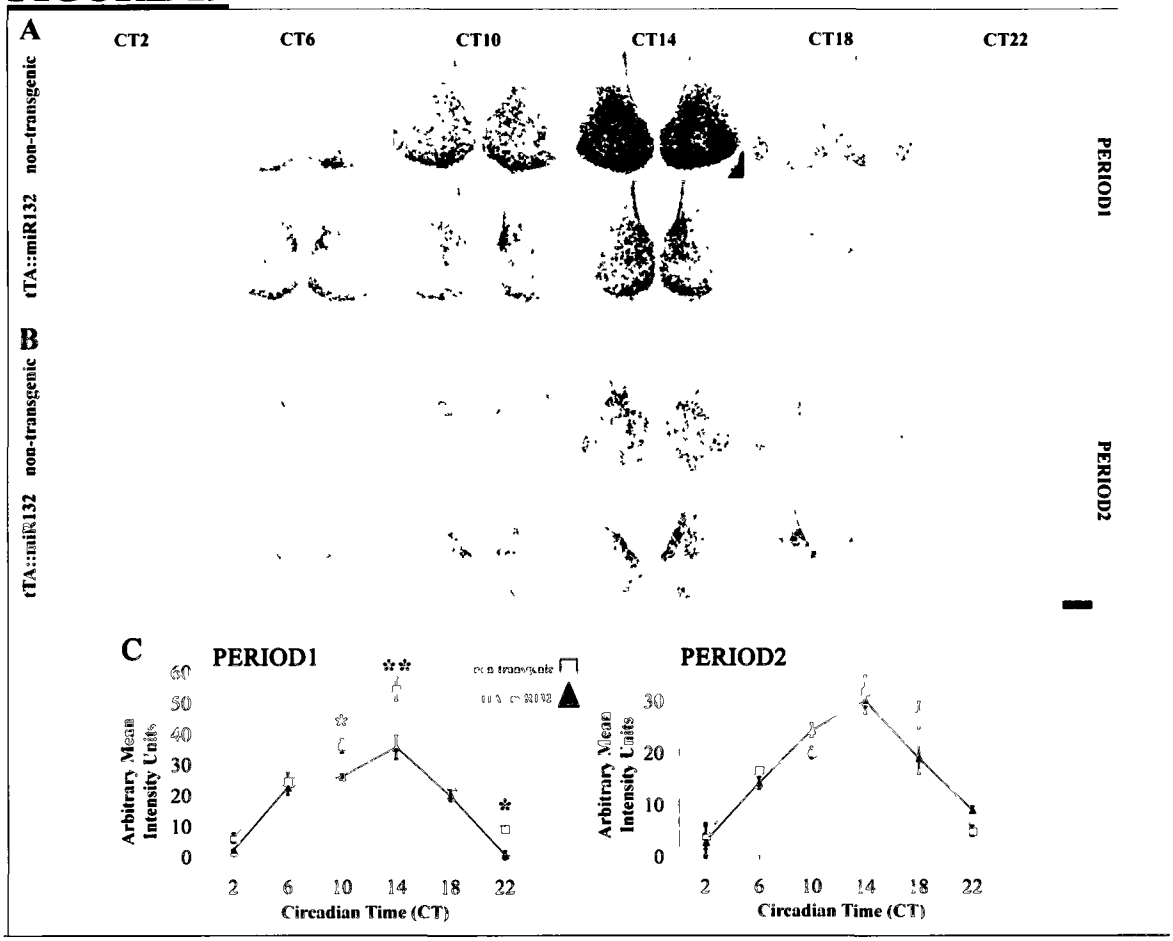

Figure 19. miR-132 overexpression in the SCN dampens PER1 protein rhythms
(A, B) Rhythms of PER1, but not PER2, expression are dampened in the SCN of tTA::miR-132 mice. SCN tissue was harvested from tTA::miR-132 mice (bottom row) and non-transgenic controls (top row) at defined CT times across a full circadian cycle, and analyzed for **(A)** PER1 and **(B)** PER2 expression by immunohistochemistry. Note the decreased amplitude of PER1 rhythms in miR-132 transgenic mice (A & C). Scale bar = 100μm. **(C)** Quantitation of PER1 (left graph) and PER2 rhythms (right graph) from (A) and (B), respectively. Values on the y-axis indicate the number of PER1- or PER2-immunoreactive nuclei in the bilateral SCN. Values are presented as mean ± SEM. n = 6 mice per genotype. *$p<0.05$, **$p<0.01$ (Fisher's LSD). Images captured using a Zeiss Axiovert Observer Z1 epifluorescent/light microscope and quantitated on grayscale with ImageJ software. This figure and figure legend are reproduced from the manuscript Alvarez-Saavedra et al, circa November 2009. Experimental design and tissue harvesting jointly performed by MAS & HYMC. Bright-field imaging and figure design performed by MAS. Quantitation software for analysis of immunohistochemical labeling conceived and written in ImageJ by Daniel Cornejo-Palma, University of Ottawa, Canada. Quantitative analysis and statistics in panel C performed by DCP under the supervision of MAS.

FIGURE 20

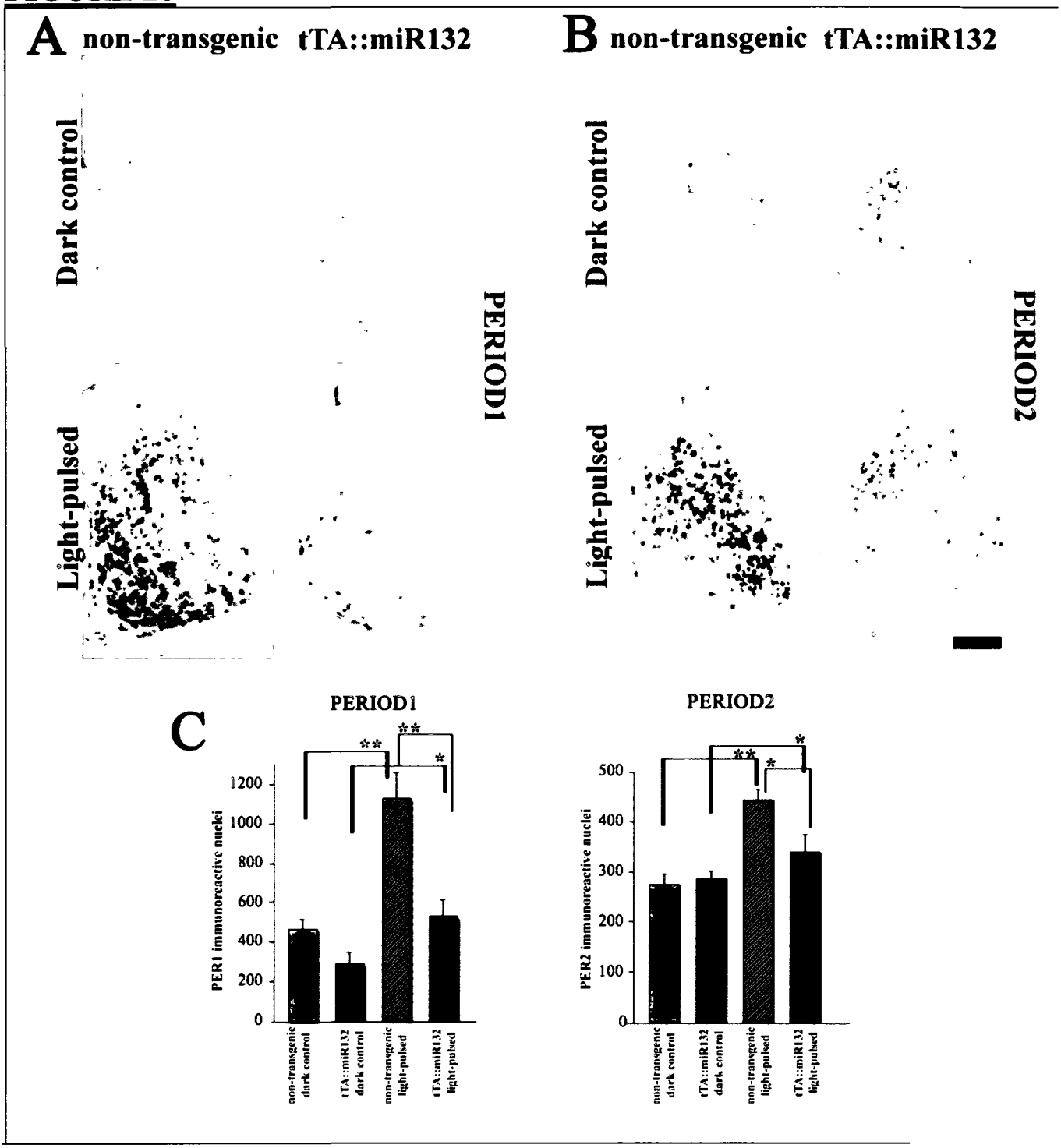

Figure 20. miR-132 overexpression in the SCN suppresses light-induced expression of PER1 and PER2.

(A, B) Induction of PER1 and PER2 expression in the SCN in response to photic stimulation is attenuated in tTA::miR-132 mice. Non-transgenic and tTA::miR-132 mice

received a brief light pulse (15 min, 40 lux) at CT 15 and SCN tissue was harvested 4 hrs later for determination of **(A)** PER1 and **(B)** PER2 levels by immunohistochemistry. Dark control mice were not exposed to light but were killed at the same circadian time. Note the decreased labeling intensity of both proteins in light-pulsed miR-132 transgenic mice vs. light-pulsed non-transgenic mice (bottom rows). Basal DD levels are similar in both genotypes (top rows). Scale bars = 50μm. **(C)** Quantitation of light-inducible PER1 (left) and PER2 (right) expression from (A) and (B), respectively. Values on the y-axis indicate the number of PER1- or PER2-immunoreactive nuclei in the bilateral SCN. Values are presented as mean ± SEM. n = 6 mice per genotype. $*p<0.05$, $**p<0.01$ (Fisher's LSD). Images captured using a Zeiss Axiovert Observer Z1 epifluorescent/light microscope and quantitated on grayscale with ImageJ software. This figure and figure legend are reproduced from the manuscript Alvarez-Saavedra et al, circa November 2009. Experimental design and tissue harvesting jointly performed by MAS & HYMC. Bright-field imaging and figure design performed by MAS. Quantitation software for analysis of immunohistochemical labeling conceived and written in ImageJ by Daniel Cornejo-Palma, University of Ottawa, Canada. Quantitative analysis and statistics in panel C performed by DCP under the supervision of MAS.

to dark controls (Figure 20A & Figure 20C). However, the number of PER1-ir nuclei after a light pulse in the transgenics was one-half of that observed in non-transgenic

controls (Figure 20A & Figure 20C). Light exposure did not significantly induce the abundance of PER2-ir cells in the SCN of tTA::miR-132 mice relative to dark controls (Figures 20B & Figure 20C). The number of PER2-ir nuclei in light-pulsed tTA::miR-132 mice was markedly fewer than that observed in light-pulsed non-transgenic controls (Figures 20B & Figure 20C). These data indicate that miR-132 overexpression negatively modulates light-inducible expression of PER1 and PER2 in the SCN.

A deficit in a photic input pathway that couples light to the molecular clock, for example, the ERK/MAPK cascade leading to CREB-dependent transcription (33), could account for the attenuation of both light-induced behavioural phase shifts and light-induced PERIOD protein expression in the SCN in tTA::miR-132 mice. However, I found no differences in phosphorylated CREB in the SCN of tTA::miR-132 mice vs. non-transgenic controls following photic stimulation (Figure 21), thereby ruling out the possibility that the observed phenotypes in the miR-132 mice are the result of an impairment in an input pathway that functions upstream of miR-132. Importantly, the data indicate that miR-132 transgene expression in the SCN suppresses light-induced PER1 and PER2 protein expression via mechanisms that are downstream of CREB activation.

xi. MeCP2-dependent transcriptional modulation of the Period genes

The next challenge was to identify miR-132 modulated *trans*-acting factors that may be involved in the transcriptional regulation of the *Per1* and *Per2* genes. Several studies have already demonstrated that p300 positively regulates CLOCK-mediated transcription

FIGURE 21

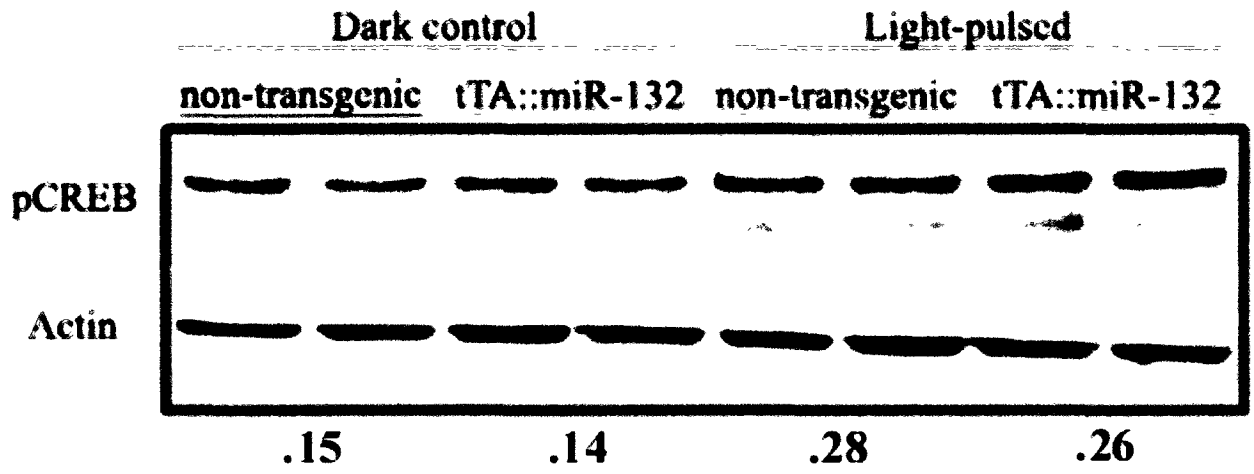

Figure 21. miR-132 overexpression does not alter CREB phosphorylation at serine 133 in miR-132 transgenic mice.
pCREB (pSerine 133) activation in the SCN of tTA::miR-132 transgenic mice and non-transgenic controls as determined by Western blotting. Non-transgenic (lanes 1,2,5,6) and tTA::miR-132 transgenic mice (lanes 3,4,7,8) received a brief light pulse (15 min, 40 lux) at CT 15. Tissue was harvested 30 min after onset of light treatment and analyzed for expression of pCREB. Dark control mice were not exposed to light but were killed at the same circadian time. Membrane was stripped and re-blotted with ß-actin as loading control. n = 8 mice per condition, grouped in pools of 2. Values presented below each blot represent the mean relative abundance of the protein examined, normalized to actin expression, for each genotype and treatment. Note pCREB activation in the light-pulsed mice of both genotypes, relative to dark controls. Images quantitated on grayscale with ImageJ software. This figure and figure legend are reproduced from the manuscript Alvarez-Saavedra et al, circa March 2010. Tissue harvest jointly performed by MAS & HYMC. Western blots, quantitations and figure design performed by MAS.

via histone H3 acetylation (80,175). Nevertheless, the role of MeCP2 in clock gene regulation has not been characterized. MeCP2 has been classically viewed as a transcriptional repressor due to its affinity for methylated DNA (158,176). Nevertheless, recent evidence suggests that MeCP2-binding sites are located not only in CpG islands but may also be found within intragenic regions (177). Moreover, it has been shown via genome-wide promoter analysis that subsets of gene promoters bound by MeCP2 are actively expressed (160). These data suggest that MeCP2, besides acting as a transcriptional repressor, may also be involved in gene activation. These data combined with the observation that MeCP2 is phosphorylated in the SCN after nocturnal light exposure (171 and this thesis), led me to investigate whether MeCP2 functions as an epigenetic modulator in light-induced clock resetting. I first began my analysis by identifying putative MeCP2 binding sites within the *Per1* and *Per2* loci. Secondly, I performed expression studies in cell culture to identify whether MeCP2 is involved in the transcriptional activation and/or repression of the *Period* genes. Thirdly, I analyzed a *Mecp2* hypomorph mouse strain to determine PERIOD expression levels in the SCN (181).

As a starting point to screen for putative MeCP2 binding sites in the *Per1* and *Per2* loci, I used the CpG plot algorithm from the European Bioinformatics Institute (http://www.ebi.ac.uk/Tools/emboss/cpgplot/index.html) to identify putative CpG islands within 10 kb of the transcription start sites (Figure 22A & Figure 22B). I identified two CpG islands in the *Per1* 5'-upstream region at bp -3333 to -3130 and at bp -3931 to -3536, herein referred to as *Per1* CpG Islands #1 and #2, respectively (Figure 22A). I also identified a putative CpG island on the *Per2* locus at bp -481 to -57 (Figure 22B). NIH-

FIGURE 22

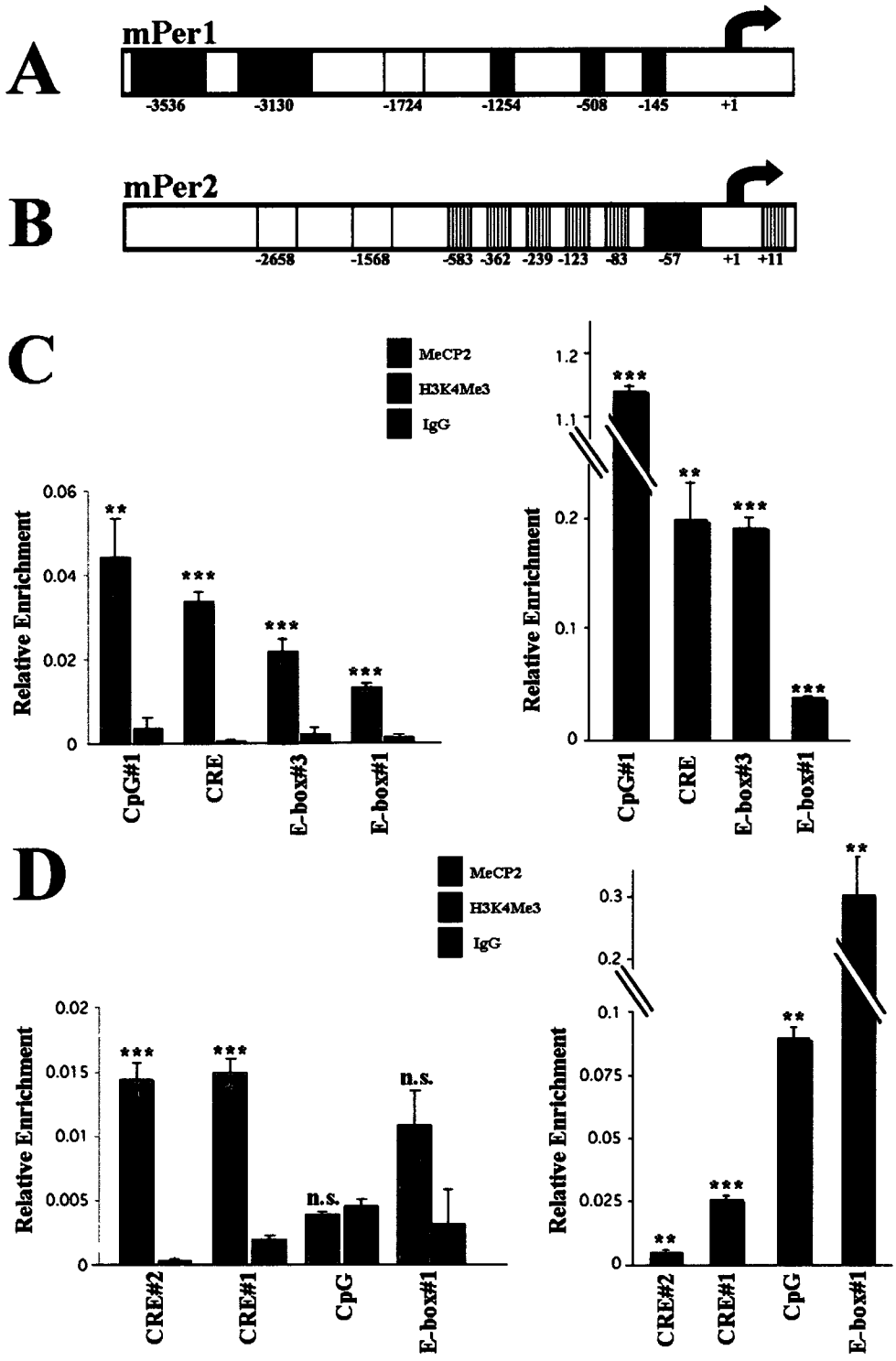
A
mPer1
-3536
-3130
-1724
-1254
-508
-145
+1
B
mPer2
-2658
-1568
-583
-362
-239
-123
-83
-57
+1
+11
C
MeCP2
H3K4Me3
IgG
Relative Enrichment
CpG#1
CRE
E-box#3
E-box#1
D
MeCP2
H3K4Me3
IgG
Relative Enrichment
CRE#2
CRE#1
CpG
E-box#1
n.s.

Figure 22. MeCP2 binds to regulatory elements within the *mPer1* and *mPer2* gene promoters.

(A, B) Schematic representation of **(A)** *mPer1* and **(B)** *mPer2* upstream regulatory elements. The *mPer1* gene is composed of three canonical E-boxes (red boxes), one canonical CRE site (yellow box) and 2 CpG islands of ~300bp each (blue boxes). The *mPer2* gene is composed of six non-canonical E-boxes (hatched red boxes), two non-canonical CRE sites (hatched yellow boxes) and 1 CpG island of ~400bp (blue box). Numbers below each box represent the genomic location relative to the transcription start site (TSS = +1; arrows). **(C, D)** ChIP analysis for binding of MeCP2 (left; red bars) and H3K4Me3 (right; blue bars) within the **(C)** *mPer1* and **(D)** *mPer2* promoters. Immunoprecipitation using an anti-rabbit IgG served as the negative control (black bars). Regions analyzed for m*Per1* include: **(C)** CpG island #1 (position -3130), CRE site (position -1724), E-box#3 (position -1254) and E-box#1 (position -145). For *mPer2,* regions analyzed include **(D)** CRE site#1 (position -1568), CRE site#2 (position -2658), CpG island (position -57) and E-box#1 (position +11). ChIP assays were performed with chromatin harvested from NIH-3T3 cells 36 hrs following transient transfection with the MeCP2-e1-myc construct. The MeCP2 ChIP results were further validated by immunoprecipitating tagged MeCP2 with anti-c-myc antibodies (data not shown). Values on the y-axis indicate the enrichment of the immunoprecipitated (IP) DNA encompassing the specified region relative to an input control, and are presented as mean ± SEM relative enrichment. Triplicate determinations from three independent experiments were made. $**p<0.01$, $***p<0.001$, n.s. = non-significant vs. IgG (two-tailed Student's t-test). Note that the presence of H3K4Me3 in regulatory sites does not coincide with MeCP2 binding in *Per2* regulatory elements. Also note that H3K4Me3 is also present throughout CpG islands. This figure and figure legend are reproduced from the manuscript Alvarez-Saavedra et al, circa November 2009. Experimental design jointly performed by MAS & HYMC. Bioinformatics, qPCR, statistical analysis and figure design performed by MAS. Gene diagrams designed by MAS.

3T3 fibroblasts, cells that endogenously express *mPer1* and *mPer2*, were transiently transfected with the MeCP2-e1-myc isoform (143; generous gift of Dr. B. Minassian), and chromatin was harvested for chromatin immunoprecipitation (ChIP) experiments. I decided to study the MeCP2-e1 isoform, since it has been shown to be the predominant transcript in the murine hypothalamus (178,179). Nevertheless, it should be noted that the MeCP2-e2 isoform is also highly expressed in the murine brain (180-182), but functional differences between the two isoforms have not yet been characterized. Transfection efficiencies for these experiments were in the range of 15-25%. Via qPCR, enrichment of MeCP2 at CpG island #1 (4.5% relative to input, $p<0.01$; Figure 22C) and CpG island #2 (data not shown) of the *Per1* locus was identified. Interestingly, I did not identify MeCP2 enrichment (<0.5% relative to input) on the CpG island of the *Per2* locus (Figure 22D). Unexpectedly, I detected a significant enrichment of H3K4Me3 at CpG island #1 of *Per1* compared to the *Per2* CpG island (116% vs. 9% relative to input; Figure 22C & Figure 22D). This data suggest that the presence of MeCP2 in the *Per1* locus does not interfere with the enrichment of H3K4Me3 in its vicinity, suggesting that the *Per1* gene is actively transcribed even in the presence of MeCP2.

In a second set of experiments, I screened for MeCP2 enrichment at CRE (cAMP response element) sites and E-boxes of the *Per1* and *Per2* loci, known sites of light-inducible and circadian transcriptional regulation, respectively (61,66,183-185). I found MeCP2 enrichment (3% relative to input, $p<0.001$) at the *Per1* CRE site (Figures 22A & 22C). In addition, I identified MeCP2 enrichment at the previously characterized E-box#3 and E-box#1 of the *Per1* locus (2.1 and 1.3%, respectively, relative to input; Figure 22A & Figure 22C; 183). Similarly, MeCP2 enrichment was identified at both

Per2 CRE site #1 and *Per2* CRE site #2 (1.5% relative to input, $p<0.001$; Figure 22B & Figure 22D). Most interestingly, I did not identify significant MeCP2 enrichment at the non-canonical E-box enhancer (E-box#1) found 11 nucleotides downstream of the *mPer2* transcription start site (Figure 22B & Figure 22D). A previous study indicated that this site accounts for most circadian transcriptional drive of the *mPer2* locus by CLOCK/BMAL1 heterodimers (185). In addition, all *Per2* E-boxes found upstream of E-box#1 also failed to show MeCP2 enrichment (MAS & HYMC, unpublished), suggesting that MeCP2 is more highly enriched throughout the *Per1* domain in comparison.

In order to investigate whether MeCP2 activates or represses transcription of the *Period* genes and, if so, whether this regulation is mediated *via* a CREB-dependent mechanism, I transiently transfected N2A cells with constructs expressing MeCP2-e1 or dominant-negative CREB (K-CREB), or both (186). I immunoblotted for total PER1 and PER2 proteins and found that MeCP2-e1 overexpression alone induced ~2-fold induction of both proteins, relative to empty vector control transfections (Figure 23). Importantly, MeCP2-dependent upregulation of PER1 and PER2 was completely abolished by co-transfection with K-CREB (Figure 23). Altogether, these results suggest that MeCP2 binds to the *Per1* and *Per2* 5' regulatory regions, and that MeCP2 mediates transcription of the *Per1* and *Per2* genes *via* a CREB-dependent mechanism.

In order to dissect the *in-vivo* role of MeCP2 in circadian biology and to investigate whether MeCP2 plays a regulatory role in PER1 and PER2 expression in the SCN, as suggested by the ChIP and *in-vitro* transfection assays, I analyzed a MeCP2 hypomorph mouse strain (herein referred to as $Mecp2^{floxed/y}$ mice) that has been previously developed and characterized (181,187,188). It has previously been shown that $Mecp2^{floxed/y}$ mice

FIGURE 23

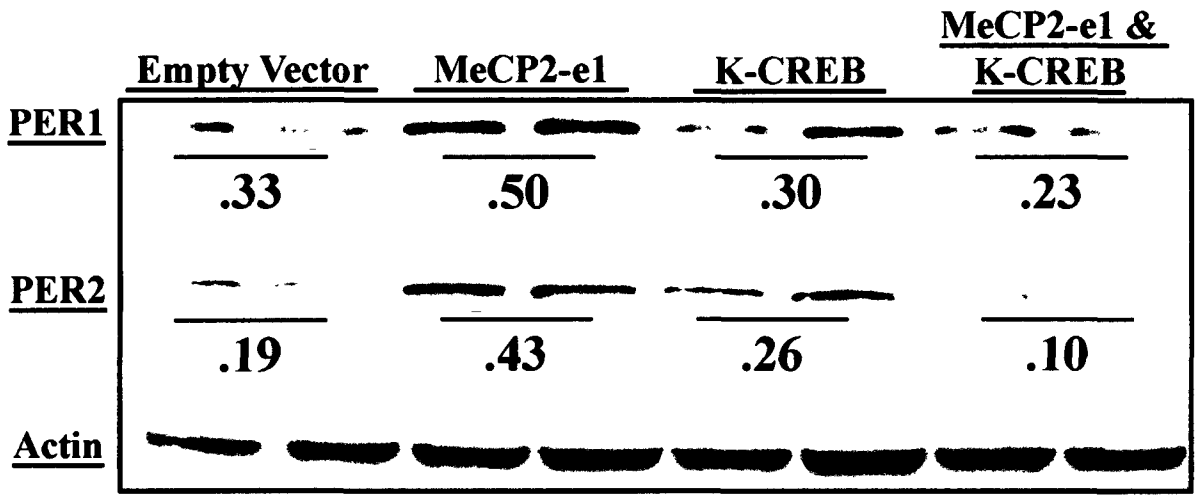

Figure 23. Overexpression of the MeCP2-e1 isoform modulates the transcriptional activation of PER1 and PER2 in a CREB-dependent manner.

(A) N2A cells were transiently transfected with constructs encoding MeCP2-e1-myc (lanes 3 and 4), dominant-negative K-CREB (lanes 5 and 6) or both (lanes 7 and 8), and PER1 (top row) and PER2 (middle row) protein levels were examined 36 hrs later by Western blotting. Transfection with empty vector pcDNA3 (lanes 1 and 2) served as the negative control. β-actin expression served as the loading control. Values presented below each blot represent the mean relative abundance of the protein examined, normalized to β-actin expression, for each condition. n = 3 per condition. Images quantitated on grayscale with ImageJ software. Experimental design jointly performed by MAS & HYMC. Western blotting, data analysis, quantitations and figure design performed by MAS.

have an ~50% reduction of MeCP2 protein levels in the brain compared to WT mice, similar to the decreased levels of MeCP2 seen in the miR-132 transgenic mice (Figure 13; 187,188). As a first step in this characterization, I verified via qRT-PCR that *Mecp2* transcript levels are decreased in the SCN of *Mecp2*$^{floxed/y}$ mice at CT8 vs. wild-type littermate control mice (Figure 24A). In addition, I characterized that *Mecp2*$^{floxed/y}$ mice have an ~60% reduction of MeCP2 total protein levels in the SCN at CT12 vs. wild-type littermate controls (Figure 24B), as previously shown for other brain regions (187,188).

In order to investigate whether MeCP2 plays a regulatory role in PER1 and PER2 expression, I harvested SCN tissue from *Mecp2*$^{floxed/y}$ mice and wild-type littermate controls at CT12, the peak of expression of PER1 and PER2 proteins (Figure 20), and analyzed them for PER1 and PER2 total protein levels via immunohistochemistry. Interestingly, a marked reduction in PER1 nuclear intensity was seen in the *Mecp2*$^{floxed/y}$ mice compared to wild-type littermate controls (Figures 25A-B). Conversely, only a modest reduction in PER2 proteins levels was seen in *Mecp2*$^{floxed/y}$ mice at CT12 compared to wild-type littermate controls (Figures 26A-B). These data suggest that MeCP2 is preferentially involved in the *in-vivo* transcriptional modulation of the *Period1* gene in the mouse SCN. Future studies will determine whether MeCP2 modulates the *Period* genes within the SCN in distinct manners, as suggested by the present data.

xii. PAIP2A-depedent translational control of the Period genes

The data thus far strongly implicate miR-132 as a negative modulator of light-induced clock resetting. This seems to be orchestrated by miR-132 targeting the translational repression (i.e. downregulation) of specific chromatin remodeling factors such as MeCP2 and p300 (this thesis) that would otherwise participate in transcriptional activation of the

FIGURE 24

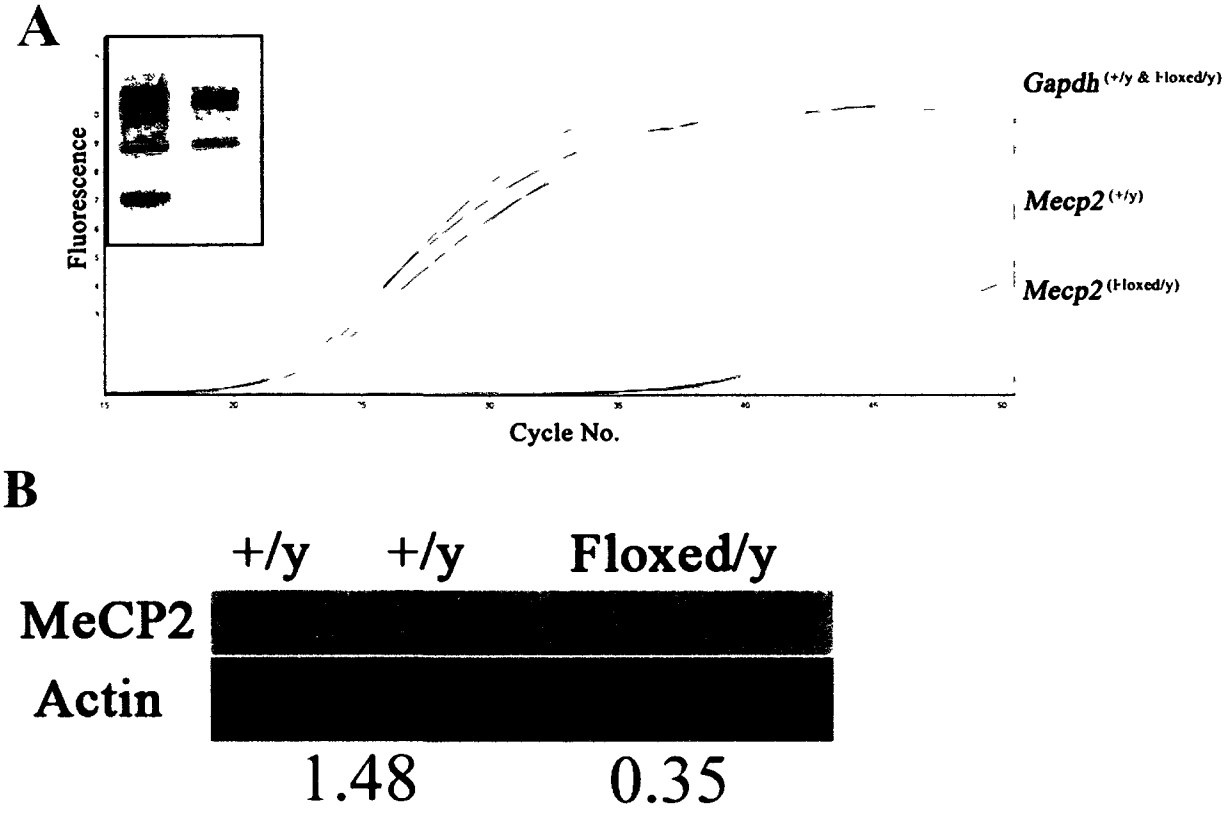

Figure 24. *Mecp2*$^{Floxed/y}$ mice have decreased *Mecp2* transcript and MeCP2 protein expression in the SCN.

(A) *Mecp2*$^{Floxed/y}$ mice and wild-type male littermates (*Mecp2*$^{+/y}$) were killed at CT8 and SCN was analyzed via qRT-PCR for *Mecp2* transcript abundance. *Gapdh* served as internal control. Note decreased amplification curves of the *Mecp2* transcript in *Mecp2*$^{Floxed/y}$ mice vs. *Mecp2*$^{+/y}$ mice. Raw data are presented as fluorescence intensity vs. number of PCR cycles. SCN tissues from 2 mice were pooled for each sample, from which quadruplicate determinations were made. n = 3 per genotype. *INSET:* RNA integrity of random analyzed samples. **(B)** *Mecp2*$^{Floxed/y}$ mice and *Mecp2*$^{+/y}$ mice were killed at CT12 and SCN protein extracts were analyzed via western blotting with a monoclonal anti-MeCP2 antibody. β-actin was used as loading control. *Mecp2*$^{Floxed/y}$ mice have an ~60% reduction of MeCP2 protein levels vs. wild-type littermates. SCN tissues from 2 mice were pooled for each sample. n = 3 per genotype. . Values presented below each blot represent the mean relative abundance of the protein examined, normalized to β-actin expression, for each condition. n = 3 per condition. Images quantitated on grayscale with ImageJ software. Tissue harvest performed by MAS at the laboratory of Dr. Juan I. Young, Centro de Estudios Científicos (CECS), Chile. Western blotting, RNA extraction and cDNA synthesis performed by MAS while in Chile. cDNA was shipped to Ottawa. qPCR performed by MAS in Ottawa. Data analysis and figure compiled by MAS.

FIGURE 25

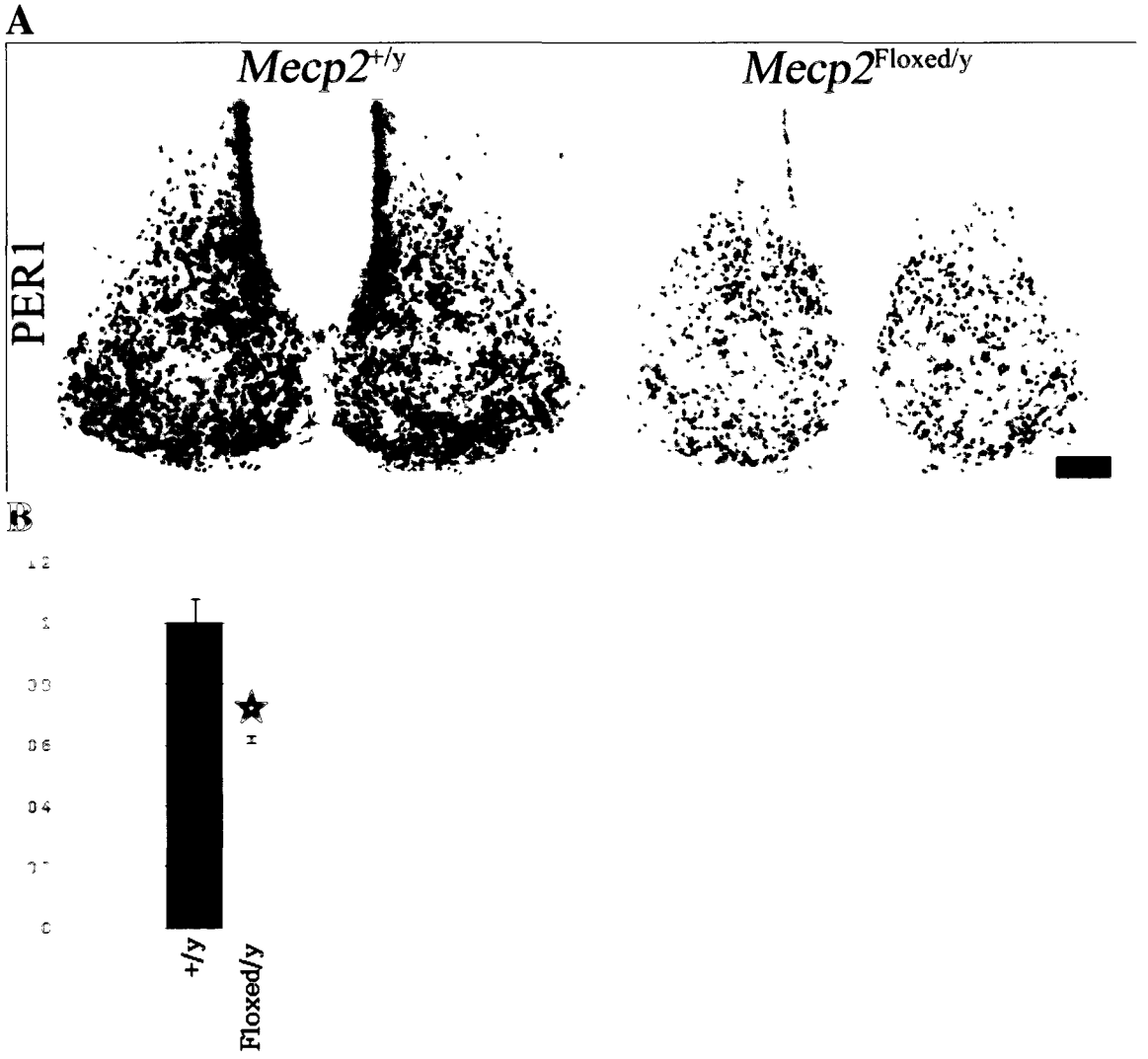

Figure 25. *Mecp2*$^{Floxed/y}$ mice have attenuated expression of PER1 protein in the SCN.

(A) *Mecp2*$^{Floxed/y}$ mice and *Mecp2*$^{+/y}$ wild-type male littermate controls were killed at CT12 and SCN sections were immunolabeled for PER1 expression. *Mecp2*$^{Floxed/y}$ mice have a clear nuclear reduction of PER1 protein levels vs. *Mecp2*$^{+/y}$ mice. n = 6 per genotype. Scale bar = 50μm. **(B)** Quantitation of PER1 SCN basal expression in *Mecp2*$^{Floxed/y}$ mice vs. non-transgenic littermate controls. Values on the y-axis represent arbitrary mean fluorescence intensity for the unilateral SCN. Values are presented as mean ± SEM. n = 6 mice per condition. *p<0.05 vs. non-transgenic controls (two-tailed Student's t-test). Images captured using a Zeiss Axiovert Observer Z1 epifluorescent/light microscope and quantitated on grayscale with ImageJ software. Tissue harvest performed by MAS while in Chile. Tissue was shipped to Ottawa. Immunolabeling performed by MAS in Ottawa. Bright-field imaging, quantitations, data analysis and figure design performed by MAS.

FIGURE 26

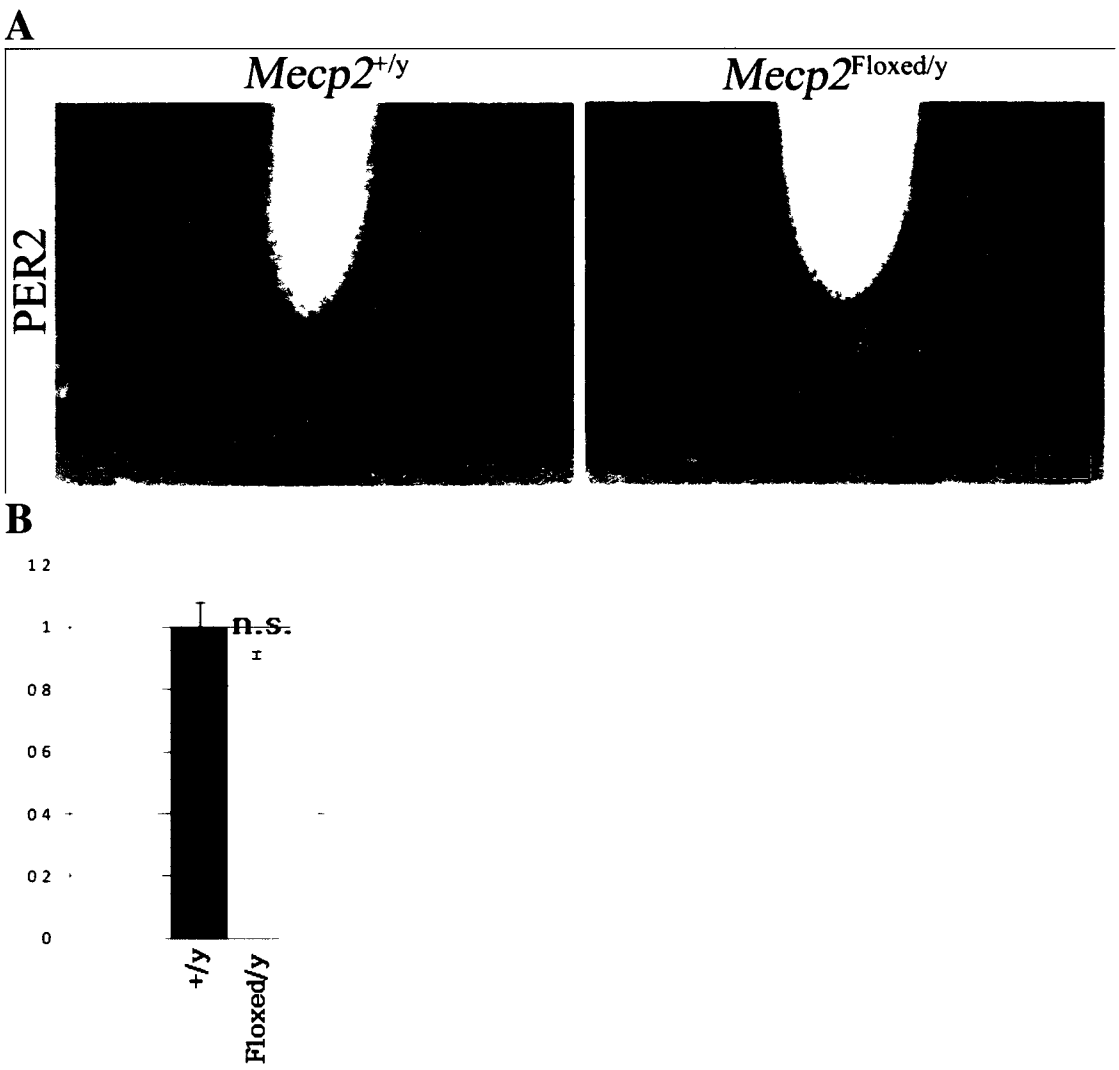

Figure 26. *Mecp2*$^{Floxed/y}$ mice have unperturbed PER2 protein levels in the SCN. **(A)** *Mecp2*$^{Floxed/y}$ mice and *Mecp2*$^{+/y}$ wild-type littermate controls were killed at CT12 and SCN sections were immunolabeled for PER2 expression. *Mecp2*$^{Floxed/y}$ mice have no qualitative differences of PER2 protein levels vs. *Mecp2*$^{+/y}$ mice. n = 6 per genotype. Scale bar = 50μm. **(B)** Quantitation of PER2 SCN basal expression in *Mecp2*$^{Floxed/y}$ mice vs. non-transgenic littermate controls. Values on the y-axis represent arbitrary mean fluorescence intensity for the unilateral SCN. Values are presented as mean ± SEM. n = 6 mice per condition. n.s. = non-significant vs. non-transgenic controls (two-tailed Student's t-test). Images captured using a Zeiss Axiovert Observer Z1 epifluorescent/light microscope and quantitated on grayscale with ImageJ software. Tissue harvest performed by MAS while in Chile. Tissue was shipped to Ottawa. Immunolabeling performed by MAS in Ottawa. Bright-field imaging, quantitations, data analysis and figure design performed by MAS.

Period genes. Nevertheless, the observed reduction in PER1 and PER2 protein levels in the SCN of tTA::miR-132 mice may also be affected by the balance of other cellular processes that are perturbed in these mice, including regulation of protein translation. Therefore, I began to characterize the possible role of *Paip2a* in the translational control of the PERIOD proteins. It is then possible that the elevated expression of PAIP2A, a suppressor of eukaryotic translation, in the SCN of tTA::miR-132 mice may be contributing to the downregulation of PER1 and PER2 proteins seen in these mice.

I obtained *Paip2a*-null mice from the Sonenberg laboratory (189) and analyzed the expression of PER1 and PER2 proteins levels in the SCN. First, I verified via western blotting the absence of PAIP2A protein in the brains of *Paip2a* knockout ($Paip2a^{-/-}$) mice. Total brain lysates were obtained at CT10 and immunoblotted against PAIP2A, PAIP2B and PABP. PAIP2A protein expression was completely abolished in the $Paip2a^{-/-}$ and $Paip2a^{-/-}/Paip2b^{-/-}$ double knock-out mice, as expected (Figure 27). Importantly, PABP protein expression was not affected in any of the mouse models analyzed, suggesting that the PAIP2A ablation does not affect the expression of PABP, a key player in eukaryotic translational mechanisms (Figure 27). Secondly, in order to argue against the possibility that the absence of PAIP2A is globally affecting the SCN proteome, I did not detect any changes in the basal expression of MeCP2 or p300 at CT14 (Figures 28A-E), two key transcriptional modulators of brain physiology and *in-vivo* miR-132 targets (this thesis).

I then examined the effect of PAIP2A ablation on the basal expression of PER1 and PER2 within the SCN during an 8-hr window of a circadian cycle, from the late subjective day (CT 10) to mid-subjective night (CT 18). This interval was chosen because

FIGURE 27

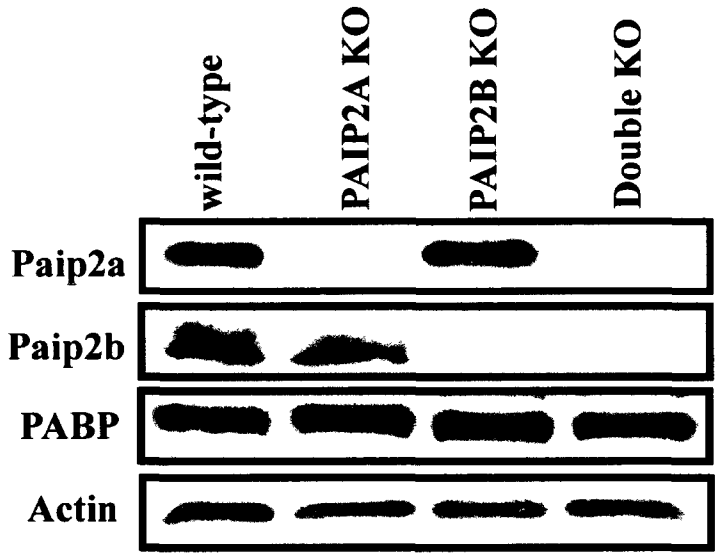

Figure 27. The absence of PAIP2A protein in the *Paip2a*$^{-/-}$ mouse brain.
Brain extracts (containing SCN tissue) from C57Bl/6 (wild-type), *Paip2a*$^{-/-}$ (PAIP2A KO), *Paip2b*$^{-/-}$ (PAIP2B KO) and *Paip2a*$^{-/-}$*Paip2b*$^{-/-}$ (double KO) mice were analyzed via western blotting for PAIP2A, PAIP2B and poly(A)-binding protein (PABP) protein expression. β-actin expression was used as a loading control. n = 3 per genotype (see Ref. 196 for mouse generation). Note the absence of PAIP2A in the *Paip2a*$^{-/-}$ mouse brain. *Paip2A*$^{-/-}$ and *Paip2B*$^{-/-}$ mice generated by Dr. Akiko Yanagiya & Dr. Nahum Sonenberg at McGill University, Montreal, Canada. This figure and figure legend are reproduced from the manuscript Alvarez-Saavedra et al, circa November 2009. Dr. Yanagiya performed the western blot experiments and compiled the figure.

FIGURE 28

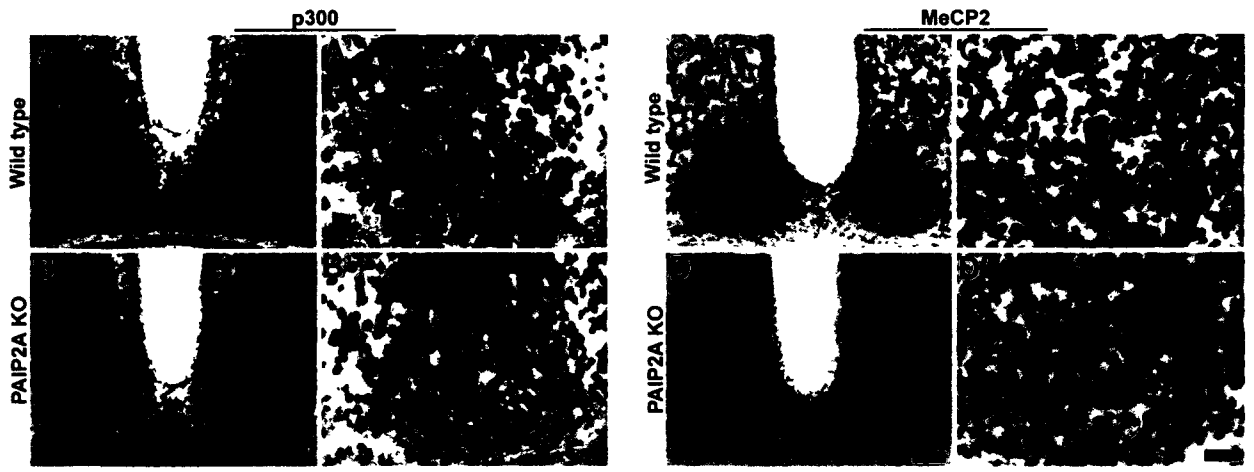

E

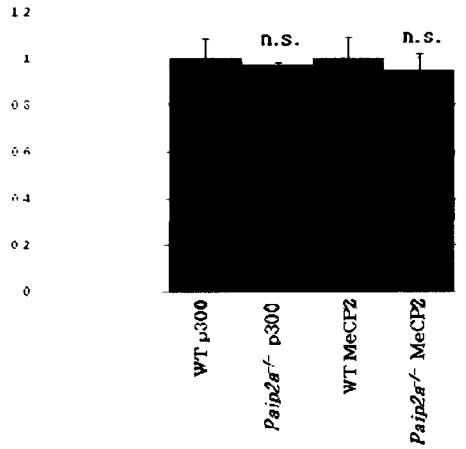

Figure 28. *Paip2a*$^{-/-}$ mice do not exhibit altered expression of the transcriptional modulators MeCP2 and p300 in the SCN.

(A, A', B, B') p300 and **(C, C', D, D')** MeCP2 protein expression in the SCN of **(B, B', D, D')** *Paip2a*$^{-/-}$ mice and **(A, A', C, C')** wild-type controls at CT14 via immunohistochemistry. Expression of **(A', B')** p300 and **(C', D')** MeCP2 in the ventrolateral SCN is given in higher magnification images. Scale bars = 100μm (A-D) and 20μm (A'-D'). n = 3 mice per genotype. Note nuclear staining of both proteins, with clear heterochromatic foci staining for MeCP2. **(E)** Quantitation of p300 and MeCP2 SCN basal expression in *Paip2a*$^{-/-}$ mice vs. wild-type littermate controls. Values on the y-axis represent arbitrary mean fluorescence intensity for the unilateral SCN. Values are presented as mean ± SEM. n = 3 mice per condition. n.s. = non-significant vs. wild-type controls (two-tailed Student's t-test). Images captured using a Zeiss Axiovert Observer Z1 epifluorescent/light microscope and quantitated on grayscale with ImageJ software. This figure and figure legend are reproduced from the manuscript Alvarez-Saavedra et al, circa November 2009. Experimental design and tissue harvesting jointly performed by MAS & HYMC. Bright-field imaging, quantitations and figure design performed by MAS.

it analyzes the rising phase as well as the declining phase of PER1 and PER2 protein rhythms. Hence, factors that either promote or inhibit translation of the cognate transcripts are likely to play a significant role during this time interval in determining the steady-state levels of the PERIOD proteins. Via immunohistochemistry, I determined that the levels of PER1 expression in the SCN of wild-type littermates were moderate at CT 10, reached a peak at CT 12-14 (as expected) and gradually declined thereafter (Figure 29A). Notably, PER1 levels in the SCN were markedly elevated in *Paip2a*$^{-/-}$ mice at the later time points (after CT12), when steady-state PER1 levels are falling in wild-type controls (Figure 29A & Figure 29C). In contrast, no substantial difference in basal PER2 expression in the SCN of wild-type and *Paip2a*$^{-/-}$ mice at all time points examined was identified, with the sole exception of CT14 (Figure 29B & Figure 29C). Very similarly to MeCP2-dependent transcriptional modulation, there seems to be a distinct mode of translational regulation, in this case via *Paip2a*, of PER1 vs. PER2. Future studies will attempt to pinpoint to the exact mechanisms of this differential regulation via PAIP2A.

In order to determine whether PAIP2A-ablation results in a behavioural phenotype, I analyzed the *in-vivo* role of PAIP2A in light-induced behavioural phase shifts. Both *Paip2a*$^{-/-}$ and wild-type littermate control mice were able to entrain stably to a full photoperiod of 12-hr light:12-hr dark (LD 12:12) and both strains remained. The mean circadian period length was statistically indistinguishable between the two genotypes. These data indicate that *Paip2a* ablation does not compromise the generation and maintenance of circadian rhythms, period length determination and stable entrainment to a full photoperiod. After 2 weeks in DD, mice received a 15-min light pulse of medium intensity (30 lux) in the early night (CT15). In wild-type mice, this light

FIGURE 29

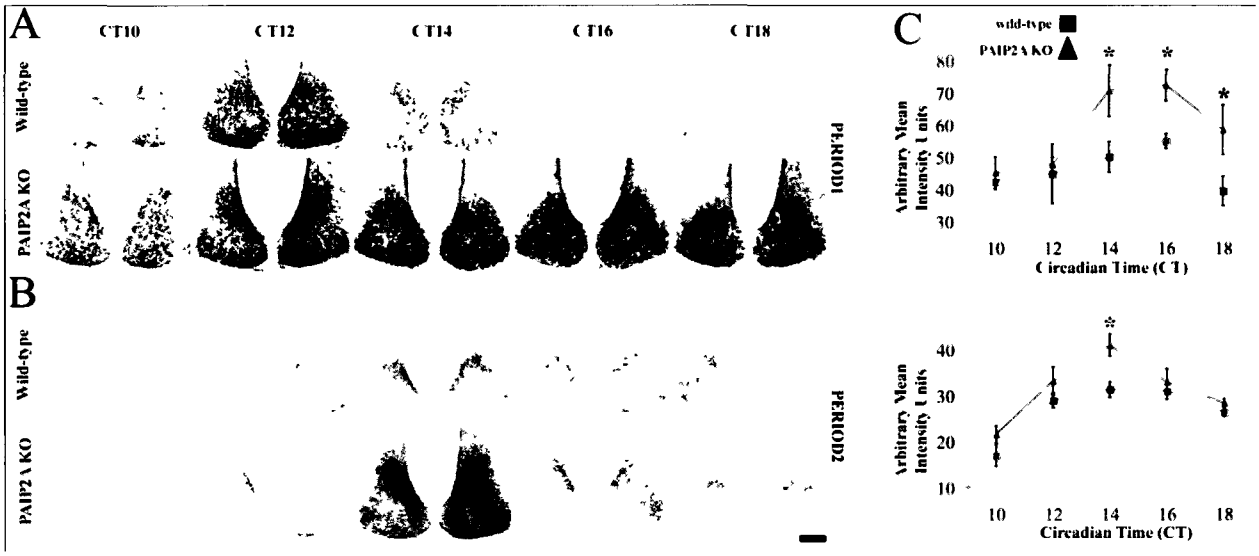

Figure 29. *Paip2a*$^{-/-}$ mice have elevated basal PER1 expression levels during the circadian night.

(**A,B**) Expression of PER1 and PER2 in the SCN of wild-type and *Paip2a*$^{-/-}$ mice from the late subjective day to the mid-subjective night. SCN tissue was harvested from wild-type (top row) and *Paip2a*$^{-/-}$ mice (bottom row) at CT 10, 12, 14, 16 and 18, and analyzed for (**A**) PER1 and (**B**) PER2 expression via immunohistochemistry. Note the decreased amplitude of PER1 rhythms in *Paip2a*$^{-/-}$ mice (A & C). Scale bar = 100 μm. (**C**) Quantitation of rhythmic PER1 (top) and PER2 (bottom) expression from (A) and (B), respectively. Values on the y-axis indicate the number of PER1- or PER2-immunoreactive nuclei in the bilateral SCN. Values are presented as mean ± SEM. n = 6 mice per genotype. *$p<0.05$, **$p<0.01$ (Fisher's LSD). Images captured using a Zeiss Axiovert Observer Z1 epifluorescent/light microscope and quantitated on grayscale with ImageJ software. This figure and figure legend are reproduced from the manuscript Alvarez-Saavedra et al, circa November 2009. Experimental design and tissue harvesting jointly performed by MAS & HYMC. Bright-field imaging and figure design performed by MAS. Quantitation software for analysis of immunohistochemical labeling conceived and written by Daniel Cornejo-Palma in ImageJ, University of Ottawa, Canada. Quantitative analysis and statistics in panel C performed by DCP under the supervision of MAS.

treatment resulted in a mean phase delay of -115 ± 10.0 minutes (Figure 30). Interestingly, light (40 lux)-induced phase delays were greatly reduced in *Paip2a*$^{-/-}$ mice (-71.3 ± 12.1 minutes, $p<0.05$; appendix I). These data indicate that PAIP2A ablation in the SCN of adult mice attenuates light-induced resetting of behavioural rhythms and suggest that PAIP2A plays an important role in the light-induced clock resetting response.

I further analyzed whether PAIP2A plays a role in regulating light-induced PER1 and PER2 expression in the SCN. This was assessed by administering a brief light pulse (15 min, 40 lux) at CT 15 to *Paip2a*$^{-/-}$ and wild-type mice, and SCN tissue harvested 4 hours later to determine PER1 and PER2 expression via immunohistochemistry. Light stimulation robustly increased the number of PER1-ir cells in the SCN of both wild-type and *Paip2a*$^{-/-}$ mice relative to their respective dark controls (Figure 31A & Figure 31C); nevertheless, the number of PER1-IR nuclei in the SCN was significantly greater in light-pulsed *Paip2a*$^{-/-}$ mice compared to light-pulsed wild-type controls (Figure 31A & Figure 31C). Similarly, photic induction of PER2 expression in SCN cells was markedly potentiated in the absence of PAIP2A (Figure 31B & Figure 31C). These data indicate that PAIP2A plays a critical role in dampening light-induced expression of PER1 and PER2.

FIGURE 30

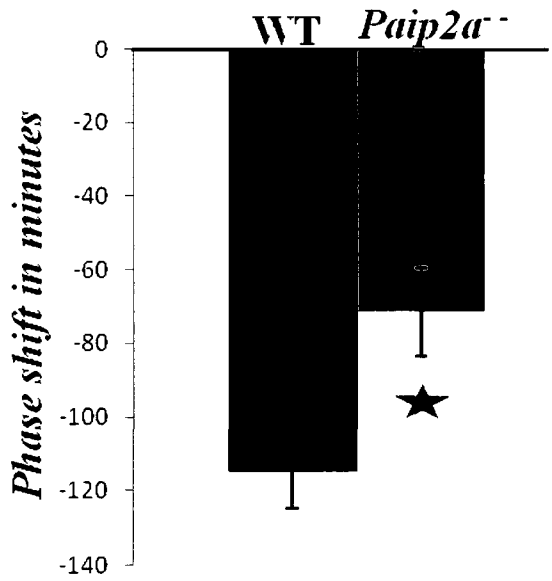

Figure 30. Light-induced clock resetting is attenuated in *Paip2a*$^{-/-}$ mice.
Wild-type (WT; black) and *Paip2a*$^{-/-}$ mice (red) were stably entrained to a fixed 12h:12h light-dark (LD) cycle prior to release into constant darkness (DD). After 2 weeks in DD, mice received a single, 15-min light pulse of 30 lux intensity at CT 15, and returned to DD. After 15 days in DD, light-induced phase shifts were quantitated. Values are presented as mean ± SEM phase shift (in min). Negative values indicate phase delays. n = 6-8 per group. *$p< 0.05$ vs. wild-type light-induced phase shifts (two-tailed Student's t-test). Please note the attenuation of light-induced phase shifts in *Paip2a*$^{-/-}$ mice. Representative actograms were not available at the time of submission of this thesis.

FIGURE 31

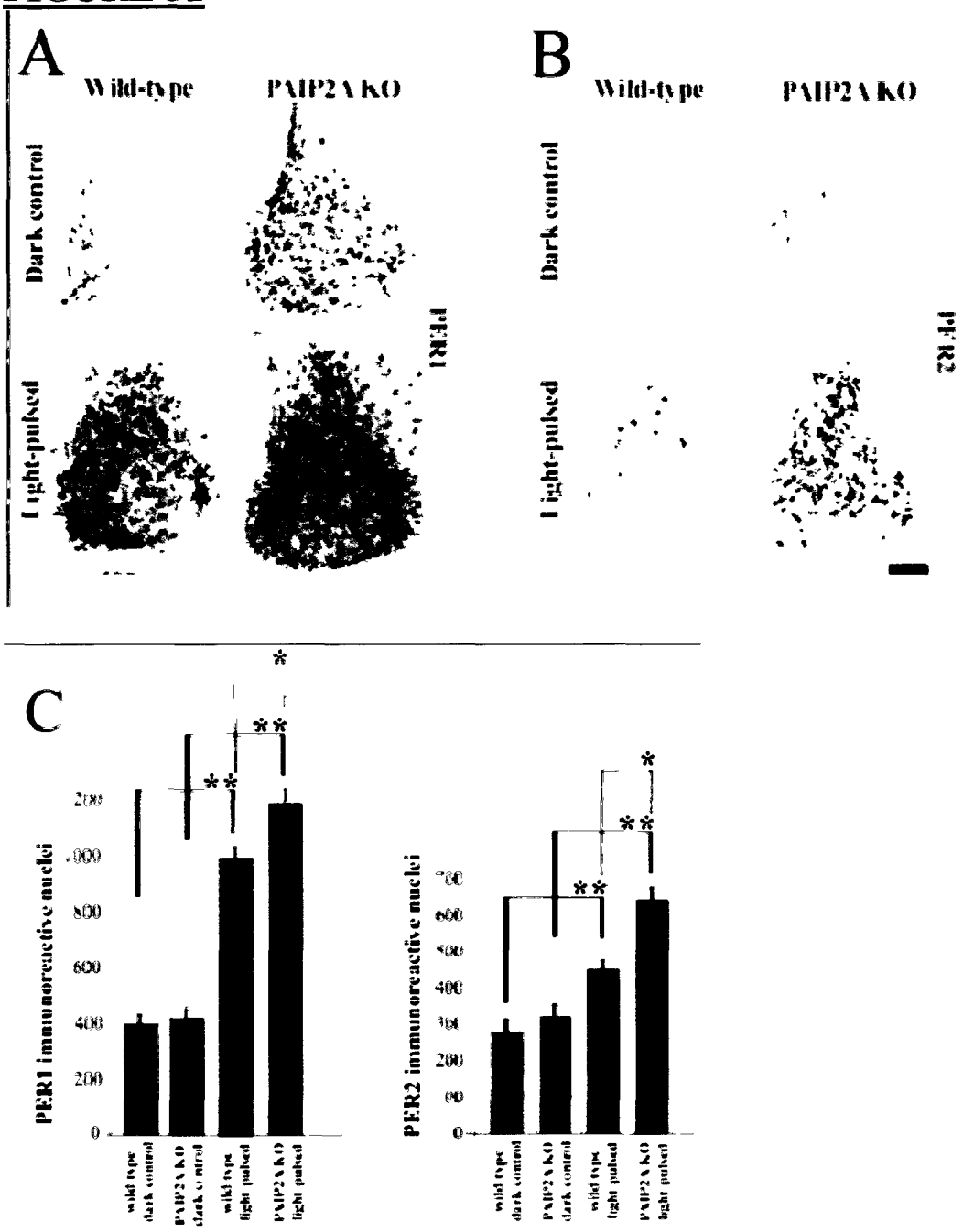

Figure 31. *Paip2a*$^{-/-}$ mice exhibit altered PER1 and PER2 light-inducible protein levels in the SCN.

(A,B) Induction of PER1 and PER2 expression in the SCN in response to photic stimulation is potentiated in the absence of PAIP2A. Wild-type and *Paip2a*$^{-/-}$ mice received a brief light pulse (15 min, 40 lux) at CT 15 and SCN tissue was harvested 4 hrs later for determination of **(A)** PER1 and **(B)** PER2 levels via immunohistochemistry. Dark control mice were not exposed to light but were killed at the same circadian time.

Note the increased labeling intensity of both proteins in light-pulsed *Paip2a*$^{-/-}$ mice vs. light-pulsed wild-type mice (bottom rows). Basal DD levels (CT19) are only increased for PER1 in the *Paip2a*$^{-/-}$ mice vs. wild-type mice (bottom rows). Scale bar = 50 μm. **(C)** Quantitation of PER1 (left) and PER2 (right) protein abundance from (A) and (B), respectively. Values on the y-axis represent the mean intensity of the unilateral SCN, given in arbitrary units. Values are presented as mean ± SEM. n = 4 - 6 mice per group. *$p<0.05$, **$p<0.01$ (Fisher's LSD). Images captured using a Zeiss Axiovert Observer Z1 epifluorescent/light microscope and quantitated on grayscale with ImageJ software. This figure and figure legend are reproduced from the manuscript Alvarez-Saavedra et al, circa November 2009. Experimental design and tissue harvesting jointly performed by MAS & HYMC. Bright-field imaging and figure design performed by MAS. Quantitation software for analysis of immunohistochemical labeling conceived and written by Daniel Cornejo-Palma in ImageJ, University of Ottawa, Canada. Quantitative analysis and statistics in panel C performed by DCP under the supervision of MAS.

DISCUSSION

i. microRNA-132 target identification

Hundreds of miRNAs have been cloned from the brain and other mammalian tissues. Nevertheless, their tissue-specific functions remain largely unknown. Only a few reports have provided mechanistic evidence for miRNA-specific regulation of neurophysiological processes (191-194). For example, it was recently shown that miR-9 and miR-124 are key mediators in the switching of chromatin remodeling complexes regulating neuronal progenitor cell differentiation in mouse development (194). In addition, it has also been shown that miR-124 is involved in regulating neuronal differentiation via regulation of splicing factors (191). In order to characterize miR-132 targets in the mouse SCN and identify their role in circadian physiology, I used 3'UTR reporter assays to demonstrate that miR-132 represses the expression of three factors implicated in chromatin remodeling (*Mecp2, p300, Jarid1a*) and two others involved in translation control (*Btg2, Paip2a*) through specific target sites, known as MREs, within the 3'UTRs of the cognate transcripts (Figure 10). In addition, via *in-vitro* and *in-vivo* knockdown experiments, as well as *in-vivo* gain-of-function, the miR-132 specific regulation of these five these targets was validated (Figures 11-14).

ii. microRNA-132 as an orchestrator of chromatin remodeling and translational control in light-induced clock resetting

The bioinformatics analysis presented in this thesis provides the novel discovery that miR-132 predicted targets are highly enriched for chromatin remodeling and translational control gene clusters. I further provide evidence to support this hypothesis via the *in vivo* characterization of miR-132 dependent regulation of five selected genes involved in these

two functional processes. In addition, there are two key mechanistic lines of evidence that further support the role of miR-132 as an orchestrator of chromatin remodeling and translational control: 1) MeCP2-dependent transcriptional modulation of the *Period* genes; and 2) PAIP2A-dependent translational control of the *Period* genes.

I provide evidence for the establishment of a mechanistic link between MeCP2 and PER1 and PER2 expression. Via ChIP experiments, I demonstrate that MeCP2 is enriched at all 5' regulatory elements within 10 kb of the *mPer1* transcription start site (TSS) that were examined: this encompasses a CpG island, a CRE site and previously characterized E-boxes proximal to the TSS. This is in stark contrast to the distribution of MeCP2 within the *mPer2* promoter: MeCP2 enrichment was restricted to the two CRE sites examined, and was not detected within a region proximal to the TSS that encompasses a CpG island and a functional E-box enhancer (Figure 22). These data raise the possibility that MeCP2 differentially regulates *mPer1* vs. *mPer2* transcription via uncharacterized mechanisms. This hypothesis is further supported via the miR-132 transgenic data, since only PER1 exhibits a dampening of rhythmic expression, even though light-inducible expression is attenuated for both proteins. In addition, a MeCP2 hypomorph mouse model (*Mecp2*$^{\text{floxed/y mice}}$) reveals that PER1 protein levels are markedly reduced vs. PER2 protein levels (Figures 25-26). Previous work has hinted at the possibility that *mPer1* and *mPer2* expression are regulated by overlapping but distinct mechanisms (13, 146). It is not inconceivable that the dampening of PER1 rhythms in the tTA::miR-132 transgenics may be due, in part, to a reduction in a potential facilitatory effect of MeCP2 on E-box-mediated transcription of the *mPer1* gene, but not of the *mPer2* gene. It would also be interesting to explore the possibility of a functional

interaction between MeCP2 and p300, which has been shown to augment CLOCK/BMAL1-mediated transcription (80), at the *mPer1* E-boxes. It is noteworthy mentioning that even though H3K4Me3 expression was enhanced in the SCN of our transgenics (arguably due to suppressed JARID1A expression), neither a global increase in gene expression nor a gene-specific increase in *Per1* or *Per2* expression was observed. This is consistent with the notion that the H3K4Me3 mark places chromatin in a transcriptionally permissive state, but other factors are required in order to fully activate a particular gene.

It is important to note that while MeCP2 was originally characterized as a transcriptional repressor, a recent report profiling hypothalamic gene expression in *Mecp2*-null as well as *Mecp2*-overexpressing mice revealed that MeCP2 activates, rather than represses, the majority (~85%) of the genes that displayed altered expression (160). In addition, this report showed, in the case of MeCP2-activated genes, that MeCP2 physically interacts with CREB at promoter sites to activate gene transcription (80). This functional interplay between MeCP2 and CREB is of potential relevance in the case of light-triggered transcriptional activation within the SCN, which requires the actions of CREB. I provide mechanistic evidence supporting this notion since MeCP2 activation of PER1 is dependent upon CREB (Figure 23). In addition, it is tempting to further propose that light-induced phosphorylation of MeCP2 facilitates the functional dynamic between MeCP2 and CREB, thereby enhancing CREB-dependent transcription in the SCN.

Collectively, the discovery of MeCP2 in the modulation of circadian rhythmicity is highly suggestive of a light-induced clock entrainment model that primarily occurs via rapid and dynamic changes at the level of histone epigenetics and DNA methylation

coupled to CREB-induced transcriptional activation of miR-132. This is shown in this thesis via MeCP2 binding in the *Per1* and *Per2* gene promoters, coupled to dynamic changes in H3K4 trimethylation and MeCP2 pS421 phosphorylation (171 and Figure 18). A recent report (195) has shown dynamic changes in DNA methylation at the *Zif268* gene promoter that serve both repressive and activating transcriptional roles during long-term memory formation. This coincides with the present data suggesting that MeCP2 may play an activating role in the transcriptional regulation of *Per1* during clock entrainment. It remains to be determined whether light may trigger *Per1*- and *Per2*-specific methylation events within their regulatory elements. In summary, I propose that MeCP2 functions as a transcriptional modulator that interacts with various molecular components of the SCN clock that affect the epigenetic status of SCN-cell networks. Furthermore, the characterization of *Jarid1a,* an H3K4-specific demethylase, as a miR-132 target hints at a role of its demethylase activity in light entrainment of the mammalian clock and/or other neurobiological processes.

This thesis also provides evidence to support the notion that miR-132 orchestrates translational control of the clock resetting response via PAIP2A regulation of *Per1* and *Per2* translation. Extensive biochemical analyses have established PAIP2A as a potent translational inhibitor via displacement of PABP from the poly(A) tail, thereby abrogating PABP-dependent enhancement of eIF4G-mediated translation. However, the physiological processes that are affected by altered PAIP2A expression have not as yet been reported in the literature. I show that PAIP2A is an essential negative modulator of light-induced PER1 and PER2 expression, since genetic deletion of *Paip2a* potentiates the expression of both proteins in response to photic stimulation. Furthermore, in the

absence of PAIP2A, rhythmic expression of PER1 during the first half of the circadian night is elevated. The effect of *Paip2a* abrogation on basal PER2 expression is more subtle by comparison (Figure 29). Notably, these results correlate with those obtained in miR-132 transgenic mice, since PER1 rhythms are dampened without a discernible effect on PER2 rhythms (Figure 19). Clearly, the data suggest differential regulation of *Per1* vs. *Per2* translational control via PAIP2A.

iii. Light-induction of molecular waves that regulate the clock-resetting response:

The light-induced molecular waves hypothesis

Not only does light induce the expression of endogenous miR-132 within the SCN (130), but the expression or activity of the targets studied herein is also light-responsive. I show that a brief nocturnal photic stimulation activates phosphorylation of MeCP2, trimethylation at lysine 4 of H3, as well as PAIP2A and BTG2 total protein levels (Figures 18). The collective data leads me to propose a biological model where light triggers waves of molecular events that initially facilitate the resetting response, but also sets in motion events (e.g. induction of miR-132) that, later on, act in a feedback inhibitory fashion to dampen the response and restore the SCN to homeostasis (see Figure 32 for proposed model).

Briefly, in mammals, light-induced clock resetting is governed via circadian photic entrainment from sunlight. Light travels through the retinohypothalamic tract onto SCN neurons that trigger intracellular signaling pathways that lead to the following post-translational modifications, amongst others:

A. Phosphorylation of CREB at S133 (37).

B. pERK1/2 phosphorylation (33).

FIGURE 32

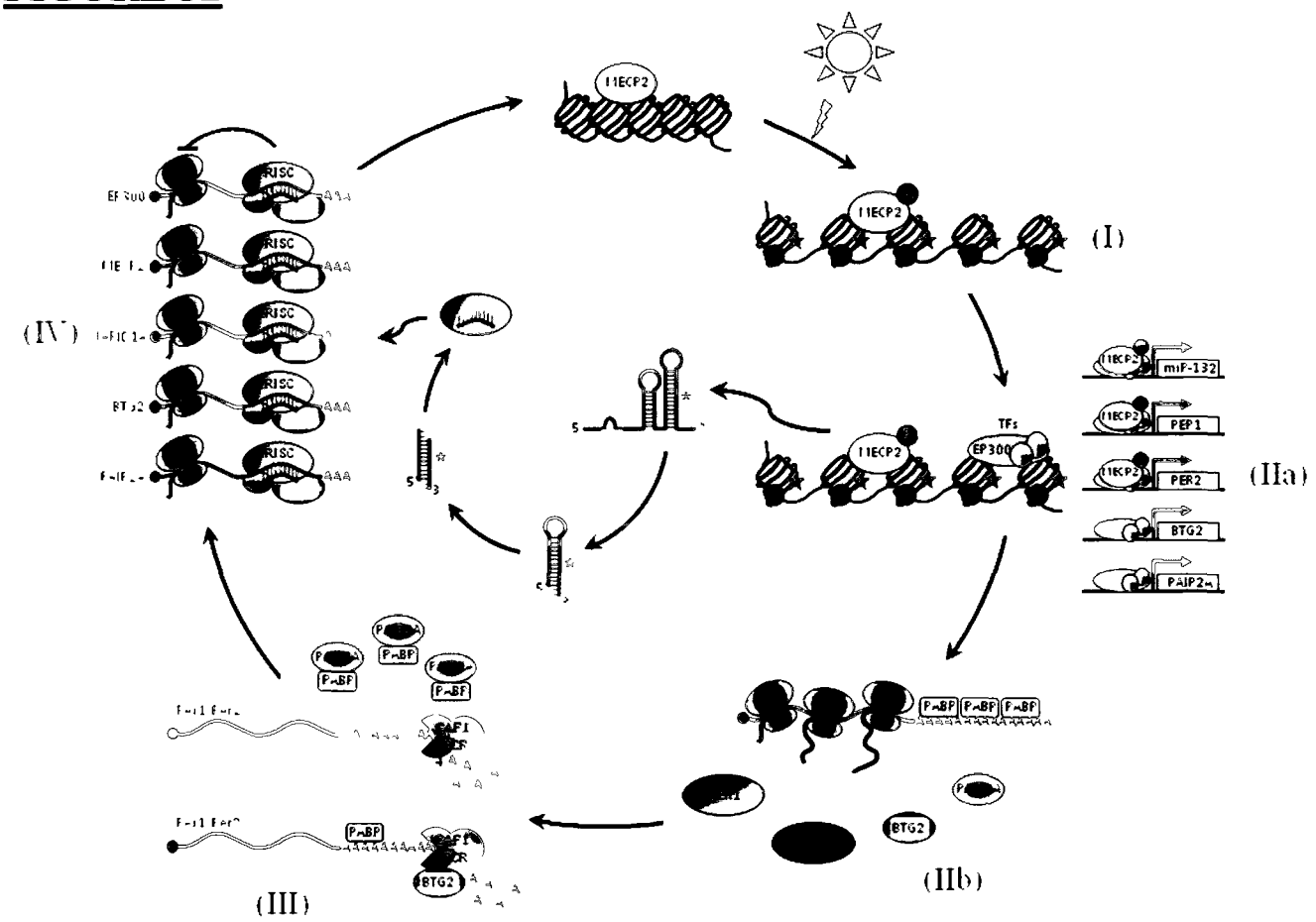

Figure 31. miR-132-dependent post-transcriptional regulation of clock entrainment physiology via modulation of chromatin remodeling and translational control gene targets:

The Light-Induced Molecular Waves Hypothesis.

(Wave I) Nocturnal light exposure triggers rapid, post-translational events in SCN neurons that promote remodeling of chromatin to a transcriptionally permissive state. For instance, a brief light pulse elicits the phosphorylation (P) of MeCP2 at Ser421 (171 and Figure 18), trimethylation (M) of histone H3 at lysine 4 (Figure 18) and acetylation (A) of histone H2A.Z at lysine residues K4, K7 and K11 (purple circle; MAS & HYMC, unpublished). **(Wave IIa)** As a result, transcription factors (TFs) and their co-modulators (e.g. MeCP2 and EP300) gain access to gene promoters and transactivate a number of light-responsive genes, including *Per1, Per2, Btg2, Paip2a* as well as miR-132 (130). Interestingly, my data suggests that MeCP2 phosphorylation positively regulates the expression of *mPer1* and *mPer2* (Figure 23). **(Wave IIb)** Subsequent mRNA translation leads to increased protein abundance of PER1, PER2, BTG2 and PAIP2A. Polyadenylate binding protein (PABP) physically associates with the polyA tails of the transcripts and facilitates translation (165). **(Wave IIb')** Meanwhile, the primary miR-132 transcript

generate the pre-miR-132 stem loop and the miRNA duplex, export of pre-miR-132 to the cytoplasm, and incorporation of the mature strand (denoted by the red asterisk) into the RNA induced silencing complex (RISC). (**Wave III**) As the levels of BTG2 and PAIP2A proteins increase, further translation of *Per1* and *Per2* transcripts is inhibited. PAIP2A competes with the polyA tail for binding to PABP, thus inhibiting PABP-dependent facilitation of translation (165); moreover, PAIP2A may also promote transcript degradation (198). BTG2 can physically associate with the CAF1/CCR4 deadenylase complex and enhances CAF1/CCR4-mediated deadenylation and mRNA decay (162). (**Wave IV**) With rising levels of mature miR-132, miRNA-mediated translational repression of miR-132 targets (*Ep300, Mecp2, Jarid1a, Btg2, Paip2a*) ensues, restoring homeostasis to those processes that were triggered by light. This figure and figure legend were adapted from the manuscript Alvarez-Saavedra et al, circa March 2010. This model was jointly conceived by MAS & HYMC, from data generated by MAS from August 2008 to March 2010 at the University of Ottawa. The powerpoint model was designed by HYMC. The "light-induced molecular waves concept" was created by MAS.

C. Phosphorylation of MeCP2 at S421 (171 and Figure 18).

D. Trimethylation of H3K4 (Figure 18).

E. Triacetylation of H2.AZ at K4-K7-K11 (data not available at the time of publication of this thesis).

In combination, these post-translational modifications trigger the relaxation of nuclear chromatin into a permissive state that leads to transcriptional activation of target genes via specific transcription factors that bind to DNA regulatory sequence motifs (e.g. CRE, E-box, CpG islands, etc.) of the genes coding for miR-132, *Mecp2*, *Jarid1a*, *Ep300*, *Btg2*, *Paip2a*, and the clock genes *Per1* and *Per2*. Some of these genes are themselves transcriptionally regulated via MeCP2 and/or CREB, as in the case of miR-132 (130) and *Per1* and *Per2* (Figure 22 & Figure 23), suggesting a feedback model of regulation. Subsequently, the *Mecp2*, *Jarid1a*, *Ep300*, *Btg2*, *Paip2a, Per1* and *Per2* transcripts are further processed for translation at the same time as pri-miR-132 processing begins. Once physiological levels of PER1 and PER2 proteins accumulate in the cytoplasm, PAIP2A- and BTG2-dependent control of *Per1* and *Per2* translation begins. PAIP2A competes with the poly(A)-tail for binding to PABP, thus inhibiting PABP-dependent facilitation of translation (165). On the other hand, BTG2 can physically associate with the CAF1/CCR4 deadenylase complex and enhances CAF1/CCR4-mediated deadenylation and mRNA decay (162). Meanwhile the light-induced proteins perform their clock-resetting functions, pre-miR-132 undergoes a series of processing steps, including sequential proteolytic cleavages to generate the pre-miR-132 stem loop and the miRNA duplex, export of pre-miR-132 to the cytoplasm, and incorporation of the mature strand (denoted by the star) into the RNA induced silencing complex (RISC). As mature miR-132 levels arise, miR-132 dependent translational regulation of *Ep300, Jarid1a, Mecp2,*

Btg2 and *Paip2a* occurs, restoring homeostasis to this network/cascade of events that were first induced by photic stimulation (see Figure 31 for schematic model).

iv. Outlook

From a broader perspective, this work raises the tantalizing possibility that miRNAs in general regulate specific physiological processes, not necessarily through their repressive action on a single target, but through coordinated regulation of multiple targets that play a role in a common biological response. I propose that miRNAs have evolved to orchestrate and tightly regulate tissue-specific physiological processes via their actions on related genes. Future studies will undoubtedly identify novel gene clusters that are under the regulation of other miRNAs and whether these processes may be regulated via a single miRNA or as functional miRNA clusters.

In addition, I foresee that future research will focus on the characterization of the specific roles that miRNAs may have in specific tissues and cell-types, besides the discovery of novel, previously unsequenced miRNAs. Future effort will also focus on the identification of *cis*-acting elements that regulate miRNA transcription. It is possible that there is a new layer of transcriptional regulation via unknown transcriptional modules that specifically regulate miRNA genes. In order to begin to address these questions in mammalian systems, it is crucial to create a library of inducible miRNA knock-in mouse strains that allow for cell- and/or tissue-specific deletion and inducible expression (i.e. inducible rescue) of a miRNA. Future efforts should be emphasized on the creation and establishment of such a library in order to decipher the role(s) of miRNAs in mammalian physiology.

BIBLIOGRAPHY

1. Nelson, RJ (2005). An Introduction to Behavioral Endocrinology. Sunderland, MA: Sinauer Associates.

2. Bretzl, H (1903). Botanische Forschungen des Alexanderzuges. Leipzig: BG Teubner.

3. de Mairan, J (1729). Observation botanique. Histoire de l'Academie Royale des Sciences, 35–36.

4. Refinetti, Roberto (2005). Circadian Physiology, Second edition. Florence, KY: CRC Press.

5. Candolle, AP de (1832). Physiologie Végétale. Paris: Béchet.

6. Kalmus, H (1935). Biologia Generalis *11*:93.

7. Bünning, E (1935). Ber. Deut. Botan. Ges. *53*:594.

8. Konopka, RJ, Benzer, S (1971). Clock mutants of Drosophila melanogaster. PNAS *68*(9):2112-6.

9. Ralph, MR, Menaker, M (1988). A mutation of the circadian system in golden hamsters. Science *241* (4870):1225-7.

10. Lowrey PL, Shimomura K, Antoch MP, Yamazaki S, Zemenides PD, Ralph MR, Menaker M, Takahashi JS (2000). Positional syntenic cloning and functional characterization of the mammalian circadian mutation tau. Science *288*(54650):483-92.

11. Sun ZS, Albrecht U, Zhuchenko O, Bailey J, Eichele G, Lee CC (1997) RIGUI, a putative mammalian ortholog of the Drosophila period gene. Cell *90*(6):1003-11.

12. Tei H, Okamura H, Shigeyoshi Y, Fukuhara C, Ozawa R, Hirose M, Sakaki Y (1997). Circadian oscillation of a mammalian homologue of the Drosophila period gene. Nature *389*(6650):512-6.

13. Shearman LP, Zylka MJ, Weaver DR, Kolakowski LF Jr, Reppert SM (1997). Two period homologs: circadian expression and photic regulation in the suprachiasmatic nuclei. Neuron *19*(6):1261-9.

14. Takumi T, Matsubara C, Shigeyoshi Y, Taguchi K, Yagita K, Maebayashi Y, Sakakida Y, Okumura K, Takashima N, Okamura H (1998). A new mammalian period gene predominantly expressed in the suprachiasmatic nucleus. Genes cells *3*(3):167-76.

15. King DP, Zhao Y, Sangoram AM, Wilsbacher LD, Tanaka M, Antoch MP, Steeves TD, Vitaterna MH, Kornhauser JM, Lowrey PL, Turek FW, Takahashi JS (1997). Positional cloning of the mouse circadian clock gene. Cell *89*(4):641-53.

16. Kondo T, Strayer CA, Kulkarni RD, Taylor W, Ishiura M, Golden SS, Johnson CH (1993). Circadian rhythms in prokaryotes: luciferase as a reporter of circadian gene expression in cyanobacteria. PNAS *90*(12):5672-6.

17. Moore RY, Eichler VB (1972). Loss of a circadian adrenal corticosterone rhythm following suprachiasmatic lesions in the rat. Brain Research *42*(1):201-6.

18. Stephan FK, Zucker I (1972). Circadian rhythms in drinking behavior and locomotor activity of rats are eliminated by hypothalamic lesions. PNAS *69*(6):1583-6.

19. van Esseveldt, KE, Lehman MN, Boer GJ (2000). The suprachiasmatic nucleus and the circadian time-keeping system revisited. Brain Res Brain Res Rev. *33*(1):34-77.

20. Inouye ST, Kawamura H (1979). Persistence of circadian rhythmicity in a mammalian hypothalamic "island" containing the suprachiasmatic nucleus. PNAS *76*(11):5962-6.

21. Green DJ, Gillette R (1982). Circadian rhythm of firing rate recorded from single cells in the rat suprachiasmatic brain slice. Brain Research *245*(1): 198-200.

22. Groos GA, Hendriks J (1979). Regularly firing neurones in the rat suprachiasmatic nucleus. Experientia *35*(12):1597-8.

23. Ralph MR, Foster RG, Davis FC, Menaker M (1990). Transplanted suprachiasmatic nucleus determines circadian period. Science *247*(4945):975-8.

4. Takahashi JS, Hong HK, Ko CH, McDearmon EL (2008). The genetics of mammalian circadian order and disorder: implications for physiology and disease. Nat Rev Genet. *9*(10):764-75.

25. Foster RG, Provencio I, Hudson D, Fiske S, De Grip W, Menaker M (1991). Circadian photoreception in the retinally degenerate mouse (rd/rd). J Comp Physiol A. *169*(1):39-50.

26. Provencio I, Cooper HM, Foster RG (1998). Retinal projections in mice with inherited retinal degeneration: implications for circadian photoentrainment. J Comp Neurol. *395*(4):417-39.

27. Provencio I, Rollag MD, Castrucci AM (2002). Photoreceptive net in the mammalian retina. This mesh of cells may explain how some blind mice can still tell day from night. Nature *415*(6871):493.

28. Berson DM, Dunn FA, Takao M (2002). Phototransduction by retinal ganglion cells that set the circadian clock. Science *295*(5557):1070-3.

29. Hattar S, Liao HW, Takao M, Berson DM, Yau KW (2002). Melanopsin-containing retinal ganglion cells: architecture, projections, and intrinsic photosensitivity. Science *295*(5557):1065-70.

30. Hannibal J, Møller M, Ottersen OP, Fahrenkrug J (2000). PACAP and glutamate are co-stored in the retinohypothalamic tract. J Comp Neurol. *418*(2):147-55.

31. Colwell CS, Foster RG, Menaker M (1991). NMDA receptor antagonists block the effects of light on circadian behavior in the mouse. Brain Res. *554*(1-2):105-10.

32. Liou SY, Shibata S, Iwasaki K, Ueki S (1986). Optic nerve stimulation-induced increase of release of 3H-glutamate and 3H-aspartate but not 3H-GABA from the suprachiasmatic nucleus in slices of rat hypothalamus. Brain Res Bull. *16*(4):527-31.

33. Obrietan K, Impey S, Storm DR (1998). Light and circadian rhythmicity regulate MAP kinase activation in the suprachiasmatic nuclei. Nat Neurosci. *1*(8):693-700.

34. Lee B, Almad A, Butcher GQ, Obrietan K (2007). Protein kinase C modulates the phase-delaying effects of light in the mammalian circadian clock. Eur J Neurosci. 26(2):451-62.

35. Butcher GQ, Lee B, Cheng HY, Obrietan K (2005). Light stimulates MSK1 activation in the suprachiasmatic nucleus via a PACAP-ERK/MAP kinase-dependent mechanism. J Neurosci. *25*(22):5305-13.

36. Kornhauser JM, Nelson DE, Mayo KE, Takahashi JS (1990). Photic and circadian regulation of c-fos gene expression in the hamster suprachiasmatic nucleus. Neuron *5*(2):127-34.

37. Ginty DD, Kornhauser JM, Thompson MA, Bading H, Mayo KE, Takahashi JS, Greenberg ME (1993). Regulation of CREB phosphorylation in the suprachiasmatic nucleus by light and a circadian clock. Science *260*(5105):238-41.

38. Obrietan K, Impey S, Smith D, Athos J, Storm DR (1999). Circadian regulation of cAMP response element-mediated gene expression in the suprachiasmatic nuclei. J Biol Chem. *274*(25):17748-56.

39. Güldner FH (1983). Numbers of neurons and astroglial cells in the suprachiasmatic nucleus of male and female rats. Exp Brain Res. *50*(2-3):373-6.

40. Moore RY, Speh JC, Leak RK (2002). Suprachiasmatic nucleus organization. Cell Tissue Res. *309*(1):89-98.

41. Altman J, Bayer SA (1986). The development of the rat hypothalamus. Adv Anat Embryol Cell Biol. *100*:1-178.

42. Moore RY, Speh JC (1993). GABA is the principal neurotransmitter of the circadian system. Neurosci Lett. *150*(1):112-6.

43. Moore RY, Speh JC, Leak RK (2002). Suprachiasmatic nucleus organization. Cell Tissue Res. *309*(1):89-98.

44. Moore RY, Lenn NJ (1972). A retinohypothalamic projection in the rat. J Comp Neurol. *146*(1):1-14.

45. Hendrickson AE, Wagoner N, Cowan WM (1972). An autoradiographic and electron microscopic study of retino-hypothalamic connections. Z Zellforsch Mikrosk Anat. 135(1):1-26.

46. Vandesande F, Dierickx K (1975). Identification of the vasopressin producing and of the oxytocin producing neurons in the hypothalamic magnocellular neurosecretory system of the rat. Cell Tissue Res. *164*(2):153-62.

47. Sofroniew MV, Weindl A (1978). Projections from the parvocellular vasopressin- and neurophysin-containing neurons of the suprachiasmatic nucleus. Am J Anat. *153*(3):391-429.

48. Card JP, Brecha N, Karten HJ, Moore RY (1981). Immunocytochemical localization of vasoactive intestinal polypeptide-containing cells and processes in the suprachiasmatic nucleus of the rat: light and electron microscopic analysis. J Neurosci. *1*(11):1289-303.

49. Watts AG, Swanson LW, Sanchez-Watts G (1987). Efferent projections of the suprachiasmatic nucleus: I. Studies using anterograde transport of Phaseolus vulgaris leucoagglutinin in the rat. J Comp Neurol. *258*(2):204-29.

50. Moga MM, Weis RP, Moore RY (1995). Efferent projections of the paraventricular thalamic nucleus in the rat. J Comp Neurol. *1359*(2):221-38.

51. Watts AG, Swanson LW (1987). Efferent projections of the suprachiasmatic nucleus: II. Studies using retrograde transport of fluorescent dyes and simultaneous peptide immunohistochemistry in the rat. J Comp Neurol. *258*(2):230-52.

52. Thompson RH, Swanson LW (1998). Organization of inputs to the dorsomedial nucleus of the hypothalamus: a reexamination with Fluorogold and PHAL in the rat. Brain Res Brain Res Rev. *27*(2):89-118.

53. Leak RK, Moore RY (2001). Topographic organization of suprachiasmatic nucleus projection neurons. J Comp Neurol. *433*(3):312-34.

54. Reddy P, Jacquier AC, Abovich N, Petersen G, Rosbash M (1986). The period clock locus of D. melanogaster codes for a proteoglycan. Cell *46*(1):53-61.

55. Citri Y, Colot HV, Jacquier AC, Yu Q, Hall JC, Baltimore D, Rosbash M (1987). A family of unusually spliced biologically active transcripts encoded by a Drosophila clock gene. Nature *326*(6108):42-7.

56. Hoffman EC, Reyes H, Chu FF, Sander F, Conley LH, Brooks BA, Hankinson O (1991). Cloning of a factor required for activity of the Ah (dioxin) receptor. Science *252*(5008):954-8.

57. Jackson FR, Bargiello TA, Yun SH, Young MW (1986). Product of per locus of Drosophila shares homology with proteoglycans. Nature *320*(6058):185-8.

58. Nambu JR, Lewis JO, Wharton KA Jr, Crews ST (1991). The Drosophila single-minded gene encodes a helix-loop-helix protein that acts as a master regulator of CNS midline development. Cell *67*(6):1157-67.

59. Lee C, Bae K, Edery I (1999). PER and TIM inhibit the DNA binding activity of a Drosophila CLOCK-CYC/dBMAL1 heterodimer without disrupting formation of the heterodimer: a basis for circadian transcription. Mol Cell Biol. *19*(8):5316-25.

60. Hardin PE, Hall JC, Rosbash M (1990). Feedback of the Drosophila period gene product on circadian cycling of its messenger RNA levels. Nature *343*(6258):536-40.

61. Hogenesch JB, Gu YZ, Jain S, Bradfield CA (1998). The basic-helix-loop-helix-PAS orphan MOP3 forms transcriptionally active complexes with circadian and hypoxia factors. Proc Natl Acad Sci *95*(10):5474-9.

62. Sangoram AM, Saez L, Antoch MP, Gekakis N, Staknis D, Whiteley A, Fruechte EM, Vitaterna MH, Shimomura K, King DP, Young MW, Weitz CJ, Takahashi JS (1998). Mammalian circadian autoregulatory loop: a timeless ortholog and mPer1 interact and negatively regulate CLOCK-BMAL1-induced transcription. Neuron *21*(5):1101-13.

63. Darlington TK, Wager-Smith K, Ceriani MF, Staknis D, Gekakis N, Steeves TD, Weitz CJ, Takahashi JS, Kay SA (1998). Closing the circadian loop: CLOCK-induced transcription of its own inhibitors per and tim. Science *280*(5369):1599-603.

64. Kume K, Zylka MJ, Sriram S, Shearman LP, Weaver DR, Jin X, Maywood ES, Hastings MH, Reppert SM (1999). mCRY1 and mCRY2 are essential components of the negative limb of the circadian clock feedback loop. Cell *98*(2):193-205.

65. Hao H, Allen DL, Hardin PE (1997). A circadian enhancer mediates PER-dependent mRNA cycling in Drosophila melanogaster. Mol Cell Biol. *17*(7):3687-93.

66. Gekakis N, Staknis D, Nguyen HB, Davis FC, Wilsbacher LD, King DP, Takahashi JS, Weitz CJ (1998). Role of the CLOCK protein in the mammalian circadian mechanism. Science *280*(5369):1564-9.

67. Allada R, White NE, So WV, Hall JC, Rosbash M (1998). A mutant Drosophila homolog of mammalian Clock disrupts circadian rhythms and transcription of period and timeless. Cell *93*(5):791-804.

68. Rutila JE, Suri V, Le M, So WV, Rosbash M, Hall JC (1998). CYCLE is a second bHLH-PAS clock protein essential for circadian rhythmicity and transcription of Drosophila period and timeless. Cell *93*(5):805-14.

69. Bell-Pedersen D, Cassone VM, Earnest DJ, Golden SS, Hardin PE, Thomas TL, Zoran MJ (2005). Circadian rhythms from multiple oscillators: lessons from diverse organisms. Nat Rev Genet. *6*(7):544-56.

70. Lee C, Etchegaray JP, Cagampang FR, Loudon AS, Reppert SM (2001). Posttranslational mechanisms regulate the mammalian circadian clock. Cell *107*(7):855-67.

71. Zheng B, Albrecht U, Kaasik K, Sage M, Lu W, Vaishnav S, Li Q, Sun ZS, Eichele G, Bradley A, Lee CC (2001). Nonredundant roles of the mPer1 and mPer2 genes in the mammalian circadian clock. Cell *105*(5):683-94.

72. Preitner N, Damiola F, Lopez-Molina L, Zakany J, Duboule D, Albrecht U, Schibler U (2002). The orphan nuclear receptor REV-ERBalpha controls circadian transcription within the positive limb of the mammalian circadian oscillator. Cell *110*(2):251-60.

73. Gallego M, Virshup DM (2007). Post-translational modifications regulate the ticking of the circadian clock. Nat Rev Mol Cell Biol. *8*(2):139-48.

74. Meng QJ, Logunova L, Maywood ES, Gallego M, Lebiecki J, Brown TM, Sládek M, Semikhodskii AS, Glossop NR, Piggins HD, Chesham JE, Bechtold DA, Yoo SH, Takahashi (2008). Setting clock speed in mammals: the CK1 epsilon tau mutation in mice accelerates circadian pacemakers by selectively destabilizing PERIOD proteins. Neuron *58*(1):78-88.

75. Eide EJ, Woolf MF, Kang H, Woolf P, Hurst W, Camacho F, Vielhaber EL, Giovanni A, Virshup DM (2005). Control of mammalian circadian rhythm by CKIepsilon-regulated proteasome-mediated PER2 degradation. Mol Cell Biol. *25*(7):2795-807.

76. Shirogane T, Jin J, Ang XL, Harper JW (2005). SCFbeta-TRCP controls clock-dependent transcription via casein kinase 1-dependent degradation of the mammalian period-1 (Per1) protein. J Biol Chem. *280*(29):26863-72.

77. Reischl S, Vanselow K, Westermark PO, Thierfelder N, Maier B, Herzel H, Kramer A (2007). Beta-TrCP1-mediated degradation of PERIOD2 is essential for circadian dynamics. J Biol Rhythms. *22*(5):375-86.

78. Busino L, Bassermann F, Maiolica A, Lee C, Nolan PM, Godinho SI, Draetta GF, Pagano M (2007). SCFFbxl3 controls the oscillation of the circadian clock by directing the degradation of cryptochrome proteins. Science *316*(5826):900-4.

79. Siepka SM, Yoo SH, Park J, Song W, Kumar V, Hu Y, Lee C, Takahashi JS (2007). Circadian mutant Overtime reveals F-box protein FBXL3 regulation of cryptochrome and period gene expression. Cell *129*(5):1011-23.

80. Etchegaray JP, Lee C, Wade PA, Reppert SM (2002). Rhythmic histone acetylation underlies transcription in the mammalian circadian clock. Nature 421(6919):177-82.

81. Ripperger JA, Schibler U (2006). Rhythmic CLOCK-BMAL1 binding to multiple E-box motifs drives circadian Dbp transcription and chromatin transitions. Nat Genet. *38*(3):369-74.

82. Doi M, Hirayama J, Sassone-Corsi P (2006). Circadian regulator CLOCK is a histone acetyltransferase. Cell *125*(3):497-508.

83. Hirayama J, Sahar S, Grimaldi B, Tamaru T, Takamatsu K, Nakahata Y, Sassone-Corsi P (2007). CLOCK-mediated acetylation of BMAL1 controls circadian function. Nature *50*(7172):1086-90.

84. Nakahata Y, Kaluzova M, Grimaldi B, Sahar S, Hirayama J, Chen D, Guarente LP, Sassone-Corsi P (2008). The NAD+-dependent deacetylase SIRT1 modulates CLOCK-mediated chromatin remodeling and circadian control. Cell *134*(2):329-40.

85. Asher G, Gatfield D, Stratmann M, Reinke H, Dibner C, Kreppel F, Mostoslavsky R, Alt FW, Schibler U (2008). SIRT1 regulates circadian clock gene expression through PER2 deacetylation. Cell *134*(2):317-28.

86. Borbély AA, Achermann P (1999). Sleep homeostasis and models of sleep regulation. J Biol Rhythms *14*(6):557-68.

87. Sack RL, Auckley D, Auger RR, Carskadon MA, Wright KP Jr, Vitiello MV, Zhdanova (2007). Circadian rhythm sleep disorders: part II, advanced sleep phase

disorder, delayed sleep phase disorder, free-running disorder, and irregular sleep-wake rhythm. An American Academy of Sleep Medicine review. Sleep *30*(11):1484-501.

88. Jones CR, Campbell SS, Zone SE, Cooper F, DeSano A, Murphy PJ, Jones B, Czajkowski L, Ptácek LJ (1999). Familial advanced sleep-phase syndrome: A short-period circadian rhythm variant in humans. Nat Med. *5*(9):1062-5.

89. Reid KJ, Chang AM, Dubocovich ML, Turek FW, Takahashi JS, Zee PC (2001). Familial advanced sleep phase syndrome. Arch Neurol. *58(7)*:1089-94.

90. Toh KL, Jones CR, He Y, Eide EJ, Hinz WA, Virshup DM, Ptácek LJ, Fu YH (2001). An hPer2 phosphorylation site mutation in familial advanced sleep phase syndrome. Science *291*(5506):1040-3.

91. Xu Y, Toh KL, Jones CR, Shin JY, Fu YH, Ptácek LJ (2007). Modeling of a human circadian mutation yields insights into clock regulation by PER2. Cell *128*(1):59-70.

92. Ebisawa T, Uchiyama M, Kajimura N, Mishima K, Kamei Y, Katoh M, Watanabe T, Sekimoto M, Shibui K, Kim K, Kudo Y, Ozeki Y, Sugishita M, Toyoshima R, Inoue Y, Yamada N, Nagase T, Ozaki N, Ohara O, Ishida N, Okawa M, Takahashi K, Yamauchi T (2001). Association of structural polymorphisms in the human period3 gene with delayed sleep phase syndrome. EMBO Rep. *2*(4):342-6.

93. Suganuma T, Workman JL (2008). Crosstalk among Histone Modifications. Cell *135*(4):604-7.

94. Ooi SK, O'Donnell AH, Bestor TH (2009). Mammalian cytosine methylation at a glance. J Cell Sci. *122*(Pt 16):2787-91.

95. Etchegaray JP, Yang X, DeBruyne JP, Peters AH, Weaver DR, Jenuwein T, Reppert SM (2006). The polycomb group protein EZH2 is required for mammalian circadian clock function. J Biol Chem. *281*(30):21209-15.

96. Alenghat T, Meyers K, Mullican SE, Leitner K, Adeniji-Adele A, Avila J, Bućan M, Ahima RS, Kaestner KH, Lazar MA (2008). Nuclear receptor corepressor and histone deacetylase 3 govern circadian metabolic physiology. Nature *456*(7224):997-1000.

97. Wakiyama M, Imataka H, Sonenberg N (2000). Interaction of eIF4G with poly(A)-binding protein stimulates translation and is critical for Xenopus oocyte maturation. Curr Biol. *10*(18):1147-50.

98. Price JL, Blau J, Rothenfluh A, Abodeely M, Kloss B, Young MW (1998). double-time is a novel Drosophila clock gene that regulates PERIOD protein accumulation. Cell *94*(1):83-95.

99. Baggs JE, Green CB (2003). Nocturnin, a deadenylase in Xenopus laevis retina: a mechanism for posttranscriptional control of circadian-related mRNA. Curr Biol. *13*(3):189-98.

100. Cao R, Lee B, Cho HY, Saklayen S, Obrietan K (2008). Photic regulation of the mTOR signaling pathway in the suprachiasmatic circadian clock. Mol Cell Neurosci. *38*(3):312-24.

101. Denli AM, Tops BB, Plasterk RH, Ketting RF, Hannon GJ (2004). Processing of primary microRNAs by the Microprocessor complex. Nature *432*(7014):231-5.

102. Gregory RI, Yan KP, Amuthan G, Chendrimada T, Doratotaj B, Cooch N, Shiekhattar R (2004). The Microprocessor complex mediates the genesis of microRNAs. Nature *432*(7014):235-40.

103. Han J, Lee Y, Yeom KH, Kim YK, Jin H, Kim VN (2004). The Drosha-DGCR8 complex in primary microRNA processing. Genes Dev. *18*(24):3016-27.

104. Landthaler M, Yalcin A, Tuschl T (2004). The human DiGeorge syndrome critical region gene 8 and Its D. melanogaster homolog are required for miRNA biogenesis. Curr Biol. *14*(23):2162-7.

105. Bohnsack MT, Czaplinski K, Gorlich D (2004). Exportin 5 is a RanGTP-dependent dsRNA-binding protein that mediates nuclear export of pre-miRNAs. RNA *10*(2):185-91.

106. Lund E, Güttinger S, Calado A, Dahlberg JE, Kutay U (2004). Nuclear export of microRNA precursors. Science *303*(5654):95-8.

107. Park MY, Wu G, Gonzalez-Sulser A, Vaucheret H, Poethig RS (2005). Nuclear processing and export of microRNAs in Arabidopsis. Proc Natl Acad Sci *102*(10):3691-6.

108. Yi R, Qin Y, Macara IG, Cullen BR (2003). Exportin-5 mediates the nuclear export of pre-microRNAs and short hairpin RNAs. Genes Dev. *17*(24):3011-6.

109. Khvorova A, Reynolds A, Jayasena SD (2003). Functional siRNAs and miRNAs exhibit strand bias. Cell *115*(2):209-16.

110. Schwarz DS, Hutvágner G, Du T, Xu Z, Aronin N, Zamore PD (2003). Asymmetry in the assembly of the RNAi enzyme complex. Cell *115*(2):199-208.

111. Kim VN (2005). MicroRNA biogenesis: coordinated cropping and dicing. Nat Rev Mol Cell Biol. *6*(5):376-85.

112. Chalfie M, Horvitz HR, Sulston JE (1981). Mutations that lead to reiterations in the cell lineages of C. elegans. Cell *24*(1):59-69.

113. Lee RC, Feinbaum RL, Ambros V (1993). The C. elegans heterochronic gene lin-4 encodes small RNAs with antisense complementarity to lin-14. Cell *75*(5):843-54.

114. Ha I, Wightman B, Ruvkun G (1996). A bulged lin-4/lin-14 RNA duplex is sufficient for Caenorhabditis elegans lin-14 temporal gradient formation. Genes Dev. *10*(23):3041-50.

115. Olsen PH, Ambros V (1999). The lin-4 regulatory RNA controls developmental timing in Caenorhabditis elegans by blocking LIN-14 protein synthesis after the initiation of translation. Dev Biol. *216*(2):671-80.

116. Wightman B, Ha I, Ruvkun G (1993). Posttranscriptional regulation of the heterochronic gene lin-14 by lin-4 mediates temporal pattern formation in C. elegans. Cell *75*(5):855-62.

117. Moss EG, Lee RC, Ambros V. The cold shock domain protein LIN-28 controls developmental timing in C. elegans and is regulated by the lin-4 RNA. Cell *88*(5):637-46.

118. Reinhart BJ, Slack FJ, Basson M, Pasquinelli AE, Bettinger JC, Rougvie AE, Horvitz HR, Ruvkun G (2000). The 21-nucleotide let-7 RNA regulates developmental timing in Caenorhabditis elegans. Nature *403*(6772):901-6

119. Lagos-Quintana M, Rauhut R, Lendeckel W, Tuschl T (2001). Identification of novel genes coding for small expressed RNAs. Science *294*(5543):853-8.

120. Lee RC, Ambros V (2001). An extensive class of small RNAs in Caenorhabditis elegans. Science *294*(5543):862-4.

121. Lau NC, Lim LP, Weinstein EG, Bartel DP (2001). An abundant class of tiny RNAs with probable regulatory roles in Caenorhabditis elegans. Science *294*(5543):858-62.

122. Stark A, Brennecke J, Bushati N, Russell RB, Cohen SM (2005). Animal MicroRNAs confer robustness to gene expression and have a significant impact on 3'UTR evolution. Cell *123*(6):1133-46.

123. Kloosterman WP, Wienholds E, Ketting RF, Plasterk RH (2004). Substrate requirements for let-7 function in the developing zebrafish embryo. Nucleic Acids Res. *32*(21):6284-91.

124. Vella MC, Choi EY, Lin SY, Reinert K, Slack FJ (2004). The C. elegans microRNA let-7 binds to imperfect let-7 complementary sites from the lin-41 3'UTR. Genes Dev. *18*(2):132-7.

125. Doench JG, Sharp PA (2004). Specificity of microRNA target selection in translational repression. Genes Dev. *18*(5):504-11.

126. Enright AJ, John B, Gaul U, Tuschl T, Sander C, Marks DS (2003). MicroRNA targets in Drosophila. Genome Biol. *5*(1):R1.

127. Lewis BP, Shih IH, Jones-Rhoades MW, Bartel DP, Burge CB (2003). Prediction of mammalian microRNA targets. Cell *115*(7):787-98.

128. Rajewsky N, Socci ND (2004). Computational identification of microRNA targets. Dev Biol. *267*(2):529-35.

129. Stark A, Brennecke J, Russell RB, Cohen SM (2003). Identification of Drosophila MicroRNA targets. PLoS Biol. *1*(3):E60.

130. Cheng HY, Papp JW, Varlamova O, Dziema H, Russell B, Curfman JP, Nakazawa T, Shimizu K, Okamura H, Impey S, Obrietan K (2007). microRNA modulation of circadian-clock period and entrainment. Neuron *54*(5):813-29.

131. Gatfield D, Le Martelot G, Vejnar CE, Gerlach D, Schaad O, Fleury-Olela F, Ruskeepää AL, Oresic M, Esau CC, Zdobnov EM, Schibler U (2009). Integration of microRNA miR-122 in hepatic circadian gene expression. Genes Dev. *23*(11):1313-26.

132. Impey S, McCorkle SR, Cha-Molstad H, Dwyer JM, Yochum GS, Boss JM, McWeeney S, Dunn JJ, Mandel G, Goodman RH (2004). Defining the CREB regulon: a genome-wide analysis of transcription factor regulatory regions. Cell *119*(7):1041-54.

133. Friedman RC, Farh KK, Burge CB, Bartel DP (2008). Most mammalian mRNAs are conserved targets of microRNAs. Genome Res. *19*(1):92-105.

134. Lim LP, Lau NC, Garrett-Engele P, Grimson A, Schelter JM, Castle J, Bartel DP, Linsley PS, Johnson JM (2005). Microarray analysis shows that some microRNAs downregulate large numbers of target mRNAs. Nature *433*(7027):769-73.

135. Lagos-Quintana M, Rauhut R, Yalcin A, Meyer J, Lendeckel W, Tuschl T (2002). Identification of tissue-specific microRNAs from mouse. Curr Biol. *12*(9):735-9.

136. Krichevsky AM, King KS, Donahue CP, Khrapko K, Kosik KS (2003). A microRNA array reveals extensive regulation of microRNAs during brain development. RNA *9*(10):1274-81.

137. Kim J, Krichevsky A, Grad Y, Hayes GD, Kosik KS, Church GM, Ruvkun G (2003). Identification of many microRNAs that copurify with polyribosomes in mammalian neurons. Proc Natl Acad Sci *101*(1):360-5.

138. Sempere LF, Freemantle S, Pitha-Rowe I, Moss E, Dmitrovsky E, Ambros V (2004). Expression profiling of mammalian microRNAs uncovers a subset of brain-expressed microRNAs with possible roles in murine and human neuronal differentiation. Genome Biol. *5*(3):R13.

139. Miska EA, Alvarez-Saavedra E, Townsend M, Yoshii A, Sestan N, Rakic P, Constantine-Paton M, Horvitz HR (2004). Microarray analysis of microRNA expression in the developing mammalian brain. Genome Biol. *5*(9):R68.

140. Wheeler G, Ntounia-Fousara S, Granda B, Rathjen T, Dalmay T (2006). Identification of new central nervous system specific mouse microRNAs. FEBS Lett. *580*(9):2195-200.

141. Berezikov E, Thuemmler F, van Laake LW, Kondova I, Bontrop R, Cuppen E, Plasterk RH (2006). Diversity of microRNAs in human and chimpanzee brain. Nat Genet. *38*(12):1375-7.

142. Vo N, Klein ME, Varlamova O, Keller DM, Yamamoto T, Goodman RH, Impey S (2005). A cAMP-response element binding protein-induced microRNA regulates neuronal morphogenesis. Proc Natl Acad Sci *2*(45):16426-31.

143. Mnatzakanian GN, Lohi H, Munteanu I, Alfred SE, Yamada T, MacLeod PJ, Jones JR, Scherer SW, Schanen NC, Friez MJ, Vincent JB, Minassian BA (2004). A previously unidentified MECP2 open reading frame defines a new protein isoform relevant to Rett syndrome. Nat Genet. *36*(4):339-41.

144. Berlanga JJ, Baass A, Sonenberg N (2006). Regulation of poly(A) binding protein function in translation: Characterization of the Paip2 homolog, Paip2B. RNA *12*(8):1556-68.

145. Rekas A, Alattia JR, Nagai T, Miyawaki A, Ikura M (2002). Crystal structure of venus, a yellow fluorescent protein with improved maturation and reduced environmental sensitivity. J Biol Chem. *277*(52):50573-8.

146. Cheng HY, Alvarez-Saavedra M, Dziema H, Choi YS, Li A, Obrietan K (2009). Segregation of expression of mPeriod gene homologs in neurons and glia: possible divergent roles of mPeriod1 and mPeriod2 in the brain. Hum Mol Genet. *18*(16):3110-24.

147. Mayford M, Bach ME, Huang YY, Wang L, Hawkins RD, Kandel ER (1996). Control of memory formation through regulated expression of a CaMKII transgene. Science *274*(5293):1678-83.

148. Klein ME, Lioy DT, Ma L, Impey S, Mandel G, Goodman RH (2007). Homeostatic regulation of MeCP2 expression by a CREB-induced microRNA. Nat Neurosci. *10*(12):1513-4.

149. Alvarez-Saavedra M, Sáez MA, Kang D, Zoghbi HY, Young JI (2007). Cell-specific expression of wild-type MeCP2 in mouse models of Rett syndrome yields insight about pathogenesis. Hum Mol Genet. *16*(19):2315-25.

150. Lewis BP, Burge CB, Bartel DP (2005). Conserved seed pairing, often flanked by adenosines, indicates that thousands of human genes are microRNA targets. Cell *120*(1):15-20.

151. John B, Enright AJ, Aravin A, Tuschl T, Sander C, Marks DS (2004). Human MicroRNA targets. PLoS Biol. 2(11):e363.

152. Krek A, Grün D, Poy MN, Wolf R, Rosenberg L, Epstein EJ, MacMenamin P, da Piedade I, Gunsalus KC, Stoffel M, Rajewsky N (2005). Combinatorial microRNA target predictions. Nat Genet. *37*(5):495-500.

153. Vo N, Goodman RH (2001). CREB-binding protein and p300 in transcriptional regulation. J Biol Chem. *276*(17):13505-8.

155. Jenuwein T, Allis CD (2001). Translating the histone code. Science *293*(5532):1074-80.

156. DNA Nan X, Tate P, Li E, Bird A (1996). DNA methylation specifies chromosomal localization of MeCP2. Mol Cell Biol. *16*(1):414-21.

157. MeCP2 Nan X, Campoy FJ, Bird A (1997). MeCP2 is a transcriptional repressor with abundant binding sites in genomic chromatin. Cell *88*(4):471-81.

158. Nan X, Ng HH, Johnson CA, Laherty CD, Turner BM, Eisenman RN, Bird A (1998). Transcriptional repression by the methyl-CpG-binding protein MeCP2 involves a histone deacetylase complex. Nature *393*(6683):386-9.

159. Young JI, Hong EP, Castle JC, Crespo-Barreto J, Bowman AB, Rose MF, Kang D, Richman R, Johnson JM, Berget S, Zoghbi HY (2005). Regulation of RNA splicing by the methylation-dependent transcriptional repressor methyl-CpG binding protein 2. Proc Natl Acad Sci *102*(49):17551-8.

160. Chahrour M, Jung SY, Shaw C, Zhou X, Wong ST, Qin J, Zoghbi HY (2008). MeCP2, a key contributor to neurological disease, activates and represses transcription. Science *320*(5880):1224-9.

161. Piazza CC, Fisher W, Kiesewetter K, Bowman L, Moser H (1990). Aberrant sleep patterns in children with the Rett syndrome. Brain Dev. *12*(5):488-93.

162. Mauxion F, Faux C, Séraphin B (2008). The BTG2 protein is a general activator of mRNA deadenylation. EMBO J. *27*(7):1039-48.

163. Woo KC, Kim TD, Lee KH, Kim DY, Kim W, Lee KY, Kim KT (2008). Mouse period 2 mRNA circadian oscillation is modulated by PTB-mediated rhythmic mRNA degradation. Nucleic Acids Res. *37*(1):26-37.

164. Imataka H, Gradi A, Sonenberg N (1998). A newly identified N-terminal amino acid sequence of human eIF4G binds poly(A)-binding protein and functions in poly(A)-dependent translation. EMBO J. *17*(24):7480-9.

165. Khaleghpour K, Kahvejian A, De Crescenzo G, Roy G, Svitkin YV, Imataka H, O'Connor-McCourt M, Sonenberg N (2001). Dual interactions of the translational repressor Paip2 with poly(A) binding protein. Mol Cell Biol. *21*(15):5200-13.

166. Ueda HR, Chen W, Adachi A, Wakamatsu H, Hayashi S, Takasugi T, Nagano M, Nakahama K, Suzuki Y, Sugano S, Iino M, Shigeyoshi Y, Hashimoto S (2002). A transcription factor response element for gene expression during circadian night. Nature *418*(6897):534-9.

167. Ogryzko VV, Schiltz RL, Russanova V, Howard BH, Nakatani Y (1996). The transcriptional coactivators p300 and CBP are histone acetyltransferases. Cell *87*(5):953-9.

168. Chan HM, La Thangue NB (2001). p300/CBP proteins: HATs for transcriptional bridges and scaffolds. J Cell Sci. *114*(Pt 13):2363-73.

169. Thompson PR, Wang D, Wang L, Fulco M, Pediconi N, Zhang D, An W, Ge Q, Roeder RG, Wong J, Levrero M, Sartorelli V, Cotter RJ, Cole PA (2004). Regulation of the p300 HAT domain via a novel activation loop. Nat Struct Mol Biol. *11*(4):308-15.

170. Impey S, Fong AL, Wang Y, Cardinaux JR, Fass DM, Obrietan K, Wayman GA, Storm DR, Soderling TR, Goodman RH (2002). Phosphorylation of CBP mediates transcriptional activation by neural activity and CaM kinase IV. Neuron *34*(2):235-44.

171. Zhou Z, Hong EJ, Cohen S, Zhao WN, Ho HY, Schmidt L, Chen WG, Lin Y, Savner E, Griffith EC, Hu L, Steen JA, Weitz CJ, Greenberg ME (2006). Brain-specific phosphorylation of MeCP2 regulates activity-dependent Bdnf transcription, dendritic growth, and spine maturation. Neuron *52*(2):255-69.

172. Bonenfant D, Coulot M, Towbin H, Schindler P, van Oostrum J (2006). Characterization of histone H2A and H2B variants and their post-translational modifications by mass spectrometry. Mol Cell Proteomics. *5*(3):541-52.

173. Shigeyoshi Y, Taguchi K, Yamamoto S, Takekida S, Yan L, Tei H, Moriya T, Shibata S, Loros JJ, Dunlap JC, Okamura H (1997). Light-induced resetting of a mammalian circadian clock is associated with rapid induction of the mPer1 transcript. Cell *91*(7):1043-53.

174. Yan L, Silver R (2004). Resetting the brain clock: time course and localization of mPER1 and mPER2 protein expression in suprachiasmatic nuclei during phase shifts. Eur J Neurosci. *19*(4):1105-9.

175. Curtis AM, Seo SB, Westgate EJ, Rudic RD, Smyth EM, Chakravarti D, FitzGerald GA, McNamara P (2004). Histone acetyltransferase-dependent chromatin remodeling and the vascular clock. J Biol Chem. *279*(8):7091-7..

176. Jones PL, Veenstra GJ, Wade PA, Vermaak D, Kass SU, Landsberger N, Strouboulis J, Wolffe AP (1998). Methylated DNA and MeCP2 recruit histone deacetylase to repress transcription. Nat Genet. *19*(2):187-91.

177. Yasui DH, Peddada S, Bieda MC, Vallero RO, Hogart A, Nagarajan RP, Thatcher KN, Farnham PJ, Lasalle JM (2007). Integrated epigenomic analyses of neuronal MeCP2 reveal a role for long-range interaction with active genes. Proc Natl Acad Sci. *104*(49):19416-21.

178. Dragich JM, Kim YH, Arnold AP, Schanen NC (2007). Differential distribution of the MeCP2 splice variants in the postnatal mouse brain. J Comp Neurol. *501*(4):526-42.

179. Kriaucionis S, Bird A (2004). The major form of MeCP2 has a novel N-terminus generated by alternative splicing. Nucleic Acids Res. *32*(5):1818-23.

180. Shahbazian MD, Antalffy B, Armstrong DL, Zoghbi HY (2002). Insight into Rett syndrome: MeCP2 levels display tissue- and cell-specific differences and correlate with neuronal maturation. Hum Mol Genet. *11*(2):115-24.

181. Guy J, Hendrich B, Holmes M, Martin JE, Bird A (2001). A mouse Mecp2-null mutation causes neurological symptoms that mimic Rett syndrome. Nat Genet. *27*(3):322-6.

182. Chen RZ, Akbarian S, Tudor M, Jaenisch R (2001). Deficiency of methyl-CpG binding protein-2 in CNS neurons results in a Rett-like phenotype in mice. Nat Genet. *27*(3):327-31.

183. Yamaguchi S, Mitsui S, Miyake S, Yan L, Onishi H, Yagita K, Suzuki M, Shibata S, Kobayashi M, Okamura H (2000). The 5' upstream region of mPer1 gene contains two promoters and is responsible for circadian oscillation. Curr Biol. *10*(14):873-6.

184. Travnickova-Bendova Z, Cermakian N, Reppert SM, Sassone-Corsi P (2002). Bimodal regulation of mPeriod promoters by CREB-dependent signaling and CLOCK/BMAL1 activity. Proc Natl Acad Sci U S A. *99*(11):7728-33.

185. Yoo SH, Ko CH, Lowrey PL, Buhr ED, Song EJ, Chang S, Yoo OJ, Yamazaki S, Lee C, Takahashi JS (2005). A noncanonical E-box enhancer drives mouse Period2 circadian oscillations in vivo. Proc Natl Acad Sci U S A. *102*(7):2608-13.

186. Walton KM, Rehfuss RP, Chrivia JC, Lochner JE, Goodman RH (1992). A dominant repressor of cyclic adenosine 3',5'-monophosphate (cAMP)-regulated enhancer-binding protein activity inhibits the cAMP-mediated induction of the somatostatin promoter in vivo. Mol Endocrinol. *6*(4):647-55.

187. Kerr B, Alvarez-Saavedra M, Sáez MA, Saona A, Young JI (2008). Defective body-weight regulation, motor control and abnormal social interactions in Mecp2 hypomorphic mice. Hum Mol Genet. *17*(12):1707-17.

188. Samaco RC, Fryer JD, Ren J, Fyffe S, Chao HT, Sun Y, Greer JJ, Zoghbi HY, Neul JL (2008). A partial loss of function allele of methyl-CpG-binding protein 2 predicts a human neurodevelopmental syndrome. Hum Mol Genet. *17*(12):1718-27.

189. Yanagiya, A, Sonenberg, N (2010). Translational control in late spermatogenesis by the poly(A) binding protein partner, Paip2a. *Submitted.*

190. Schratt GM, Tuebing F, Nigh EA, Kane CG, Sabatini ME, Kiebler M, Greenberg ME (2006). A brain-specific microRNA regulates dendritic spine development. Nature *439*(7074):283-9.

191. Makeyev EV, Zhang J, Carrasco MA, Maniatis T (2007). The MicroRNA miR-124 promotes neuronal differentiation by triggering brain-specific alternative pre-mRNA splicing. Mol Cell. *27*(3):435-48.

192. Tay YM, Tam WL, Ang YS, Gaughwin PM, Yang H, Wang W, Liu R, George J, Ng HH, Perera RJ, Lufkin T, Rigoutsos I, Thomson AM, Lim B (2008). MicroRNA-134 modulates the differentiation of mouse embryonic stem cells, where it causes post-transcriptional attenuation of Nanog and LRH1. Stem Cells. *26*(1):17-29

193. Tay Y, Zhang J, Thomson AM, Lim B, Rigoutsos I (2008). MicroRNAs to Nanog, Oct4 and Sox2 coding regions modulate embryonic stem cell differentiation. Nature *455*(7216):1124-8.

194. Yoo AS, Staahl BT, Chen L, Crabtree GR (2009). MicroRNA-mediated switching of chromatin-remodeling complexes in neural development. Nature *460*(7255):642-6..

195. Gupta S, Kim SY, Artis S, Molfese DL, Schumacher A, Sweatt JD, Paylor RE, Lubin FD (2010). Histone methylation regulates memory formation. J Neurosci. *30*(10):3589-99.

196. Xiao F, Zuo Z, Cai G, Kang S, Gao X, Li T (2008). miRecords: an integrated resource for microRNA-target interactions. Nucleic Acids Res. *37*(Database issue):D105-10.

197. Reppert SM, Weaver DR (2002). Coordination of circadian timing in mammals. Nature *418*(6901):935-41.

198. Onesto C, Berra E, Grépin R, Pagès G (2004). Poly(A)-binding protein-interacting protein 2, a strong regulator of vascular endothelial growth factor mRNA. J Biol Chem. *279*(33):34217-26.

CONTRIBUTIONS OF COLLABORATORS

Dr. Carolina Perez-Iratxeta at the Ottawa Health Research Institute (OHRI) performed the computational analysis of miR-132 predicted targets from TargetScan5.1. She also provided Figure 9A & Figure 9B, as well as Table 3 and Table 4. This data was incorporated into a revised version of the manuscript Alvarez-Saavedra et al, circa March 2010.

Drs. Nahum Sonenberg and Akiko Yanagiya at the Rosalind and Morris Goodman Cancer Centre, McGill University, provided the *Paip2a*$^{-/-}$ mice. Brains were harvested at their laboratory and tissue was transported to Ottawa. Dr. Akiko Yanagiya performed the western blot to verify the absence of PAIP2A in *Paip2a*$^{-/-}$ brain tissue and provided Figure 27.

Dr. Juan I. Young, presently at the Hussman Institute for Human Genomics, University of Miami, provided the *Mecp2*$^{\text{Floxed/y mice}}$. Brains were harvested at the Centre for Scientific Studies (Centro de Estudios Científicos) in Valdivia, Chile and tissues and cDNAs shipped to Ottawa. Thanks to Dr. Bredford Kerr and Juan Manuel Baamonde, at the CECS transgenic facility, for genotyping and mouse handling while in Chile.

Dr. Karl Obrietan and Heather Dziema at the Neuroscience Department, Ohio State University, performed the C57/B6 mouse cannulations and miR-132, miR-219, miR-1 and vehicle antagomir infusions. They shipped the dissected SCN tissue to the Cheng lab where western blotting was performed to validate the identified targets via *in-vivo* knockdown of miR-132.

All cloning strategies, except where noted, were designed by Matías Alvarez-Saavedra (MAS) with helpful input from Dr. Hai-Ying Mary Cheng (HYMC). All MeCP2 ChIP

binding motifs were identified by MAS. All experiments were jointly designed, executed and analyzed by MAS & HYMC, as indicated in greater detail in the figure legends. The proposed model was originally conceived by MAS & HYMC, from data generated by MAS from August 2008 to March 2010. All figures in this thesis were designed by MAS. MAS wrote parts of the manuscript and designed all figures, including supplementary figures, for the manuscripts Alvarez-Saavedra et al, circa November 2009 (submitted to *Neuron*) and Alvarez-Saavedra et al, circa March 2010 (unsubmitted).

This work and MAS' funding was financed by an operating grant from the Canadian Institute of Health Research (CIHR) no. 086549, as well as funds from the Early Researcher Award, Canada Research Chair program, and University of Ottawa start-up funds, awarded to HYMC.

CURRICULUM VITAE

Matías Alberto Alvarez-Saavedra, B.Sc.

BORN: May 06 1980, Santiago, Chile.

EDUCATION:

University of Ottawa, Canada — September 2008 –August 010
Master of Science, Department of Biochemistry, Microbiology & Immuno.
Thesis: microRNA-132-dependent post-transcriptional regulation of clock entrainment physiology via modulation of chromatin remodeling and translational control gene targets.
Advisor: Hai-Ying Mary Cheng, Ph.D.

Montclair State University, United States of America — January 2005
Bachelor of Science, Molecular Biology Major

EMPLOYMENT:

2006-2008 *Research Assistant*
Molecular Genetics Laboratory, Centro de Estudios Científicos (CECS), Valdivia, Chile.
Principal Investigator: Juan I. Young, Ph.D.

2002 *Research Technician I*
Neuroinflammation Research Laboratories, Mount Sinai Medical Center, New York, New York, USA.
Principal Investigator: Giulio Maria Pasinetti, M.D., Ph.D.

OTHER RESEARCH EXPERIENCE:

2004-2005 *Undergraduate Senior Thesis Student*
Montclair State University, Department of Biology & Molecular Biology, Montclair, New Jersey, USA.
Projects: I) Role of N-glycans on FMV receptor binding. II) Inhibition of cellular N-glycan synthesis by tunicamycin.
Advisor: Sandra D. Adams, Ph.D.

2000-2002 *Undergraduate Biology Honors Student*
Department of Neuroscience, New Jersey Neuroscience Institute, Seton Hall University/JFK Medical Centre, South Orange, New Jersey, USA
Projects: I) Cellular and molecular events following kainic acid-induced status epilepticus in postnatal and adult rats.
Advisor: Linda K. Friedman, Ph.D.

TEACHING EXPERIENCE:

2009 Teaching Assistant, Intro Biochemistry Lab (BCH2333), University of Ottawa, Ottawa, Canada.

2008 Teaching Assistant, Molecular Biology Lab (BCH3356), University of Ottawa, Ottawa, Canada.

LATEST AWARDS:

2009 Winner of "Becas Chile" Fellowship for Master of Science Studies from the Government of Chile, CONICYT, Santiago, Chile (gratefully declined).

2009 3rd Place Finish, BMI Poster Day, Department of Biochemistry, Microbiology & Immunology, Faculty of Medicine, University of Ottawa, Ottawa, Canada.

2007 Full Travel Award (US$3000), The Wellcome Trust Foundation, "Working with the Human Genome", Wellcome Trust Overseas Workshops, Pasteur Institute, Montevideo, Uruguay.

2007 Full Travel Award (US$2000), The Institute of Stem Cell Research, University of Edinburgh & The Millennium Nucleus for Developmental Biology, University of Chile, "ES cells as a model for mammalian development", University of Chile, Santiago, Chile.

PUBLICATIONS

Publications in Peer-Reviewed Journals

1. **Alvarez-Saavedra M**, Carrasco L, Sura-Trueba, S, Aiello, VD, Walz, K, Neto JX, Young JI. Elevated expression of MeCP2 in cardiac and skeletal tissues is detrimental for normal development. *Human Molecular Genetics* 2010, 19(11): 2177-2190.

2. Cheng HYM, **Alvarez-Saavedra M,** Dziema H, Choi YS, Li A, Obrietan K. Segregation of expression of *mPeriod* gene homologs in neurons and glia: Possible divergent roles of *mPeriod1* and *mPeriod2* in the brain. *Human Molecular Genetics* 2009, 18(16): 3110-3124.

3. Kerr B, **Alvarez-Saavedra M,** Saez M, Saona A, Young JI. Defective body weight regulation, motor control and abnormal social interactions in Mecp2 hypomorphic mice. *Human Molecular Genetics* 2008, 17(12): 1707-1717.

4. **Alvarez-Saavedra M,** Saez M, Kang D, Zoghbi HY, Young JI. Cell-specific expression of wild-type MeCP2 in mouse models of Rett syndrome yields insight about pathogenesis. *Human Molecular Genetics* 2007, 16(19): 2315-2325.

Manuscripts in press, submitted or in preparation

1. **Alvarez-Saavedra M**, Yanagiya A, Cornejo-Palma D, Oliva-Hernandez R, Sonenberg N, Cheng HYM. microRNA-132 orchestrates chromatin remodeling and translational control of the circadian clock (unsubmitted, circa March 2010).

2. Tian R, **Alvarez-Saavedra M**, Cheng HYM, Figeys D. Uncovering the light-responsive proteome of the master circadian clock (manuscript in preparation).

PRESENTATIONS & LECTURES

Latest Abstracts and Posters

1. Cheng HYM, **Alvarez-Saavedra M**, Obrietan K. Segregation of expression of *mPeriod* gene homologs in neurons and glia: Possible divergent roles of *mPeriod1* and *mPeriod2* in the brain. 39th Annual Meeting of the Society for Neuroscience (SFN), Chicago, Illinois, USA, October 17-21, 2009.
2. Kerr B, **Alvarez-Saavedra M,** Saez M, Young JI. MeCP2 hypomorphic mice display abnormalities in body weight regulation, motor control and social interactions. 9th Annual Rett Syndrome Symposium, Eaglewood Resort & Spa, Chicago, Illinois, USA, June 23-25, 2008.
3. Saez M, **Alvarez-Saavedra M,** Young JI. Post-transcriptional functions of MeCP2: Influenced by neuronal activity? Gene Expression & RNA Processing and Cell Biology, Signaling & Alternative Splicing Combined Meetings, EURASNET Interdisciplinary Focus Meeting, Bariloche, Argentina, November 26-30, 2007.
4. Saez M, **Alvarez-Saavedra M**, Young JI. Post-transcriptional functions of MeCP2: Influenced by neuronal activity? 8th Annual Rett Syndrome Symposium, Eaglewood Resort & Spa, Chicago, Illinois, USA, June 25-27, 2007.
5. Saez M, **Alvarez-Saavedra M**, Zoghbi HY, Young JI. Post-transcriptional functions of MeCP2. The Third Chromatin Structure & Function Meeting, Punta Cana, Dominican Republic, December 5-7, 2006.

Invited Lectures

1. **Alvarez-Saavedra, M.** "Cell-specific expression of wild-type MeCP2 in mutant mouse models for mecp2." Student Seminar for the XXI Annual Meeting of the Chilean Cell Biology Society, Pucón, Chile, October 7-11, 2007.

APPENDIX

Appendix I

NATURE PUBLISHING GROUP LICENSE
TERMS AND CONDITIONS
Jul 11, 2010

This is a License Agreement between Matias A Alvarez-Saavedra ("You") and Nature Publishing Group ("Nature Publishing Group") provided by Copyright Clearance Center ("CCC"). The license consists of your order details, the terms and conditions provided by Nature Publishing Group, and the payment terms and conditions.

All payments must be made in full to CCC. For payment instructions, please see information listed at the bottom of this form.

License Number	2464341445467
License date	Jul 08, 2010
Licensed content publisher	Nature Publishing Group
Licensed content publication	Nature
Licensed content title	Coordination of circadian timing in mammals
Licensed content author	Steven M. Reppert, David R. Weaver
Volume number	
Issue number	
Pages	
Year of publication	2002
Portion used	Figures / tables
Number of figures / tables	1
Requestor type	Student
Type of Use	Thesis / Dissertation
Billing Type	Invoice
Company	Matias A Alvarez-Saavedra
Billing Address	195 Lennox Park Avenue Ottawa, ON K1G 0K3 Canada
Customer reference info	
Total	0.00 USD
Terms and Conditions	

Terms and Conditions for Permissions

Nature Publishing Group hereby grants you a non-exclusive license to reproduce this material for this purpose, and for no other use, subject to the conditions below:

1. NPG warrants that it has, to the best of its knowledge, the rights to license reuse of this material. However, you should ensure that the material you are requesting is original to Nature Publishing Group and does not carry the copyright of another entity (as credited in the published version). If the credit line on any part of the material you have requested indicates that it was reprinted or adapted by NPG with permission from another source, then you should also seek permission from that source to reuse the material.

2. Permission granted free of charge for material in print is also usually granted for any electronic version of that work, provided that the material is incidental to the work as a whole and that the electronic version is essentially equivalent to, or substitutes for, the print version. Where print permission has been granted for a fee, separate permission must be obtained for any additional, electronic re-use (unless, as in the case of a full paper, this has already been accounted for during your initial request in the calculation of a print run). NB: In all cases, web-based use of full-text articles must be authorized separately through the 'Use on a Web Site' option when requesting permission.

3. Permission granted for a first edition does not apply to second and subsequent editions and for editions in other languages (except for signatories to the STM Permissions Guidelines, or where the first edition permission was granted for free).

4. Nature Publishing Group's permission must be acknowledged next to the figure, table or abstract in print. In electronic form, this acknowledgement must be visible at the same time as the figure/table/abstract, and must be hyperlinked to the journal's homepage.
5. The credit line should read:

   Reprinted by permission from Macmillan Publishers Ltd: [JOURNAL NAME] (reference citation), copyright (year of publication)

   For AOP papers, the credit line should read:

   Reprinted by permission from Macmillan Publishers Ltd: [JOURNAL NAME], advance online publication, day month year (doi: 10.1038/sj.[JOURNAL ACRONYM].XXXXX)

6. Adaptations of single figures do not require NPG approval. However, the adaptation

should be credited as follows:

Adapted by permission from Macmillan Publishers Ltd: [JOURNAL NAME] (reference citation), copyright (year of publication)

7. Translations of 401 words up to a whole article require NPG approval. Please visit http://www.macmillanmedicalcommunications.com for more information. Translations of up to a 400 words do not require NPG approval. The translation should be credited as follows:

   Translated by permission from Macmillan Publishers Ltd: [JOURNAL NAME] (reference citation), copyright (year of publication).

We are certain that all parties will benefit from this agreement and wish you the best in the use of this material. Thank you.

v1.1

END OF THESIS
